

**Inhibiting Protein-Protein Interactions in the Hsp70 Complex
as a Means to Regulate Protein Homeostasis**

by

Matthew Conrad Smith

A dissertation submitted in partial fulfillment
of the requirements for the degree of
Doctor of Philosophy
(Molecular and Cellular Pathology)
in The University of Michigan
2012

Doctoral Committee:

Associate Professor Jason E. Gestwicki, Chair
Professor Yoichi Osawa
Assistant Professor Tomasz Cierpicki
Assistant Professor Yali Dou
Assistant Professor Ming Lei

© Matthew Conrad Smith

2012

To Beverly

Acknowledgments

I would first like to thank Prof. Jason E. Gestwicki for being a constant source of enthusiasm, inspiration, and ideas as I navigated through graduate school. I could not have asked for a better advisor. Jason's door was always open, and I will be forever grateful for the amount of time he allotted to helping me mature as a scientist. This process had its share of challenges, but at every turn (and negative result) I was greeted with a smile and endless optimism about my project.

I would also like to thank members of the lab who helped contribute to the work in this thesis. Chris Evans was instrumental in helping to set-up the synthesis for the compounds outlined here. As well as Srikanth Patury and Andrea Thompson who helped characterize the protein-protein interaction that became a central component of my project. Countless substantive discussions with Andrea, Srikanth, Yoshi Miyata, Leah Makley, Paul Marinec, and Ashley Reinke, have helped me continually throughout my graduate career. Finally, to all of the members of the Gestwicki lab, both past and present, you have made this lab such a wonderful place to work. I thank you all, sincerely.

Nothing I have accomplished would have been possible without the support of my family. I thank my two wonderful sisters, Kendria and Christina for constantly "bothering" me with the various issues in their lives. Honestly, sometimes they felt like my only connection to the world outside of lab. My dad has supported just about every

decision I have made in my adult life, and I appreciate and admire his level of consistency. My stepfather Laci, has never missed an opportunity to tell me how proud he is of me. And his home in New York has been an invaluable retreat for me over the past five years. Lastly, to mother, Beverly: I do not have appropriate words to express my gratitude for all you have done for me. You raised me with the notion that I could do anything, that there was literally nothing outside of my grasp as long as I was willing to work for it. Your constant encouragement has pushed me to do better at every stage of my life, and I thank you so very much.

Table of Contents

Dedication	ii
Acknowledgments	iii
List of Figures	xii
List of Tables	xiv
Abstract	xv
Chapter	
1. Introduction: Protein-protein interactions as emerging drug targets	1
1.1. Abstract	1
1.2. Protein-protein interactions as novel targets in biology	2
1.3. Challenges of targeting protein-protein interactions	3
1.3.1. Surface area	3
1.3.2. Topology	4
1.3.3. Promiscuity	5
1.4. Classes of protein-protein interaction inhibitors	7
1.4.1. Protein-protein interactions "Tight and Narrow"	8
1.4.2. Protein-protein interactions "Tight and Wide"	11
1.4.3. Protein-protein interactions "Loose and Narrow"	16

1.4.4. Protein-protein interactions “Loose and Wide”	18
1.5. Advancing protein-protein interaction inhibitors in difficult systems	19
1.5.1. Heat shock protein 70	20
1.5.2. Heat shock protein 90	24
1.6. Analysis and prospectus	26
1.7. References	29
2. Characterization of the binding of the E3 ubiquitin ligase CHIP to the molecular chaperones Hsp70 and Hsp90	40
2.1. Abstract	40
2.1.1. Hsp70 and Hsp90 promote the degradation of misfolded proteins	41
2.1.2. CHIP binds to chaperones through its TPR domain	42
2.2. Results	45
2.2.1. Design of CHIP and Hsp70 truncations	45
2.2.2. Full binding of CHIP to Hsp70 and Hsp90 requires an intact TPR domain	46
2.2.3. CHIP binds to Hsp90 with weaker affinity than Hsp70	48
2.2.4. Truncation mutants reveal domains critical for the Hsp70-CHIP interaction	51
2.2.5. CHIP does not display nucleotide dependence in binding to Hsp70	53
2.2.6. TPR domain is required for the ubiquitination of Hsp70	54
2.3. Discussion	55
2.3.1. The TPR domain in CHIP and the EEVD motif in Hsp70/Hsp90 play important roles in binding but other regions also contribute	55

2.3.2. Nucleotide state does not influence CHIP binding to Hsp70	57
2.4. Materials and Methods	58
2.4.1. Protein purification	58
2.4.2. Surface plasmon resonance experiments	59
2.4.3. Analytical ultracentrifugation	59
2.4.4. Gel filtration	60
2.4.5. ATPase assays	60
2.4.6. Fluorescence quenching assays	61
2.4.7. Ubiquitination assays	62
2.5. Appendix	63
2.5.1. CHIP does not bind Hsp70 as a substrate	63
2.5.2. Hsp70-CHIP complex formation	64
2.5.3. Hsp90 can compete with Hsp70 for CHIP binding	65
2.5.4. Raw SPR curves	66
2.5.5. Free energy values calculated from SPR binding affinities	67
2.6. References	68
3. Improving the synthesis of 15-deoxyspergualin analogs using the Ugi multicomponent reaction	71
3.1. Abstract	71
3.1.1. Spergualin and its derivatives are unstable, yet biologically active, polyamines	72
3.1.2. The synthesis of spergualin derivatives remains difficult	75
3.2. Results	76
3.2.1. Optimizing the microwave irradiation-assisted Ugi reaction	76

3.2.2.	Building a focused library of spergualin analogs	76
3.2.3.	Spergualin analogs are significantly more stable than the natural product	78
3.2.4.	Spergualin analogs retain antibacterial activity	81
3.3.	Discussion	81
3.3.1.	The Ugi multicomponent reaction allows increased access to spergualin derivatives	81
3.3.2.	Spergualin analogs are more stable than and maintain biological activity of the natural product	82
3.3.3.	Conclusions	83
3.4.	Materials and methods	84
3.4.1.	Reagents and general syntheses	84
3.4.2.	Spergualin analog syntheses	87
3.4.3.	High performance liquid chromatography	89
3.4.4.	Thin-layer chromatography	89
3.5.	References	91
4.	Spergualin analogs as novel inhibitors of the Hsp70/CHIP protein-protein interaction	94
4.1.	Abstract	94
4.1.1.	Protein-protein interactions in the Hsp70 system	95
4.1.2.	The C-terminus of Hsp70 acts as a hub for TPR protein binding	95
4.1.3.	Spergualin analogs bind to the C-terminus of Hsp70	97
4.2.	Results	98
4.2.1.	A spergualin analog inhibits binding of Hsp70 to CHIP	98
4.2.2.	Screen of spergualin library reveals a potent inhibitor	100

4.2.3.	Spergualin analog disrupts the Hsc70-CHIP interaction by size-exclusion chromatography	101
4.2.4.	The effect of Spergualin analogs on other Hsp70 PPIs	102
4.2.5.	Spergualin binds the C-terminus of Hsc70	104
4.2.6.	Spergualin analog inhibits the Hsp70-TPR interactions in cells	105
4.2.7.	Inhibition of the Hsc70-CHIP interaction in cells causes Tau accumulation	107
4.3.	Discussion	108
4.3.1.	Rational design of a novel Hsc70 inhibitor	108
4.3.2.	Re-investigating a promising chemical scaffold	109
4.3.3.	Conclusions	110
4.4.	Materials and methods	111
4.4.1.	Reagents and general syntheses	111
4.4.2.	Spergualin analog syntheses	112
4.4.3.	Characterization of spergualin analogs	113
4.4.4.	Protein purification	116
4.4.5.	Fluorescence quenching assay	117
4.4.6.	Gel filtration assays	118
4.4.7.	ATPase assays	119
4.4.8.	Plasmids, transfections and co-immunoprecipitation	119
4.4.9.	MAPT stability assays	120
4.5.	Appendix	121
4.5.1.	Characterizing Hsc70 PPIs by fluorescence-quenching assay	121
4.5.2.	Gly-DSG (1) has a modest effect on tau burden	122

4.5.3. Administration of spergualins does not effect BHQ-10 absorbance	123
4.6. References	124
5. Conclusions and future directions	127
5.1. Abstract	127
5.2. Conclusions	128
5.2.1. Targeting protein quality control using small molecules: Rationale for targeting the Hsp70-CHIP interface	128
5.2.2. Summary of major advances and characterization of spergualin analogs as inhibitors of the Hsp70-CHIP PPI	129
5.3. Future directions	132
5.3.1. Improving potency and building selectivity	132
5.3.2. Re-exploring the therapeutic potential of spergualins	134
5.4. Appendix	136
5.4.1. Spergualin effect on the Hsp90-CHIP interaction	136
5.5. References	137
Appendix: A chemical biology approach to exploring protein-protein interactions in neurodegeneration	139
A.1. Abstract	139
A.1.1. Protein aggregation in neurodegeneration	140
A.1.2. Aggresome formation and protein quality control	141
A.2. Results	142
A.2.1. A <i>Saccharomyces cerevisiae</i> model of aggresome formation	142
A.2.2. Modulation of the Hsp70-Hsp40 interaction inhibits aggresome formation	144
A.2.3. The pharmacological inhibition of aggresome formation	144

is persistent over time	
A.2.4. Inhibiting aggresome formation decreases cellular longevity	146
A.3. Conclusions	148
A.3.1. Aggresome formation facilitates cell survival during high misfolded protein burden	148
A.3.2. Protein quality control directs the formation of aggresomes	149
A.4. Materials and methods	150
A.4.1. General materials	150
A.4.2. Yeast growth and induction	150
A.4.3. Yeast aging assay	150
A.4.4. Fluorescence microscopy	151
A.5. Appendix	152
A.5.1. Live cells harboring aggresomes accumulate with age	152
A.6. References	153

List of Figures

1.1 Categorization of protein-protein interactions (PPIs) and their inhibitors	6
1.2 Protein-protein interaction classes versus average inhibitor affinities	9
1.3 Inhibition of protein-protein interactions in the chaperone complexes	24
2.1 Domain architecture of CHIP, Hsp70 and Hsp90 and design of truncations	43
2.2 Binding of Hsp70/Hsp90 to CHIP by fluorescence quenching	46
2.3 Full-length CHIP binds Hsp70 and Hsp90 by surface plasmon resonance (SPR)	50
2.4 CHIP interaction with Hsp70 is independent of nucleotide state	54
2.5 Ubiquitination of Hsp70 by CHIP requires the TPR domains	56
3.1 Chemical structures of the natural product, spergualin, and two of its derivatives	72
3.2 Comparison of the retrosynthetic analysis	74
3.3 Synthesis of spergualin analogs	79
3.4 Synthetic derivatives of spergualin are more stable than the natural product	80
4.1 TPR-proteins coordinate substrate fate	96
4.2 Spergualin analogs inhibit the Hsc70-CHIP PPI by FRET	99
4.3 Inhibitory effect of compound seen by gel filtration	103
4.4 Compound effect on Hsc70 PPIs	105
4.5 The cellular disruption of Hsc70 PPIs by compound 5b	106

4.6 Compound administration causes tau accumulation	108
4.7 Model of compound 5b activity	110
5.1 The co-chaperone mediated activity of Hsp70	129
5.2 The discovery of a novel PPI inhibitor of the Hsp70 system	131
5.3 Structural differences between Hsp70-TPR interactions	133
A.1 Characterization of the Huntingtin gene	141
A.2 SW02 causes the inhibition of aggresome formation	143
A.3 The inhibition of aggresome formation is persistent over time	145
A.4 Inhibiting aggresome formation causes toxicity	147
A.5 Spergualin analog administration also inhibits aggresome formation	148

List of Tables

1.1 Features of select PPIs and their inhibitors	17
2.1 Binding affinities (K_i values in nM), as measured by fluorescence quench	48
2.2 Binding affinities (K_D values in nM) for binding of Hsp70 to CHIP, as measured by SPR	52
3.1 Optimization of the Ugi reaction conditions	77
4.1 Characterization of compound effect in fluorescence quenching assay	100

Abstract

The molecular chaperone, heat shock protein 70 (Hsp70), is an important regulator of protein homeostasis that has roles in both primary protein folding and clearance of misfolded proteins. Several studies have suggested that it is the interaction between Hsp70 and a network of co-chaperones that might determine the fate Hsp70-bound substrates. For example, a complex formed between Hsp70 and the E3 ubiquitin ligase CHIP, is thought to guide substrates to the proteasome. However the mechanism governing how co-chaperones assemble on Hsp70 remains unresolved. We wanted to explore how interactions between Hsp70 and CHIP govern the ubiquitin-mediated degradation of chaperone substrates. Moreover, we hypothesize that chemical disruption of the Hsp70-CHIP contact might decrease turnover of these substrates and, thereby, alter protein homeostasis.

This thesis work involves the biophysical and structural characterization of the Hsp70-CHIP complex and synthesis of chemical probes that block CHIP binding to Hsp70. Using truncations and biochemical assays, we determined that the

tetratricopeptide repeat (TPR) domain of CHIP, along with an important secondary interaction in the charged coiled-coil domain govern binding of CHIP to Hsp70. In addition, we developed a dramatically improved synthesis of the promising natural product, spergualin, and created a collection of more potent and stable derivatives. We then showed that these compounds disrupt the Hsp70-CHIP interaction *in vitro* and in cells. Together, these findings provide a quantitative exploration of the CHIP-Hsp70 complex and the first set of chemical tools that can be used to regulate Hsp70 interactions with CHIP. We expect that these probes will be useful in further studying Hsp70-mediated protein quality control.

Chapter 1

Introduction: Protein-protein interactions as emerging drug targets

1.1. Abstract

Protein-protein interactions (PPIs) control the assembly of multi-protein complexes and, thus, these contacts have enormous potential as drug targets. However, the field has produced a mix of both exciting success stories and frustrating challenges, begging the question of how best to go after these difficult targets. Here, we review known examples and explore how the physical features of a PPI, such as its affinity, hotspots, off-rates, buried surface area and topology, may influence the chances of success in finding inhibitors. This analysis affirms that concise, tight binding PPIs are most amenable to inhibition. However, emerging technical methods are expanding the repertoire of “druggable” protein contacts and increasing the odds against difficult targets. In particular, natural product-like compound libraries, high throughput screens specifically designed for PPIs and approaches that favor discovery of allosteric inhibitors appear to be attractive routes. The first group of PPI inhibitors has entered clinical trials, further motivating the need to understand the challenges and opportunities in pursuing these types of targets.

1.2. Protein-protein interactions as novel targets in biology

As revealed by proteomic and two-hybrid strategies, protein-protein interactions (PPIs) are extensive and ubiquitous in biology [1, 2]. PPIs hold together the key multi-protein complexes of the cell, guide sub-cellular trafficking and form the backbone of its major signaling pathways [3-6]. Accordingly, many PPIs are also potential therapeutic targets in disease [7, 8] and inhibiting PPIs has become an increasingly attractive goal for both drug discovery and the generation of new research probes [9].

The last twenty years has witnessed considerable progress in the area of small molecule-based PPI inhibitors, with an explosion of literature reports and multiple PPI inhibitors entering clinical trials [10, 11]. For example, a search of PubChem for projects involving “protein-protein” interactions reveals more than 800 results. In these projects, research groups are employing a wide array of methodologies and often these methods are particularly suited for PPIs. At the same time, structural and computational biologists are becoming more adept at predicting PPIs and many groups are studying these interfaces to identify common topological features [12-15]. Clearly, this field is maturing rapidly and “tricks” are being developed to overcome the challenges associated with targeting PPIs. The prevailing attitude has changed considerably in the last two decades and PPIs are no longer considered uniformly “undruggable”. In this review, we

retrospectively analyze a subset of successful cases to explore what lessons can be learned.

1.3. Challenges of targeting protein-protein interactions

1.3.1. Surface area

Despite advances, small molecule inhibitors of PPIs remain a relatively daunting challenge, an idea clearly articulated in a number of recent reviews [16-23]. Informal polls of colleagues in the field suggest that successes are equally balanced with frustrations. There are several, well-described factors that contribute to this issue. Firstly, proteins that interact with other proteins typically do so using relatively large contact surfaces (1500 to 3000 Å²) [3]. This value is much larger than the average size of the contact area between a small molecule and protein target, which is estimated to be between 300 to 1000 Å² [24]. This larger surface creates problems because molecules that target PPIs through competitive binding must typically have a high molecular weight to overcome the distributed free energy (ΔG) of the larger contact surface [16]. Accordingly, the resulting compounds may have difficulty fitting within the reported limits on the size of orally available drugs, as summarized by the Rule of Five (RO5) [25]. RO5 violations may shelve traditional drug leads, however a strict adherence to the RO5 for PPI programs seems likely to prove detrimental. In fact, the chemical properties of successful PPI antagonists have steadily shifted away from this benchmark [10]. Still, the sheer size of many PPIs poses an unavoidable

challenge. One possible solution to this problem is that 'hotspots' within some PPI sites create a scenario in which a handful of amino acids contribute a disproportionate amount of the binding ΔG [26, 27]. Thus, targeting these specific regions typically has a more dramatic influence on the overall affinity and effectiveness of a small molecule. One of the earliest strategies to take advantage of this idea was the tethering method explored by Wells and colleagues [26]. In this approach, compound fragments are covalently directed to hotspots to maximize the chances of developing potent PPI inhibitors. More recently, fragment-based screening by mass spectrometry, crystallography and nuclear magnetic resonance (NMR) have become next-generation platforms for this type of discovery [28]. NMR, in particular, has proven a powerful method for finding building blocks that bind to topologically or energetically interesting sites on protein targets.

1.3.2. Topology

Another major issue related to PPI inhibition is that, compared to more traditional targets of antagonism, PPI partners often lack substantial grooves or deep pockets at their interacting surfaces [29]. For example, the Arora group reported an interesting study in which they analyzed PPI structures from the Protein Data Base (PDB), focusing on those PPIs involving α -helical interactions. They categorize these PPIs into examples with well-defined clefts and those with extended interfaces and use this information to suggest that PPIs with shallow

surfaces are less likely to be readily inhibited [30]. Regardless of the type of contact, screens for chemical PPI inhibitors often produce hits that are abnormally large, with complex topology, especially compared to traditional inhibitors [16, 25, 31]. These features can create synthetic challenges, in addition to possible issues with pharmacokinetics and solubility. As such, many groups have explored ways of improving chemical libraries to maximize the topological complexity of the library members and enrich for PPI inhibitors. The goal in these approaches, such as diversity-oriented synthesis and others [32, 33], is to produce compounds able to match the topology of PPIs. These challenges have also sparked revitalized interest in natural products as another rich source of potential PPI inhibitors, given the high average complexity of these molecules [34]. Similarly, peptidomimetics, cyclic peptides and stapled peptides are being increasingly used to inhibit PPIs [35, 36]. These ligands mimic natural protein-protein contacts by presenting multiple amino acid side chains from architecturally complex cores [37-41]. Finally, small molecule-protein hybrids have been developed to artificially increase apparent molecular mass and target the most difficult PPIs [42, 43].

1.3.3. Promiscuity

A related challenge to overcome in the search for PPI inhibitors is that a single contact surface on a protein can often have multiple binding partners [44] and, moreover, these partners can exchange in complex, dynamic equilibria [45].

Thus, PPI inhibitors may have to contend with multiple protein competitors in the

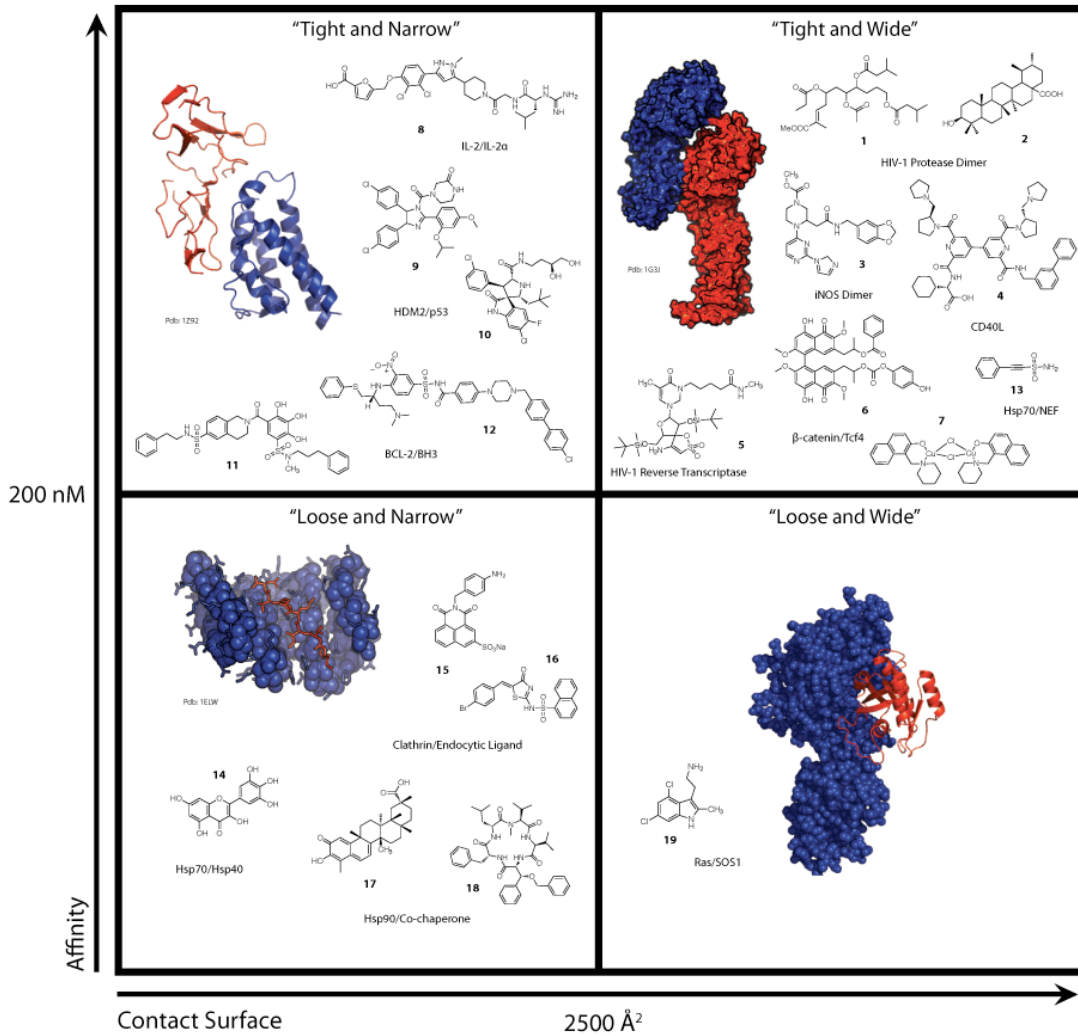


Figure 1.1 Categorization of protein-protein interactions (PPIs) and their inhibitors. PPIs are categorized by their size and affinity and representative interactions from each class are shown in blue and red. For “Tight and Wide” the interaction is between the armadillo repeat region of β -catenin and the catenin binding domain of Xenopus TCF3 (PDB: 1G3J). For “Tight and Narrow” the interaction is between IL-2 and the IL-2 α Receptor (PDB: 1Z92). For “Loose and Narrow” the interaction is between TPR1 and a C-terminal peptide of Hsc70 (PDB: 1ELW). For “Loose and Wide” the interaction is between Ras and Sos1 (PDB: 1BKD).

cell and, conversely, a single inhibitor may simultaneously disrupt multiple contacts, which could have unintended consequences on biology. Multi-protein complexes are often combinatorially assembled from a selection of possible

subunits in the cell. For example, certain chromatin-remodeling complexes and chaperone systems are built from components that bind in a mutually exclusive way [46, 47], allowing creation of complexes with distinct functions. This is the biological complexity that must be overcome when considering which PPI to target and what to expect from successful inhibition.

1.4. Classes of protein-protein interaction inhibitors

The first literary example of inhibiting a PPI came from a peptide mimic against the ribonucleotide reductase (RR) of herpes simplex virus type 1 (HSV1) in 1986. Two independent groups showed that a nonapeptide representing the C-terminus of an essential subunit in the HSV1 RR holoenzyme was sufficient to inhibit RR activity [48, 49]. Since then, the field has produced a large and ever increasing number of successful inhibitors [16, 17, 23]. With that growing list of examples, can we begin to “bin” PPIs into categories that are predictive of their relative chances of success? Similarly, can this retrospective analysis reveal common topological features that make PPIs more or less challenging?

As one way to approach these questions, we selected 19 published chemical inhibitors of PPIs (which represents a subset of the total) and ranked these in terms of buried surface area and affinity (**Figure 1.1; Table 1.1**). Using cutoffs intended to reveal whether any properties are common to clustered systems, we generated four categories of PPIs. These categories are colloquially termed

“Tight and Narrow”, “Tight and Wide”, “Loose and Narrow” and “Loose and Wide”. These terms are defined based on the size of the buried surface area and the affinity of the PPI. For surface area, narrow was defined as less than 2500 Å², while wide was greater than 2500 Å². Likewise, the affinity of the contact was separated into tight (K_d less than 200 nM) or loose (K_d greater than 200 nM).

1.4.1. Protein-protein interactions "Tight and Narrow"

To date, this category of PPI has proven most amenable to inhibition, producing the most potent inhibitors and a large number of examples (**Figure 1.2**). The reasons for this relative success could be due to the fact that the physical features shared by members of this class are most similar to traditional, enzyme targets. These PPIs are those with high affinity encompassed in a relatively small surface area. They also typically have deep pockets that are engaged by less than five major amino acids that contribute a majority of the binding ΔG . Because of these concise features, some of the strategies used in typical drug discovery campaigns, such as high throughput screening (HTS) and structure-based design, can be readily employed to target these PPIs. However, a number of PPI-specific methods have also been developed and some of those methods have subsequently been used to tackle more challenging targets.

In 1997, a group at Hoffmann-La Roche rationally designed a low micromolar inhibitor of the interaction between interleukin 2 (IL-2) and the IL-2 α receptor [50].

Based off of this molecule, researchers at Sunesis Pharmaceuticals developed the mid-nanomolar antagonist SP4206 **8** ($K_i = 60$ nM). The Sunesis group developed structure-activity relationships (SAR) by NMR, combined with tethering, to incrementally build this molecule [51]. An instructive idea that arose from that work came from the fact that the structural characterization of these compounds was originally based on their direct binding to IL-2. It was only after

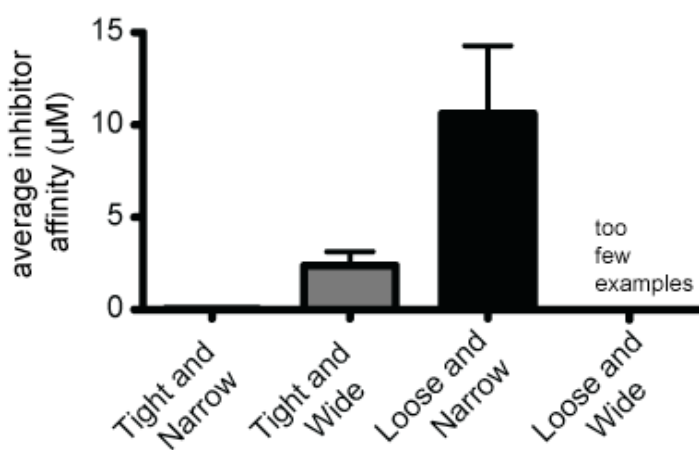


Figure 1.2 Protein-protein interaction classes versus average inhibitor affinities. The category of “loose and wide” did not have enough examples to be included.

the structure of the IL-2/IL2R α complex was solved that it became apparent that SP4206 bound to the same residues of IL-2 that are used to bind the IL-2R α .

Moreover, SP4206 induced a conformational

change at the PPI surface by interacting with residues that were shown by alanine scanning to encompass a disproportionate amount of binding ΔG (e.g. a “hotspot”) [52]. Thus, this early example of a successful PPI inhibitor uncovered a number of principles that became repetitive themes in other systems; namely, compound-induced allostery and hotspot binding.

Small-molecule inhibitors of the PPI between p53 and mouse double minute 2

(MDM2) were identified based on the results of a high throughput screen. As was observed in the case of IL2, these cis-imidazolines, termed nutlins, were shown to occupy the same binding pocket on MDM2 that is critical for binding to p53 [53]. Nutlin-3 **9** was shown to have mid-nanomolar (~70 nM) and enantioselective activity towards the p53-MDM2 complex, leading to an accumulation of p53 and subsequent tumor suppression [54]. Nutlin-3 is currently in phase I clinical trial for the treatment of retinoblastoma, illustrating the promise of PPI inhibitors as drugs and solidifying the idea that surface mimicry and hotspot binding are key tools for targeting this class of PPI. The concept of mimicking the natural interactions was also used in a parallel strategy to inhibit p53-MDM2. This strategy was inspired by the natural product spiro(oxindole-3,3'-pyrrolidine) scaffold, which mimics the indole ring of Trp23 in p53 that binds to a deep, hydrophobic cavity in MDM2 [55]. This rational-design approach, coupled with medicinal chemistry efforts yielded MI-63, which was further developed to MI-219 **10** to improve its pharmacokinetic profile. MI-219 shows low nanomolar (~5 nM) inhibition of complex formation with sub-micromolar (0.4 to 0.8 μ M) IC_{50} values for tumor growth inhibition [56]. The Wang group has pioneered additional rational design approaches in which they start with the structure of the PPI, perform alanine scans to identify possible hotspots and then design peptidomimetics and synthetic scaffolds that are intended to disrupt critical contacts [57, 58]. These examples are clear cases in which the structure of the PPI can be used to launch inhibitor programs.

Another key lesson is illustrated by the work of Abbott investigators in their search for inhibitors of B-cell lymphoma 2 (Bcl-2). Fesik and colleagues employed fragment screening by NMR, followed by extensive NMR-structure-guided medicinal chemistry to developed ABT-737 **12**, which binds the anti-apoptotic molecules Bcl-XL, Bcl-2, and Bcl-W and prevents their association with pro-apoptotic proteins BAD and BAX ($K_i > 1$ nM) [59]. This compound, and its orally bioavailable derivative ABT-263, shows anti-proliferative activity against a number of cancer cell lines, as well as anti-tumor activity in xenograft animal models [60]. ABT-263 is currently in phase I/II trial as a single agent for relapsed or refractory lymphoid malignancies, and in phase II trial for lymphatic leukemia in combination with the antibody therapeutic rituximab. This work was some of the first to document how NMR could be used as a primary discovery tool for identifying and elaborating drug leads [61]. More broadly, NMR-based design of PPI inhibitors, often combined with some form of HTS, has been particularly successful in this category of interactions, as illustrated by examples in the Runx1-CBF β [62] and MLL [63].

1.4.2. Protein-protein interactions "Tight and Wide"

Some PPIs involve extensive and often convoluted or discontinuous interaction surfaces, creating contacts with large buried contact areas and tight affinities. These features can create special difficulties in developing small-molecule

inhibitors because of the slow off rates and the large surfaces to overcome. Still, a number of successful examples have been reported and a review of these cases suggests some methodologies with potentially far-reaching utility.

Of the 15 enzymes encoded in the human immunodeficiency virus (HIV) genome, three are essential homo- or pseudo-dimers [64]. Two of these proteins, HIV-1 protease (HIVp) and reverse transcriptase (RT) have been successfully targeted with small-molecule inhibitors. The HIVp dimer has an interacting face with over 3,000 Å² of buried surface area [65] and a K_d value in the low nanomolar range [66]. Similarly, the HIV-1 RT multimer interface buries 2,730 Å² [67] with a K_d of 400 pM [68]. In the late 1990s, two groups identified HIVp dimerization inhibitors by screening natural products (**1**, **2**) [69, 70]. Likewise, exploration of non-nucleoside inhibitors of HIV-1 RT revealed **5**, which was subsequently shown to have anti-dimerization activity [71, 72]. These findings support the idea that topologically complex natural products are suitable scaffolds for inhibiting even complex and large PPIs. To further exemplify this idea, the interaction surface between β-catenin and Tcf/LEF family members is also particularly large (> 3000 Å²), making it another difficult target [73]. Yet, **6** was identified in a natural product screen that relied on measuring binding of Tcf4 to β-catenin [74]. However, natural products are not exclusive in their ability to inhibit these types of interactions. Recently, an *in silico* screen revealed **7**, a simpler structure that is predicted to bind to a hotspot region and inhibit the β-catenin-Tcf4 interaction

[75]. Additional structural information will be needed to fully understand the binding mode and mechanistic basis for these activities, but the findings suggest that topologically complex chemical libraries may be good starting points for identifying PPI inhibitors.

The inducible isoform of nitric oxide synthase (iNOS) has been implicated in inflammatory and autoimmune diseases [76], while the endothelial isoform plays a vital role in vascular homeostasis [77]. In an effort to identify selective inhibitors of iNOS, McMillan et al. (2000) conducted an *in vitro* screen against iNOS enzyme activity using a compound library based off of a pyrimidine-imidazole core [78]. This screen resulted in no active compounds, but a cell-based screen against nitric oxide production yielded the potent inhibitor **3**. The compound was shown to have a high affinity for the iNOS monomer and, upon binding, it allosterically inhibited subsequent dimerization, explaining why the original *in vitro* screen against the pre-formed iNOS dimer produced no inhibitors. This example nicely illustrates a growing realization that allostery and allosteric mechanisms are powerful tools in targeting larger PPIs [12, 79]. Moreover, this study illustrates how dynamics can have a large impact on success in HTS-based PPI campaigns. Only when iNOS was allowed to sample both monomeric and dimeric structures were allosteric inhibitors uncovered.

Other interesting examples of this class are found in inhibitors of the c-Myc/Max

dimer, the CD40 ligand (CD40L) trimer, and the eukaryotic translation initiation factors (eIF) eIF4E and eIF4G. A hurdle to small-molecule inhibition of c-Myc/Max dimerization is the vast increase in dimer stabilization in the presence of DNA [80]. To circumvent this issue, the Berg group developed a clever HTS approach in which c-Myc/Max binding to a fluorophore-labeled oligonucleotide was measured, revealing Mycos 1 and 2 as micromolar inhibitors [81]. This study nicely leveraged known biophysical features of the PPI to design a screen especially targeting a key aspect of the complex. Similarly, identifying inhibitors of CD40L trimerization are also difficult, given the tight affinity of this complex. Yet, a direct binding assay was used to produce BIO8898 **4**, a small molecule that populates a deep, allosteric pocket between two subunits of the trimer [82]. Binding by BIO8898 distorts the interface enough to prevent binding of CD40L to the CD40 receptor. This is a more subtle form of inhibition than seen in previous studies of the homologous TNF α , where an inhibitor was found that completely ejected one subunit from the trimer [83]. These examples suggest that even challenging PPIs can sometimes be amenable to HTS approaches, using methodologies, such as AlphaLisa, fluorescence and luminescence complementation, ELISA, SPR and FRET [84-87], and the resulting compounds, if the screen is designed carefully, can access unexpected and interesting molecular mechanisms. This concept is further re-enforced by work from the Wagner group, in which they developed a high-throughput fluorescence polarization screen against the initiation factor eIF4E using a peptide from the

binding motif of eIF4G [88]. This screen revealed the inhibitor 4EGI-1 that disrupts full-length eIF4G binding, and interestingly, clears the path for natural modulators of translation (4E-BP) to interact and thereby inhibit translation. Together, these examples demonstrate the diversity of solutions to the problem of blocking large, tight interactions.

As illustrated by the examples above, this class of PPIs has been successfully targeted and the resulting compounds access interesting mechanisms. Another example was provided by the Neubig group, in which they used a flow cytometry protein interaction assay (FCPIA) to target regulators of G-protein signaling (RGS). They identified CCG-4986, which inhibits the RGS₄-G_α PPI by covalent modification of a cysteine residue adjacent to the interaction surface [89]. This example highlights a growing resurgence of covalent modifiers as probes and drugs [90]. Covalent modifiers might be particularly attractive for PPIs because irreversible binding can be used to overcome problems of weak interactions and shallow binding sites.

Amyloids are ordered protein aggregates defined by a characteristic appearance by electron microscopy, affinity for the dye, congo red, and large contact interfaces between monomers [91]. The interface challenge is exacerbated by the repetitive structure of amyloids, involving thousands of monomer interactions and thousands of cumulative Å² of buried surface area. Amyloids underlie a

number of neurodegenerative disorders and other diseases of protein misfolding [92], so inhibitors of amyloid PPIs are of medical interest. Numerous small molecules with tight affinity for amyloids have been described, some based on synthetic scaffolds and others based on peptidomimetics [91, 93, 94]. Some of these molecules have even advanced to clinical trials in Alzheimer's disease. Interestingly, these compounds typically have good K_d values, yet their ability to block PPIs between amyloid-forming monomers (IC_{50}) is typically 10- to 1000-fold worse. The disconnect between these values is thought to arise from compound binding being insufficient to fully block the large amyloid surfaces, which often lack clear "hotspots". In 2004, it was discovered that hybrids between congo red and the FK506-binding protein (FKBP) created bifunctional inhibitors that better matched the size and complexity of the amyloid surface, producing inhibitors with nanomolar IC_{50} values [42]. Interestingly, increasing the size of the FKBP portion enhanced the apparent IC_{50} of the hybrids, suggesting that larger surfaces were more effective inhibitors [95]. Another clever solution to this problem can be found in anti-amyloid strategies using compounds that dissolve pre-formed aggregates by allostery [96]. Thus, even for some of the most extreme PPIs, allostery and other mechanisms can be used to inhibit their formation.

1.4.3. Protein-protein interactions "Loose and Narrow"

PPIs within this category are characterized by weak ($K_d > 200$ nM) binding but relatively small contact areas. Because these interactions are typically transient,

it is not unusual for the surfaces to be shared by multiple partners. These hurdles, often coupled to a lack of structural data and relatively shallow binding pockets, make these interactions especially challenging targets (**Figure 1.2**).

Table 1.1 Features of select PPIs and their inhibitors.

Interaction	Buried surface area (Å ²)	Complex affinity (μM)	Inhibitor affinity (μM) ^a	References
Tight and Wide				
HIV-1 Protease	3224	0.004	2-3	(65, 66, 69, 70)
HIV-1 Reverse Transcriptase	2730	0.0004	0.56	(67, 68, 72)
iNOS	4650	0.01	0.0022	(78, 148, 149)
β-catenin/Tcf4	4820	0.008	3-5	(73-75, 150)
Hsp70/NEF	2800	0.03	ND	(119)
CD40L	5850	0.008	25	(82)
Tight and Narrow				
IL-2/IL-2Rα	1900	0.01	0.06	(51, 151-153)
HDM2/p53 (peptide)	1498	0.1	0.005-0.067	(54, 56, 154-156)
Bcl-2/BH3 (peptide)	<2500 ^b	0.2	0.0006-0.11	(59, 157, 158)
HPV E1/E2	~2000 ^c	0.06	0.1	(159, 160)
Loose and Narrow				
Hsp70/Hsp40	1028	0.6	ND	(118, 123)
Hsp90/TPR	1000	0.3	0.4	(120, 121, 141)
Hsp90/cdc37	1600	2.5	ND	(136, 163)
Clathrin/Endolytic Ligand	<2500 ^b	1-100	12-18	(98, 161, 162)
ZipA/FtsZ (peptide)	1197	21.6	12	(164, 165)
Loose and Wide				
Ras/SOS1	3600	3.6	155	(102, 103, 105)

^aWhen direct binding data was not available, Ki or IC₅₀ values were used instead. ^bThe absolute value for surface area has not been described for these interactions. The values in the table are predictions based off of known structural information. ^cPredicted value (152).

However, in one example of a successful approach, the N-terminal β-propeller domain (TD) of the clathrin heavy chain was targeted. Clathrin heavy chain

serves as a central interacting hub for accessory proteins in the endocytic pathway [97]. Two molecules termed pitstops, one from a naphthalimide core **15** and the other from rhodanine **16** were identified in an ELISA-based high-throughput screen [98]. These compounds were shown to compete with accessory proteins for binding to a common site on the clathrin TD, limiting endocytosis and thereby inhibiting viral entry. Despite this success, general strategies for targeting this class are not yet clear.

In another interesting example that illustrates the challenges in this type of PPI, the Mapp group identified compounds that inhibit transcriptional activation within the activator complex [99]. These authors recognized that a conserved structural element of natural activation domains is that they are amphipathic. They displayed polar functionality from an isoxazolidine core and, indeed, found that the only apparent requirement for creating artificial activators was that the molecule needed to be amphipathic [100, 101]. This relatively loose structural constraint suggests that the strategies for optimizing inhibitors of this type of PPI will be substantially different than for other types of targets.

1.4.4. Protein-protein interactions “Loose and Wide”

At the extreme end of PPIs are the contacts defined by large surface areas and weak affinities. To our knowledge, few potent inhibitors of contacts within this

category have been described and these targets remain a particularly challenging area. Yet, very recent evidence suggests that inhibition at this level is possible. The interaction between the small GTP-binding protein Ras and its guanidine nucleotide exchange factor (GEF) SOS1 spans approximately 3600 Å² [102] and Ras binds to the catalytic site of SOS1 with an affinity in the low micromolar range [103], placing this PPI square within the “loose and wide” category. Recent work has produced a stapled peptide [104] and a small molecule (**19**) [105] capable of inhibiting this interaction both *in vitro* and in cells. Other biological examples of these PPIs are plentiful in the literature, especially in the area of GPCR clustering, cell-cell interactions and carbohydrate-protein interactions [106], creating a need for PPI inhibitors.

1.5. Advancing protein-protein interaction inhibitors in difficult systems

As evident from visually placing PPIs into quadrants (**Figure 1.1**), some systems, especially weaker interactions and those that make contacts over a wide area, remain notoriously resistant to inhibition. This challenge is further evident by the large differences in the average potency values for inhibitors targeting the different classes. On average, compounds that inhibit “Tight and Narrow” PPIs have 10-fold better potency than those targeting “Loose and Narrow” contacts (**Figure 2**). Many of these resistant systems have commonalities among them, such as limited structural information, transient and weak contacts and promiscuous binding interfaces. To further illustrate these ideas and highlight

methodologies developed to specifically address these challenges, we focus on the heat shock protein 70 (Hsp70) and heat shock protein 90 (Hsp90) systems for further discussion. Hsp70 and Hsp90 are molecular chaperones that each form multi-protein complexes with important roles in protein folding and stabilization. Moreover, there is compelling evidence, in both cases, to suggest that targeting PPIs in the Hsp70 and Hsp90 complexes may be an effective therapeutic strategy in cancer and neurodegeneration [107-111]. These systems also provide a convenient model for these discussions because the PPIs inherent in Hsp70 and Hsp90 complexes provide examples of nearly every type of PPI category.

1.5.1. Heat shock protein 70

Hsp70 plays important roles in normal protein homeostasis and it is implicated in several disease states, such as cancer, neurodegeneration, and amyloidosis [107, 108, 112, 113]. The protein consists of two domains, a nucleotide binding domain (NBD) that hydrolyzes ATP and a substrate-binding domain (SBD) that binds to exposed hydrophobic regions of polypeptides. NMR-based fragment screens conducted by the biotechnology company, Vernalis, have shown that the ATP-binding site of Hsp70 is not particularly amenable to discovery of selective or potent inhibitors [114]. Thus, the PPIs between Hsp70 and its numerous co-chaperones have become attractive alternatives [107, 108, 115]. There are three main classes of proteins that bind to Hsp70s. The Hsp40 (or DnaJ) superfamily is

characterized by a conserved J-domain that binds to Hsp70 and stimulates its ATPase activity [116]. This stimulation of ATP turnover promotes tight binding of substrates in the SBD via a conformational change. Nucleotide exchange factors (NEFs) bind Hsp70 and facilitate ADP release, helping to release substrates. And, finally, a family of tetratricopeptide repeat (TPR) domain-containing co-chaperones binds to the SBD, helping to arbitrate the fate of Hsp70-bound substrates [113]. Thus, either promoting or inhibiting PPIs between Hsp70 and its co-chaperones can modulate the biology of the system [107, 108].

The J domain of the prokaryotic Hsp40, DnaJ, binds to the Hsp70, DnaK, across a largely polar interface located between the NBD and SBD [117]. The K_d of this interaction is weak ($> 1 \mu\text{M}$) and a structure of the auxilin J-domain fused to mammalian Hsp70 suggests a relatively modest interaction surface (1028 \AA^2) [118]. Structures of Hsp70 bound by NEFs suggest a larger (2800 \AA^2) interaction, with much higher affinity (30 nM) [119]. Finally, the TPR domain interaction with Hsp70 is approximately $1 \mu\text{M}$ [120] and occurs over an area of 1330 \AA^2 , based on a crystal structure of a representative TPR domain with the C-terminus of Hsp70 [121]. Based on genetic studies, each of these interfaces is attractive as a therapeutic target.

Our group has become particularly interested in targeting the Hsp70-Hsp40 interaction because of the importance of the contact in chaperone biology [116].

Recent work by the Zuiderweg group has shown that the prokaryotic Hsp70-Hsp40 contact is largely polar, with a complex and shallow topology [117]. Thus, we originally considered it unlikely that a screen for direct (e.g. competitive) inhibitors of the direct PPI would be fruitful, given the weak binding of the two partners. Accordingly, we pursued a different strategy, termed “gray box screening”. In this method, the ATPase activity of Hsp70 is stimulated by reconstituting its complex with an Hsp40 *in vitro*. Any compounds that disrupt Hsp40-stimulated ATP turnover would be identified as a “hit” in the screen. This approach is termed gray box screening because it has some features in common with “black box” screens, in which whole cells or animals are used as the target. In cell-based screens, the physiological relevance of the platform is high, but target identification is a challenging task. In the gray box approach, some of the natural complexity of the system is mimicked by reconstitution of the multi-protein system. This approach has been used to identify a number of inhibitors of the Hsp70-Hsp40 complex, some of which bind directly at the PPI interface [122] and others that bind distal, allosteric sites [123]. For example, the flavonoid myricetin **14** was found to bind an unanticipated site in the NBD, about 30 Å from the Hsp70-Hsp40 interface, trapping a conformation that is not able to interact with Hsp40 [123]. Interestingly, the binding site for myricetin is not apparent in the crystal structures of the Hsp70 NBD, suggesting that dynamic movements in this region are required to open the compound-binding site [124]. Because this screening approach is amenable to HTS in low volume, large numbers of

compounds can be screened [125, 126]. This strategy might be applicable in other systems involving weak interactions, especially those in which non-enzyme partners allosterically modify the activity of a core enzyme component.

The Hsp70-TPR protein interaction, while also weak, sits at a critical point in Hsp70 biology. TPR proteins are thought to facilitate triage decisions for client proteins of Hsp70 [115, 127, 128], assisting in either folding or degradation of these clients. Therefore, this PPI is of unique interest to chemical biologists who seek to attain fine control of the Hsp70 machinery. However, to date, no inhibitors of the Hsp70-TPR domain interaction have been described in the literature, highlighting the challenge that this interface may pose. This idea will be further explored in the subsequent chapters.

The tighter Hsp70-NEF interaction has been targeted using a “black box” high throughput screen. From a cell-based assay against p53-mediated apoptosis, PES **13** was identified as a small-molecule that decreases tumor cell viability [129]. In follow-up studies, PES appears to block the binding of Hsp70 to the M isoform of bcl-2 associated anthanogene 1 (BAG-1), a NEF for Hsp70. These findings (along with the nutlin work described above) suggest that phenotypic screens can sometimes reveal PPI inhibitors, even if the target PPI is relatively large. One power of these methods is that the target PPI is allowed to undergo its natural dynamics, often providing unanticipated mechanisms of inhibition. The

challenge is that the mechanism of inhibition is not clear until follow-up studies are performed.

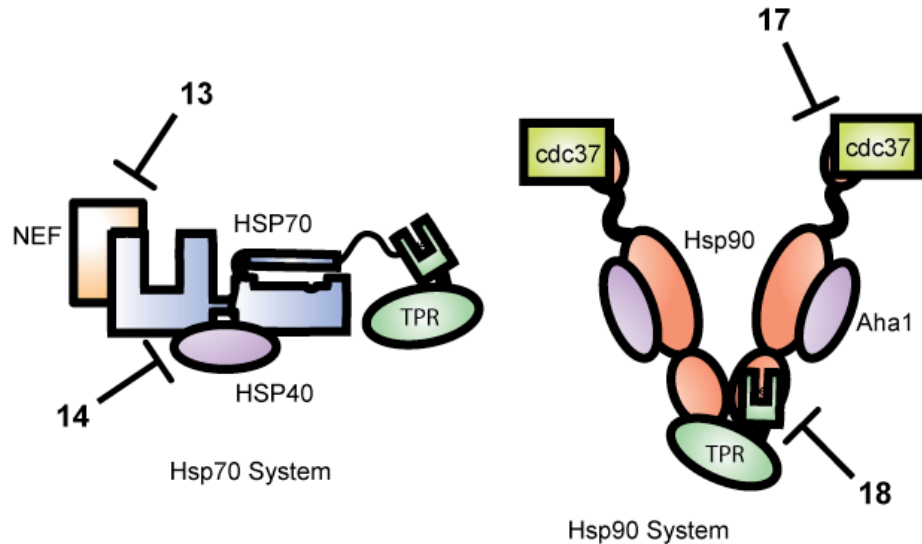


Figure 1.3 Inhibition of protein-protein interactions in the chaperone complexes. Complexes between Hsp70 and Hsp90 and their co-chaperones are shown. PES **13** inhibits the Hsp70/Bag1 interaction, myricetin **14** inhibits the Hsp70/Hsp40 interaction, celestrol **17** inhibits Hsp90/cdc37, and San A **18** inhibits the Hsp90/TPR interactions. Abbreviations: NEF, nucleotide exchange factor; TPR, tetratricopeptide repeat domain-containing co-chaperone; San A, sansalvamide A.

1.5.2. Heat shock protein 90

The Hsp70 and Hsp90 systems are linked through a shared TPR-domain co-chaperone, HOP (Hsp70-Hsp90 organizing protein) [130]. And like Hsp70, Hsp90 is an abundant molecular chaperone that relies on a network of these co-chaperones for its activity [131]. Under both stress and normal conditions, Hsp90 regulates the stability and maturation of over 200 client proteins, many of which either harbor mutations or are over-expressed in cancers [132]. In fact, inhibitors

of the ATPase activity of Hsp90, which bind to the N-terminal ATP-binding pocket, have been extensively explored and some of these have advanced to clinical trials as anti-cancer agents [133]. These inhibitors bind classically defined pockets and do not appear to directly impact co-chaperone binding. However, one drawback of these molecules is that they elicit a heat shock response, through activation of heat shock factor 1 (HSF1) [134]. This cytoprotective response has the potential to undermine the anti-proliferative effects of Hsp90 inhibition. These issues have driven interest in targeting the C-terminal ATP-binding site [135] and, importantly for this review, PPIs between Hsp90 and its co-chaperones.

Hsp90 interacts with the important co-chaperones Aha1, cdc37, p23 and a number of TPR-domain proteins [130]. These interactions tune the ATPase activity of Hsp90 and these PPIs are being recognized as potential drug targets [111]. The TPR-Hsp90 interaction surface resembles that in the TPR-Hsp70 system, being relatively weak but narrow. Cdc37 interacts with relatively poor affinity (2.5 μM) [136] to Hsp90, burying 1600 \AA^2 of solvent exposed surface area, while Aha1 binds across a very large, polar surface of Hsp90 [137] with moderate affinity (0.6 μM) [138]. Thus, like the Hsp70 system, this multi-protein complex has a wide range of affinities and surface areas.

An investigation into how the natural product, celastrol **17** inhibited Hsp90 and

elicited a heat-shock response initially revealed that the compound reduced the interaction between Hsp90 and the cancer associated co-chaperone cdc37 [139]. Upon further analysis, it was revealed that celastrol covalently binds to the Hsp90 co-chaperone, cdc37 [140]. Recently, a molecule **18** based off of another natural product, Sansalvamide A, was reported to bind to Hsp90 and inhibit the interaction of TPR domain-containing co-chaperones [141]. Other inhibitors of the Hsp90-TPR interaction have also been identified by HTS approaches [141, 142]. Thus, like in the Hsp70 system, “biology-driven” HTS was employed as a successful strategy to identify PPIs inhibitors in the Hsp90 system and natural products were common hits.

1.6. Analysis and prospectus

Protein-protein interactions are the “glue” that drives biology, especially in the context of multi-protein complexes, signaling pathways and subcellular trafficking. To take advantage of these opportunities, a growing urgency has emerged around inhibiting PPIs. In addition, a number of successes in the field of chemical inhibitors of PPIs, including initiation of multiple clinical trials, have provided a strong motivator for continued experimental focus.

What can be learned from analyzing prior success and failures in targeting PPIs with small molecules? One over-whelming observation is that PPI inhibitors are not as hard to find as one might expect. Many straightforward HTS methods have

successfully produced micromolar and nanomolar inhibitors, especially of concise PPIs. Many of the most successful PPI inhibitors have taken advantage of hotspots that effectively reduce large, flat surfaces to more manageable targets. Another common solution is found in compounds that bind allosteric sites to modify PPIs, as was the case with the IL2 inhibitors and myricetin in the Hsp70 system. These compounds utilized well-defined pockets to enact global changes at either adjacent (in the case of IL2) or distal (in the case of Hsp70) PPI contacts. Allostery can work over substantial distances [143] and through multiple components of a multi-protein complex, further suggesting that even topologically complex surfaces can be impacted. Also, allosteric sites can be versatile tools, sometimes allowing switching between agonism and antagonism [122, 144]. Finally, it seems possible that many of the allosteric sites found in PPI projects might represent the binding sites for natural ligands, such as secondary metabolites. Despite this progress, clear challenges remain. Can the pharmacokinetic and synthetic challenges of larger molecules be solved? How does one purposefully search for allosteric regulators?

What methods are best for identifying PPI inhibitors? The answer to this question appears to be dependent on the type of PPI, the specific biological goals and other factors. Rational design approaches have succeeded in cases of both large surface areas (as is the case with stapled peptides) and concise PPIs (as was seen with inhibitors of p53-MDM2). NMR is likely to continue to be a powerful

method for discovery of PPI inhibitors because it combines structural insights with fragment-based approaches (as was seen in the case of Bcl-2). Finally, unbiased HTS methods, especially gray box screening and cell-based methods, have proven surprisingly fruitful in the search for PPI inhibitors of many types. These methods seem particularly attractive in systems involving large contact surfaces, owing to their propensity to find unanticipated allosteric sites. Thus, the workhorse for drug discovery in this difficult chemical space is likely to continue to be HTS-based methodology, especially for binding partners where there exists a limited amount of structural information.

What do these studies mean for understanding the biology and “druggability” of multi-protein complexes? Many, if not all, biological processes are dependent on the function of multi-protein complexes [145-147]. These processes emerge from the coordinated activity of multiple enzyme and non-enzyme components. In a post-genomic world, medicinal chemists are viewing drug targets within the context of the multi-protein pathways and networks in which they act. This more sophisticated view includes a greater number of possible PPI targets, further lowering the barrier to projects aimed at blocking important PPIs.

1.7 References

1. Stelzl, U., et al., *A Human Protein-Protein Interaction Network: A Resource for Annotating the Proteome*. Cell, 2005. **122**(6): p. 957-968.
2. Rual, J.-F., et al., *Towards a proteome-scale map of the human protein-protein interaction network*. Nature, 2005. **437**(7062): p. 1173-1178.
3. Jones, S. and J.M. Thornton, *Principles of protein-protein interactions*. Proceedings of the National Academy of Sciences of the United States of America, 1996. **93**(1): p. 13-20.
4. Gavin, A.C., et al., *Functional organization of the yeast proteome by systematic analysis of protein complexes*. Nature, 2002. **415**(6868): p. 141-147.
5. Ryan, D.P. and J.M. Matthews, *Protein-protein interactions in human disease*. Current Opinion in Structural Biology, 2005. **15**(4): p. 441-446.
6. Kuriyan, J. and D. Eisenberg, *The origin of protein interactions and allostery in colocalization*. Nature, 2007. **450**(7172): p. 983-990.
7. Balch, W.E. and J.R. Yates, *Application of Mass Spectrometry to Study Proteomics and Interactomics in Cystic Fibrosis*. Cystic Fibrosis: Diagnosis and Protocols, Vol II: Methods and Resources to Understand Cystic Fibrosis, 2011. **742**: p. 227-247.
8. Vidal, M., M. Cusick, and A.-L. Barabasi, *Interactome Networks and Human Disease*. Cell, 2011. **144**(6): p. 986-998.
9. Arkin, M., *Protein-protein interactions and cancer: small molecules going in for the kill*. Current Opinion in Chemical Biology, 2005. **9**(3): p. 317-324.
10. Morelli, X., R. Bourgeas, and P. Roche, *Chemical and structural lessons from recent successes in protein-protein interaction inhibition (2P2I)*. Current Opinion in Chemical Biology, 2011. **15**(4): p. 475-481.
11. Thangudu, R.R., et al., *Modulating Protein-Protein Interactions with Small Molecules: The Importance of Binding Hotspots*. Journal of Molecular Biology, 2012. **415**(2): p. 443-453.
12. Reynolds, K., R. McLaughlin, and R. Ranganathan, *Hot Spots for Allosteric Regulation on Protein Surfaces*. Cell, 2011. **147**(7): p. 1564-1575.
13. Yang, C.-Y. and S. Wang, *Computational Analysis of Protein Hotspots*. ACS Medicinal Chemistry Letters, 2010. **1**(3): p. 125-129.
14. Geppert, T., et al., *Context-Based Identification of Protein-Protein Interfaces and 'Hot-Spot' Residues*. Chemistry & Biology, 2011. **18**(3): p. 344-353.
15. Reichmann, D., et al., *The modular architecture of protein-protein binding interfaces*. Proceedings of the National Academy of Sciences of the United States of America, 2005. **102**(1): p. 57-62.
16. Wells, J.A. and C.L. McClendon, *Reaching for high-hanging fruit in drug discovery at protein-protein interfaces*. Nature, 2007. **450**(7172): p. 1001-1009.

17. Keskin, O., et al., *Principles of protein-protein interactions: What are the preferred ways for proteins to interact?* Chemical Reviews, 2008. **108**(4): p. 1225-1244.
18. Berg, T., *Modulation of Protein–Protein Interactions with Small Organic Molecules*. Angewandte Chemie International Edition, 2003. **42**(22): p. 2462-2481.
19. Veselovsky, A.V., et al., *Protein–protein interactions: mechanisms and modification by drugs*. Journal of Molecular Recognition, 2002. **15**(6): p. 405-422.
20. Gordo, S. and E. Giralt, *Knitting and untying the protein network: Modulation of protein ensembles as a therapeutic strategy*. Protein Science, 2009. **18**(3): p. 481-493.
21. Meireles, L.M.C. and G. Mustata, *Discovery of Modulators of Protein-Protein Interactions: Current Approaches and Limitations*. Current Topics in Medicinal Chemistry, 2011. **11**(3): p. 248-257.
22. Toogood, P.L., *Inhibition of protein-protein association by small molecules: Approaches and progress*. Journal of Medicinal Chemistry, 2002. **45**(8): p. 1543-1558.
23. Arkin, M.R. and A. Whitty, *The road less traveled: modulating signal transduction enzymes by inhibiting their protein-protein interactions*. Current Opinion in Chemical Biology, 2009. **13**(3): p. 284-290.
24. Cheng, A.C., et al., *Structure-based maximal affinity model predicts small-molecule druggability*. Nature Biotechnology, 2007. **25**(1): p. 71-75.
25. Lipinski, C.A., et al., *Experimental and computational approaches to estimate solubility and permeability in drug discovery and development settings*. Advanced Drug Delivery Reviews, 2001. **46**(1-3): p. 3-26.
26. Clackson, T. and J. Wells, *A hot spot of binding energy in a hormone-receptor interface*. Science, 1995. **267**(5196): p. 383-386.
27. Erlanson, D.A., J.A. Wells, and A.C. Braisted, *TETHERING: Fragment-Based Drug Discovery*. Annual Review of Biophysics and Biomolecular Structure, 2004. **33**(1): p. 199-223.
28. Valkov, E., et al., *Targeting Protein–Protein Interactions and Fragment-Based Drug Discovery* *Fragment-Based Drug Discovery and X-Ray Crystallography*. 2012, Springer Berlin / Heidelberg. p. 145-179.
29. Hopkins, A.L. and C.R. Groom, *The druggable genome*. Nature Reviews Drug Discovery, 2002. **1**(9): p. 727-730.
30. Jochim, A.L. and P.S. Arora, *Systematic Analysis of Helical Protein Interfaces Reveals Targets for Synthetic Inhibitors*. Acs Chemical Biology, 2010. **5**(10): p. 919-923.
31. Walters, W.P., A. Murcko, and M.A. Murcko, *Recognizing molecules with drug-like properties*. Current Opinion in Chemical Biology, 1999. **3**(4): p. 384-387.
32. Schreiber, S.L., *Target-Oriented and Diversity-Oriented Organic Synthesis in Drug Discovery*. Science, 2000. **287**(5460): p. 1964-1969.

33. Xu, Y., et al., *A credit-card library approach for disrupting protein-protein interactions*. *Bioorganic & Medicinal Chemistry*, 2006. **14**(8): p. 2660-2673.
34. Reayi, A. and P. Arya, *Natural product-like chemical space: search for chemical dissectors of macromolecular interactions*. *Current Opinion in Chemical Biology*, 2005. **9**(3): p. 240-247.
35. Woodman, R., et al., *Design and Validation of a Neutral Protein Scaffold for the Presentation of Peptide Aptamers*. *Journal of Molecular Biology*, 2005. **352**(5): p. 1118-1133.
36. Kritzer, J.A., et al., *Miniature Protein Inhibitors of the p53-hDM2 Interaction*. *ChemBioChem*, 2006. **7**(1): p. 29-31.
37. Verdine, G.L., et al., *Chapter one - Stapled Peptides for Intracellular Drug Targets*, in *Methods in Enzymology*. 2012, Academic Press. p. 3-33.
38. Walensky, L.D., et al., *Activation of Apoptosis in Vivo by a Hydrocarbon-Stapled BH3 Helix*. *Science*, 2004. **305**(5689): p. 1466-1470.
39. Zhang, H., et al., *A Cell-penetrating Helical Peptide as a Potential HIV-1 Inhibitor*. *Journal of Molecular Biology*, 2008. **378**(3): p. 565-580.
40. Horwill, A.R., S.N. Savinov, and S.J. Benkovic, *A systematic method for identifying small-molecule modulators of protein-protein interactions*. *Proceedings of the National Academy of Sciences of the United States of America*, 2004. **101**(44): p. 15591-15596.
41. Ruvo, M., et al., *Branched Peptides for the Modulation of Protein-Protein Interactions: More Arms are Better than One?* *Current Medicinal Chemistry*, 2011. **18**(16): p. 2429-2437.
42. Gestwicki, J.E., G.R. Crabtree, and I.A. Graef, *Harnessing Chaperones to Generate Small-Molecule Inhibitors of Amyloid β Aggregation*. *Science*, 2004. **306**(5697): p. 865-869.
43. Gestwicki, J.E. and P.S. Marinec, *Chemical control over protein-protein interactions: Beyond inhibitors*. *Combinatorial Chemistry & High Throughput Screening*, 2007. **10**(8): p. 667-675.
44. DeLano, W.L., et al., *Convergent solutions to binding at a protein-protein interface*. *Science*, 2000. **287**(5456): p. 1279-1283.
45. Sprinzak, E., Y. Altuvia, and H. Margalit, *Characterization and prediction of protein-protein interactions within and between complexes*. *Proceedings of the National Academy of Sciences of the United States of America*, 2006. **103**(40): p. 14718-14723.
46. Lessard, J.A. and G.R. Crabtree, *Chromatin Regulatory Mechanisms in Pluripotency*, in *Annual Review of Cell and Developmental Biology, Vol 26*, R.G.L.L.R. Schekman, Editor. 2010. p. 503-532.
47. Hohfeld, J., D.M. Cyr, and C. Patterson, *From the cradle to the grave: molecular chaperones that may choose between folding and degradation*. *Embo Reports*, 2001. **2**(10): p. 885-890.
48. Cohen, E.A., et al., *SPECIFIC-INHIBITION OF HERPESVIRUS RIBONUCLEOTIDE REDUCTASE BY A NONAPEPTIDE DERIVED*

- FROM THE CARBOXY TERMINUS OF SUBUNIT-2*. Nature, 1986. **321**(6068): p. 441-443.
49. Dutia, B.M., et al., *SPECIFIC-INHIBITION OF HERPESVIRUS RIBONUCLEOTIDE REDUCTASE BY SYNTHETIC PEPTIDES*. Nature, 1986. **321**(6068): p. 439-441.
 50. Tilley, J.W., et al., *Identification of a Small Molecule Inhibitor of the IL-2/IL-2RCE± Receptor Interaction Which Binds to IL-2*. Journal of the American Chemical Society, 1997. **119**(32): p. 7589-7590.
 51. Raimundo, B.C., et al., *Integrating Fragment Assembly and Biophysical Methods in the Chemical Advancement of Small-Molecule Antagonists of IL-2; An Approach for Inhibiting Protein-Protein Interactions*. Journal of Medicinal Chemistry, 2004. **47**(12): p. 3111-3130.
 52. Thanos, C.D., W.L. DeLano, and J.A. Wells, *Hot-spot mimicry of a cytokine receptor by a small molecule*. Proceedings of the National Academy of Sciences, 2006. **103**(42): p. 15422-15427.
 53. Fry, D.C., et al., *NMR structure of a complex between MDM2 and a small molecule inhibitor*. Journal of Biomolecular NMR, 2004. **30**(2): p. 163-173.
 54. Vassilev, L.T., et al., *In vivo activation of the p53 pathway by small-molecule antagonists of MDM2*. Science, 2004. **303**(5659): p. 844-848.
 55. Ding, K., et al., *Structure-Based Design of Potent Non-Peptide MDM2 Inhibitors*. Journal of the American Chemical Society, 2005. **127**(29): p. 10130-10131.
 56. Shangary, S., et al., *Temporal activation of p53 by a specific MDM2 inhibitor is selectively toxic to tumors and leads to complete tumor growth inhibition*. Proceedings of the National Academy of Sciences, 2008. **105**(10): p. 3933-3938.
 57. Wang, G.P., et al., *Structure-based design of potent small-molecule inhibitors of anti-apoptotic Bcl-2 proteins*. Journal of Medicinal Chemistry, 2006. **49**(21): p. 6139-6142.
 58. Ding, K., et al., *Structure-based design of spiro-oxindoles as potent, specific small-molecule inhibitors of the MDM2-p53 interaction*. Journal of Medicinal Chemistry, 2006. **49**(12): p. 3432-3435.
 59. Bruncko, M., et al., *Studies leading to potent, dual inhibitors of bcl-2 and Bcl-xL*. Journal of Medicinal Chemistry, 2007. **50**(4): p. 641-662.
 60. Oltersdorf, T., et al., *An inhibitor of Bcl-2 family proteins induces regression of solid tumours*. Nature, 2005. **435**(7042): p. 677-681.
 61. Murray, C.W. and D.C. Rees, *The rise of fragment-based drug discovery*. Nat Chem, 2009. **1**(3): p. 187-192.
 62. Gorczynski, M.J., et al., *Allosteric inhibition of the protein-protein interaction between the leukemia-associated proteins Runx1 and CBF beta*. Chemistry & Biology, 2007. **14**(10): p. 1186-1197.
 63. Grembecka, J., et al., *Menin-MLL inhibitors reverse oncogenic activity of MLL fusion proteins in leukemia*. Nature Chemical Biology, 2012. **8**(3): p. 277-284.

64. Frankel, A.D. and J.A.T. Young, *HIV-1: Fifteen Proteins and an RNA*. Annual Review of Biochemistry, 1998. **67**(1): p. 1-25.
65. Weber, I.T., *COMPARISON OF THE CRYSTAL-STRUCTURES AND INTERSUBUNIT INTERACTIONS OF HUMAN IMMUNODEFICIENCY AND ROUS-SARCOMA VIRUS PROTEASES*. Journal of Biological Chemistry, 1990. **265**(18): p. 10492-10496.
66. Zhang, Z.Y., et al., *DISSOCIATIVE INHIBITION OF DIMERIC ENZYMES - KINETIC CHARACTERIZATION OF THE INHIBITION OF HIV-1 PROTEASE BY ITS COOH-TERMINAL TETRAPEPTIDE*. Journal of Biological Chemistry, 1991. **266**(24): p. 15591-15594.
67. Ding, J., et al., *Buried surface analysis of HIV-1 reverse transcriptase p66/p51 heterodimer and its interaction with dsDNA template/primer*. Journal of Molecular Recognition, 1994. **7**(2): p. 157-161.
68. Divita, G., T. Restle, and R.S. Goody, *CHARACTERIZATION OF THE DIMERIZATION PROCESS OF HIV-1 REVERSE-TRANSCRIPTASE HETERODIMER USING INTRINSIC PROTEIN FLUORESCENCE*. Febs Letters, 1993. **324**(2): p. 153-158.
69. Fan, X., G.R. Flentke, and D.H. Rich, *Inhibition of HIV-1 Protease by a Subunit of Didemnaketal A*. Journal of the American Chemical Society, 1998. **120**(34): p. 8893-8894.
70. Quere, L., T. Wenger, and H.J. Schramm, *Triterpenes as Potential Dimerization Inhibitors of HIV-1 Protease*. Biochemical and Biophysical Research Communications, 1996. **227**(2): p. 484-488.
71. Balzarini, J., et al., *2',5'-Bis-O-(tert-butyl dimethylsilyl)-3'-spiro-5''-(4''-amino-1'',2''-oxathiole-2'',2'-dioxide)pyrimidine (TSAO) nucleoside analogues: highly selective inhibitors of human immunodeficiency virus type 1 that are targeted at the viral reverse transcriptase*. Proceedings of the National Academy of Sciences, 1992. **89**(10): p. 4392-4396.
72. Bonache, M.a.-C., et al., *Improving the Antiviral Efficacy and Selectivity of HIV-1 Reverse Transcriptase Inhibitor TSAO-T by the Introduction of Functional Groups at the N-3 Position*. Journal of Medicinal Chemistry, 2005. **48**(21): p. 6653-6660.
73. Graham, T.A., et al., *Crystal Structure of a β -Catenin/Tcf Complex*. Cell, 2000. **103**(6): p. 885-896.
74. Lepourcelet, M., et al., *Small-molecule antagonists of the oncogenic Tcf/ β -catenin protein complex*. Cancer Cell, 2004. **5**(1): p. 91-102.
75. Tian, W., et al., *Structure-Based Discovery of a Novel Inhibitor Targeting the β -Catenin/Tcf4 Interaction*. Biochemistry, 2012. **51**(2): p. 724-731.
76. Amin, A.R. and S.B. Abramson, *The role of nitric oxide in articular cartilage breakdown in osteoarthritis*. Current Opinion in Rheumatology, 1998. **10**(3): p. 263-268.
77. Nathan, C. and Q.W. Xie, *NITRIC-OXIDE SYNTHASES - ROLES, TOLLS, AND CONTROLS*. Cell, 1994. **78**(6): p. 915-918.

78. McMillan, K., et al., *Allosteric inhibitors of inducible nitric oxide synthase dimerization discovered via combinatorial chemistry*. Proceedings of the National Academy of Sciences, 2000. **97**(4): p. 1506-1511.
79. Lee, G.M. and C.S. Craik, *Trapping Moving Targets with Small Molecules*. Science, 2009. **324**(5924): p. 213-215.
80. Fieber, W., et al., *Structure, function, and dynamics of the dimerization and DNA-binding domain of oncogenic transcription factor v-Myc*. Journal of Molecular Biology, 2001. **307**(5): p. 1395-1410.
81. Kiessling, A., et al., *Selective inhibition of c-Myc/Max dimerization and DNA binding by small molecules*. Chemistry & Biology, 2006. **13**(7): p. 745-751.
82. Silvian, L.F., et al., *Small Molecule Inhibition of the TNF Family Cytokine CD40 Ligand through a Subunit Fracture Mechanism*. Acs Chemical Biology, 2011. **6**(6): p. 636-647.
83. He, M.M., et al., *Small-molecule inhibition of TNF-alpha*. Science, 2005. **310**(5750): p. 1022-1025.
84. Magliery, T.J., et al., *Detecting protein-protein interactions with a green fluorescent protein fragment reassembly trap: Scope and mechanism*. Journal of the American Chemical Society, 2005. **127**(1): p. 146-157.
85. Liu, B., et al., *Label Transfer Chemistry for the Characterization of Protein-Protein Interactions*. Journal of the American Chemical Society, 2007. **129**(41): p. 12348-12349.
86. Heeres, J.T., et al., *Identifying Modulators of Protein-Protein Interactions Using Photonic Crystal Biosensors*. Journal of the American Chemical Society, 2009. **131**(51): p. 18202-18203.
87. Porter, J.R., et al., *A General and Rapid Cell-Free Approach for the Interrogation of Protein-Protein, Protein-DNA, and Protein-RNA Interactions and their Antagonists Utilizing Split-Protein Reporters*. Journal of the American Chemical Society, 2008. **130**(20): p. 6488-6497.
88. Moerke, N.J., et al., *Small-molecule inhibition of the interaction between the translation initiation factors eIF4E and eIF4G*. Cell, 2007. **128**(2): p. 257-267.
89. Roman, D.L., et al., *Identification of Small-Molecule Inhibitors of RGS4 Using a High-Throughput Flow Cytometry Protein Interaction Assay*. Molecular Pharmacology, 2007. **71**(1): p. 169-175.
90. Potashman, M.H. and M.E. Duggan, *Covalent Modifiers: An Orthogonal Approach to Drug Design*. Journal of Medicinal Chemistry, 2009. **52**(5): p. 1231-1246.
91. Reinke, A.A. and J.E. Gestwicki, *Insight into Amyloid Structure Using Chemical Probes*. Chemical Biology & Drug Design, 2011. **77**(6): p. 399-411.
92. Eisenberg, D. and M. Jucker, *The amyloid state of proteins in human diseases*. Cell, 2012. **148**(6): p. 1188-203.

93. Findeis, M.A., *Approaches to discovery and characterization of inhibitors of amyloid beta-peptide polymerization*. Biochimica Et Biophysica Acta-Molecular Basis of Disease, 2000. **1502**(1): p. 76-84.
94. Lee, V.M.Y., *Amyloid binding ligands as Alzheimer's disease therapies*. Neurobiology of Aging, 2002. **23**(6): p. 1039-1042.
95. Bose, M., et al., *'Nature-inspired' drug-protein complexes as inhibitors of A beta aggregation*. Biochemical Society Transactions, 2005. **33**: p. 543-547.
96. Roberts, B.E., et al., *A synergistic small-molecule combination directly eradicates diverse prion strain structures*. Nat Chem Biol, 2009. **5**(12): p. 936-946.
97. Schmid, E.M. and H.T. McMahon, *Integrating molecular and network biology to decode endocytosis*. Nature, 2007. **448**(7156): p. 883-888.
98. von Kleist, L., et al., *Role of the Clathrin Terminal Domain in Regulating Coated Pit Dynamics Revealed by Small Molecule Inhibition*. Cell, 2011. **146**(3): p. 471-484.
99. Lee, L.W. and A.K. Mapp, *Transcriptional Switches: Chemical Approaches to Gene Regulation*. Journal of Biological Chemistry, 2010. **285**(15): p. 11033-11038.
100. Buhrlage, S.J., et al., *Amphipathic Small Molecules Mimic the Binding Mode and Function of Endogenous Transcription Factors*. ACS Chemical Biology, 2009. **4**(5): p. 335-344.
101. Casey, R.J., et al., *Expanding the repertoire of small molecule transcriptional activation domains*. Bioorganic & Medicinal Chemistry, 2009. **17**(3): p. 1034-1043.
102. Boriack-Sjodin, P.A., et al., *The structural basis of the activation of Ras by Sos*. Nature, 1998. **394**(6691): p. 337-343.
103. Sondermann, H., et al., *Structural Analysis of Autoinhibition in the Ras Activator Son of Sevenless*. Cell, 2004. **119**(3): p. 393-405.
104. Patgiri, A., et al., *An orthosteric inhibitor of the Ras-Sos interaction*. Nat Chem Biol, 2011. **7**(9): p. 585-587.
105. Maurer, T., et al., *Small-molecule ligands bind to a distinct pocket in Ras and inhibit SOS-mediated nucleotide exchange activity*. Proceedings of the National Academy of Sciences, 2012. **109**(14): p. 5299-5304.
106. Kiessling, L.L., J.E. Gestwicki, and L.E. Strong, *Synthetic Multivalent Ligands as Probes of Signal Transduction*. Angewandte Chemie International Edition, 2006. **45**(15): p. 2348-2368.
107. Evans, C.G., L. Chang, and J.E. Gestwicki, *Heat Shock Protein 70 (Hsp70) as an Emerging Drug Target*. Journal of Medicinal Chemistry, 2010. **53**(12): p. 4585-4602.
108. Patury, S., Y. Miyata, and J.E. Gestwicki, *Pharmacological Targeting of the Hsp70 Chaperone*. Current Topics in Medicinal Chemistry, 2009. **9**(15): p. 1337-1351.

109. Brodsky, J.L. and G. Chiosis, *Hsp70 molecular chaperones: Emerging roles in human disease and identification of small molecule modulators*. Current Topics in Medicinal Chemistry, 2006. **6**(11): p. 1215-1225.
110. Brandt, G.E.L. and B.S.J. Blagg, *Alternate Strategies of Hsp90 Modulation for the Treatment of Cancer and Other Diseases*. Current Topics in Medicinal Chemistry, 2009. **9**(15): p. 1447-1461.
111. Powers, M.V. and P. Workman, *Inhibitors of the heat shock response: Biology and pharmacology*. Febs Letters, 2007. **581**(19): p. 3758-3769.
112. Hartl, F.U. and M. Hayer-Hartl, *Converging concepts of protein folding in vitro and in vivo*. Nat Struct Mol Biol, 2009. **16**(6): p. 574-581.
113. Meimaridou, E., S.B. Gooljar, and J.P. Chapple, *From hatching to dispatching: the multiple cellular roles of the Hsp70 molecular chaperone machinery*. Journal of Molecular Endocrinology, 2009. **42**(1-2): p. 1-9.
114. Massey, A.J., *ATPases as Drug Targets: Insights from Heat Shock Proteins 70 and 90*. Journal of Medicinal Chemistry, 2010. **53**(20): p. 7280-7286.
115. Miyata, Y., et al., *Molecular chaperones and regulation of tau quality control: strategies for drug discovery in tauopathies*. Future Medicinal Chemistry, 2011. **3**(12): p. 1523-1537.
116. Kampinga, H.H. and E.A. Craig, *The HSP70 chaperone machinery: J proteins as drivers of functional specificity*. Nature Reviews Molecular Cell Biology, 2010. **11**(8): p. 579-592.
117. Ahmad, A., et al., *Heat shock protein 70- τ kDa chaperone/DnaJ cochaperone complex employs an unusual dynamic interface*. Proceedings of the National Academy of Sciences, 2011. **108**(47): p. 18966-18971.
118. Jiang, J., et al., *Structural Basis of J Cochaperone Binding and Regulation of Hsp70*. Molecular cell, 2007. **28**(3): p. 422-433.
119. Harrison, C.J., et al., *Crystal Structure of the Nucleotide Exchange Factor GrpE Bound to the ATPase Domain of the Molecular Chaperone DnaK*. Science, 1997. **276**(5311): p. 431-435.
120. Schmid, A.B., et al., *The architecture of functional modules in the Hsp90 co-chaperone Sti1/Hop*. EMBO J, 2012. **31**(6): p. 1506-1517.
121. Scheufler, C., et al., *Structure of TPR Domain-Peptide Complexes: Critical Elements in the Assembly of the Hsp70-Hsp90 Multichaperone Machine*. Cell, 2000. **101**(2): p. 199-210.
122. Wisen, S., et al., *Binding of a Small Molecule at a Protein-Protein Interface Regulates the Chaperone Activity of Hsp70-Hsp40*. Acs Chemical Biology, 2010. **5**(6): p. 611-622.
123. Chang, L., et al., *Chemical Screens against a Reconstituted Multiprotein Complex: Myricetin Blocks DnaJ Regulation of DnaK through an Allosteric Mechanism*. Chemistry & Biology, 2011. **18**(2): p. 210-221.

124. Bhattacharya, A., et al., *Allostery in Hsp70 Chaperones Is Transduced by Subdomain Rotations*. Journal of Molecular Biology, 2009. **388**(3): p. 475-490.
125. Chang, L., et al., *High-throughput screen for small molecules that modulate the ATPase activity of the molecular chaperone DnaK*. Analytical Biochemistry, 2008. **372**(2): p. 167-176.
126. Miyata, Y., et al., *High-Throughput Screen for Escherichia coli Heat Shock Protein 70 (Hsp70/DnaK): ATPase Assay in Low Volume by Exploiting Energy Transfer*. Journal of Biomolecular Screening, 2010. **15**(10): p. 1211-1219.
127. Ketterer, N., et al., *Chaperone-assisted degradation: multiple paths to destruction*. Biological Chemistry, 2011. **391**(5): p. 481-489.
128. Allan, R.K. and T. Ratajczak, *Versatile TPR domains accommodate different modes of target protein recognition and function*. Cell Stress & Chaperones, 2011. **16**(4): p. 353-367.
129. Leu, J.I.J., et al., *A Small Molecule Inhibitor of Inducible Heat Shock Protein 70*. Molecular cell, 2009. **36**(1): p. 15-27.
130. Li, J., J. Soroka, and J. Buchner, *The Hsp90 chaperone machinery: Conformational dynamics and regulation by co-chaperones*. Biochimica et Biophysica Acta (BBA) - Molecular Cell Research, 2012. **1823**(3): p. 624-635.
131. Kamal, A., M.F. Boehm, and F.J. Burrows, *Therapeutic and diagnostic implications of Hsp90 activation*. Trends in molecular medicine, 2004. **10**(6): p. 283-290.
132. Whitesell, L. and S.L. Lindquist, *HSP90 and the chaperoning of cancer*. Nat Rev Cancer, 2005. **5**(10): p. 761-772.
133. Porter, J.R., C.C. Fritz, and K.M. Depew, *Discovery and development of Hsp90 inhibitors: a promising pathway for cancer therapy*. Current Opinion in Chemical Biology, 2010. **14**(3): p. 412-420.
134. Bagatell, R., et al., *Induction of a Heat Shock Factor 1-dependent Stress Response Alters the Cytotoxic Activity of Hsp90-binding Agents*. Clinical Cancer Research, 2000. **6**(8): p. 3312-3318.
135. Donnelly, A. and B.S.J. Blagg, *Novobiocin and Additional Inhibitors of the Hsp90 C-Terminal Nucleotide-binding Pocket*. Current Medicinal Chemistry, 2008. **15**(26): p. 2702-2717.
136. Sreeramulu, S., et al., *The Human Cdc37.Hsp90 Complex Studied by Heteronuclear NMR Spectroscopy*. Journal of Biological Chemistry, 2009. **284**(6): p. 3885-3896.
137. Meyer, P., et al., *Structural basis for recruitment of the ATPase activator Aha1 to the Hsp90 chaperone machinery*. EMBO J, 2004. **23**(3): p. 511-519.
138. Siligardi, G., et al., *Co-chaperone Regulation of Conformational Switching in the Hsp90 ATPase Cycle*. Journal of Biological Chemistry, 2004. **279**(50): p. 51989-51998.

139. Zhang, T., et al., *Characterization of Celastrol to Inhibit Hsp90 and Cdc37 Interaction*. Journal of Biological Chemistry, 2009. **284**(51): p. 35381-35389.
140. Sreeramulu, S., et al., *Molecular Mechanism of Inhibition of the Human Protein Complex Hsp90–Cdc37, a Kinome Chaperone–Cochaperone, by Triterpene Celastrol*. Angewandte Chemie International Edition, 2009. **48**(32): p. 5853-5855.
141. Ardi, V.C., et al., *Macrocycles That Inhibit the Binding between Heat Shock Protein 90 and TPR-Containing Proteins*. Acs Chemical Biology, 2011. **6**(12): p. 1357-1366.
142. Yi, F. and L. Regan, *A Novel Class of Small Molecule Inhibitors of Hsp90*. Acs Chemical Biology, 2008. **3**(10): p. 645-654.
143. Gandhi, P.S., et al., *Structural identification of the pathway of long-range communication in an allosteric enzyme*. Proceedings of the National Academy of Sciences, 2008. **105**(6): p. 1832-1837.
144. Motlagh, H.N. and V.J. Hilser, *Agonism/antagonism switching in allosteric ensembles*. Proceedings of the National Academy of Sciences, 2012. **109**(11): p. 4134-4139.
145. Chari, A. and U. Fischer, *Cellular strategies for the assembly of molecular machines*. Trends in Biochemical Sciences, 2010. **35**(12): p. 676-683.
146. Peterson-Kaufman, K.J., et al., *Nucleating the Assembly of Macromolecular Complexes*. ChemBioChem, 2010. **11**(14): p. 1955-1962.
147. Good, M.C., J.G. Zalatan, and W.A. Lim, *Scaffold Proteins: Hubs for Controlling the Flow of Cellular Information*. Science, 2011. **332**(6030): p. 680-686.
148. Cardinale, D., et al., *Homodimeric Enzymes as Drug Targets*. Current Medicinal Chemistry, 2010. **17**(9): p. 826-846.
149. Panda, K., et al., *Distinct Dimer Interaction and Regulation in Nitric-oxide Synthase Types I, II, and III*. Journal of Biological Chemistry, 2002. **277**(34): p. 31020-31030.
150. Knapp, S., et al., *Thermodynamics of the high-affinity interaction of TCF4 with β -catenin*. Journal of Molecular Biology, 2001. **306**(5): p. 1179-1189.
151. Rickert, M., et al., *The Structure of Interleukin-2 Complexed with Its Alpha Receptor*. Science, 2005. **308**(5727): p. 1477-1480.
152. Braisted, A.C., et al., *Discovery of a Potent Small Molecule IL-2 Inhibitor through Fragment Assembly*. Journal of the American Chemical Society, 2003. **125**(13): p. 3714-3715.
153. Raimundo, B.C., et al., *Integrating Fragment Assembly and Biophysical Methods in the Chemical Advancement of Small-Molecule Antagonists of IL-2: An Approach for Inhibiting Protein-Protein Interactions*. Journal of Medicinal Chemistry, 2004. **47**(12): p. 3111-3130.
154. Yu, G.W., et al., *The central region of HDM2 provides a second binding site for p53*. Proceedings of the National Academy of Sciences of the United States of America, 2006. **103**(5): p. 1227-1232.

155. Kussie, P.H., et al., *Structure of the MDM2 oncoprotein bound to the p53 tumor suppressor transactivation domain*. Science, 1996. **274**(5289): p. 948-953.
156. Grasberger, B.L., et al., *Discovery and Cocrystal Structure of Benzodiazepinedione HDM2 Antagonists That Activate p53 in Cells*. Journal of Medicinal Chemistry, 2005. **48**(4): p. 909-912.
157. Sattler, M., et al., *Structure of Bcl-x(L)-Bak peptide complex: Recognition between regulators of apoptosis*. Science, 1997. **275**(5302): p. 983-986.
158. Tang, G., et al., *Pyrogallol-Based Molecules as Potent Inhibitors of the Antiapoptotic Bcl-2 Proteins*. Journal of Medicinal Chemistry, 2007. **50**(8): p. 1723-1726.
159. Abbate, E.A., J.M. Berger, and M.R. Botchan, *The X-ray structure of the papillomavirus helicase in complex with its molecular matchmaker E2*. Genes & Development, 2004. **18**(16): p. 1981-1996.
160. Wang, Y., et al., *Crystal Structure of the E2 Transactivation Domain of Human Papillomavirus Type 11 Bound to a Protein Interaction Inhibitor*. Journal of Biological Chemistry, 2004. **279**(8): p. 6976-6985.
161. Edeling, M.A., C. Smith, and D. Owen, *Life of a clathrin coat: insights from clathrin and AP structures*. Nat Rev Mol Cell Biol, 2006. **7**(1): p. 32-44.
162. Miele, A.E., et al., *Two distinct interaction motifs in amphiphysin bind two independent sites on the clathrin terminal domain [beta]-propeller*. Nat Struct Mol Biol, 2004. **11**(3): p. 242-248.
163. Siligardi, G., et al., *Regulation of Hsp90 ATPase Activity by the Co-chaperone Cdc37p/p50 cdc37*. Journal of Biological Chemistry, 2002. **277**(23): p. 20151-20159.
164. Mosyak, L., et al., *The bacterial cell-division protein ZipA and its interaction with an FtsZ fragment revealed by X-ray crystallography*. EMBO J, 2000. **19**(13): p. 3179-3191.
165. Rush, T.S., et al., *A Shape-Based 3-D Scaffold Hopping Method and Its Application to a Bacterial Protein-Protein Interaction*. Journal of Medicinal Chemistry, 2005. **48**(5): p. 1489-1495.

Chapter 2

Characterization of the binding of the E3 ubiquitin ligase CHIP to the molecular chaperones Hsp70 and Hsp90

2.1. Abstract

One of the major cellular roles for the molecular chaperones, heat shock protein 70 (Hsp70) and heat shock protein 90 (Hsp90) is to triage misfolded proteins. Both of these chaperones use protein-protein interactions (PPIs) with the E3 ubiquitin ligase CHIP (C-terminus of Hsc70 interacting protein) to facilitate the degradation of their protein substrates. The complex between CHIP and Hsp70 or Hsp90 facilitates proteasomal degradation through the attachment of poly-ubiquitin chains to the chaperone-bound substrate. Qualitative studies have shown that CHIP binds to the C-termini of either Hsp70 or Hsp90 through its tetratricopeptide (TPR) domains, however, less is known about the affinity of the CHIP-Hsp70 and CHIP-Hsp90 interactions and whether regions outside the TPR domain contribute to binding. Towards these questions, we measured the affinity of CHIP for Hsp70 and Hsp90 using two independent assays and mapped the key interacting domains using truncation mutants. These studies showed that ~80% of the binding free energy is associated with CHIP interacting with the C-

terminal “lid” subdomain of Hsp70. However, additional contacts between the substrate-binding domain (SBD) of Hsp70 and the coiled-coil region of CHIP also make a significant contribution, resulting in a 2-fold tighter affinity of CHIP for Hsp70 compared to Hsp90. We also found that the TPR domain of CHIP is essential for *in vitro* ubiquitin transfer to Hsp70. Together, these studies suggest that multivalent interactions facilitate protein turnover, possibly by fine-tuning the relative position of chaperone, substrate and CHIP in the complex.

2.1.1. Hsp70 and Hsp90 promote the degradation of misfolded proteins

The molecular chaperones Hsp70 and Hsp90 maintain protein homeostasis by assisting in the folding, trafficking and turnover of proteins [1, 2]. Both of these chaperones are ATP hydrolyzing enzymes that bind to their “clients” in a nucleotide-dependent manner [3, 4]. When Hsp70, Hsp90 and their associated co-chaperones encounter a denatured protein, they are thought to first attempt to rescue it via the folding pathway [5, 6]. However, when these attempts fail, Hsp70 and Hsp90 have also been linked to the degradation of clients via the ubiquitin-proteasome system (UPS) [7-9]. Together, these alternating pro-folding and pro-degradation functions help coordinate protein quality control decisions and protect cells from the accumulation of potentially proteotoxic, misfolded proteins [10-12].

Proteins destined for degradation by the UPS are often labeled with a polyubiquitin chain via the activity of activating (E1), conjugating (E2) and ligase (E3) enzymes [13], which enhances the affinity of the protein for the 26S proteasome [14]. There is considerable evidence that Hsp70 and Hsp90 promote degradation of certain substrates, such as glucocorticoid receptors (GR) [15], cystic fibrosis transmembrane conductance regulator (CFTR) [16], and the microtubule associated protein tau (MAPT) [17], by directly recruiting ubiquitin E3 ligases [18, 19]. For example, the E3 ligase CHIP appears to be an especially important partner in this chaperone-mediated polyubiquitination [20-22]. For some chaperone clients, such as the GR, CHIP even appears to be the major dedicated E3 ligase responsible for turnover, whereas other substrates, such as neuronal nitric oxide synthase (nNOS), can be degraded via the chaperone-mediated action of multiple E3 ligases [23].

2.1.2. CHIP binds to chaperones through its TPR domain

CHIP is a 35 kDa protein that contains a tetratricopeptide repeat (TPR) domain. The TPR domain is a common protein-protein interaction motif characterized by a tandem arrangement of three 34 amino acid motifs that forms an anti-parallel α -helical hairpin [24, 25]. TPR domains are found in several Hsp70- and Hsp90-associated co-chaperones and both chaperones are thought to interact with TPR domains via the conserved 'EEVD' motifs located in their C-termini [20, 26]. Co-crystal structures of the TPR domain of the co-chaperone, HOP (Hsp70-Hsp90

organizing protein), bound to the EEVD motif of Hsp70 suggest that the extended polypeptide resides in a charged groove, with key electrostatic interactions between the C-terminal aspartate acting as a carboxylate clamp [27]. Outside of the EEVD motif, Hsp70 and Hsp90 have very little sequence or structural similarity, but they converge on binding to CHIP and other TPR domain co-chaperones through this shared peptide motif. These protein-protein interactions (PPIs) are thought to enable turnover of clients by recruiting ubiquitin transfer activity to the vicinity of chaperone-associated, misfolded substrates [28].

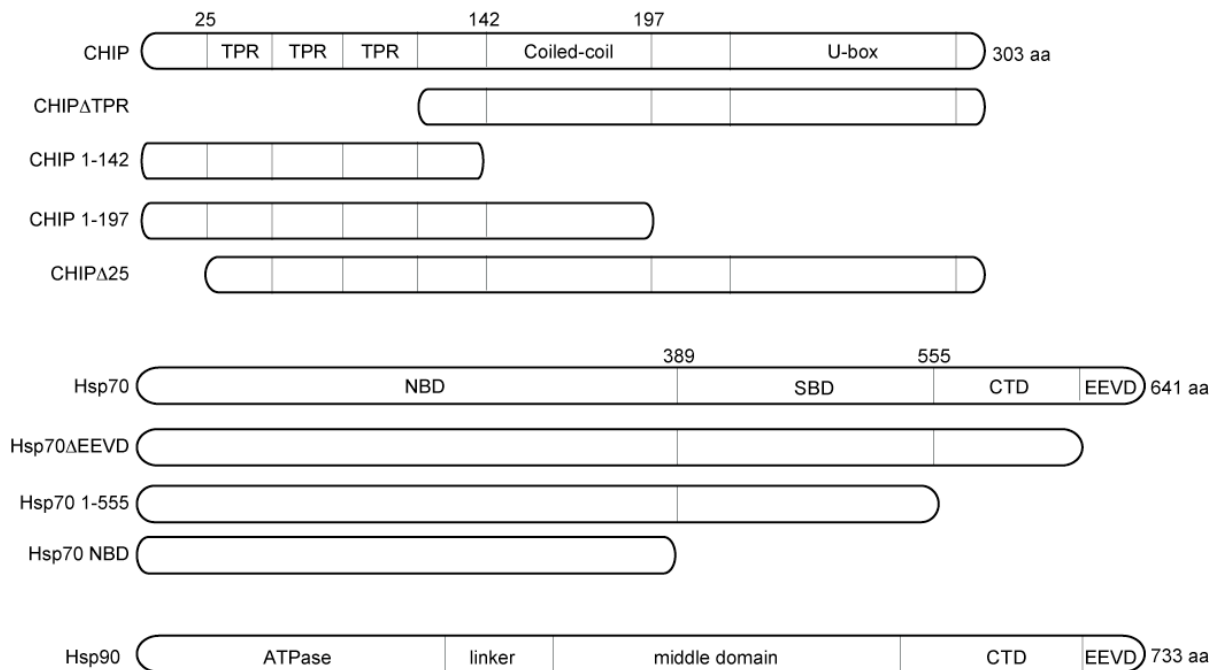


Figure 2.1 Domain architecture of CHIP, Hsp70 and Hsp90 and design of truncations. Tetratricopeptide repeat (TPR); nucleotide-binding domain (NBD); substrate-binding domain (SBD); C-terminal subdomain (CTD).

Despite the importance of the CHIP-Hsp70 and CHIP-Hsp90 complexes in protein homeostasis, surprisingly little is known about the affinities of these interactions. Moreover, it isn't clear whether contact surfaces outside the EEVD-TPR interaction also contribute to the binding free energy. Most of what is known comes from qualitative pull-down experiments, especially glutathione-S-transferase (GST) fusion protein assays [20, 28, 29]. Based on these studies, the TPR domain and an adjacent charged region of CHIP appear to be important for its interaction with Hsp70. Likewise similar approaches have been used to suggest that the carboxy terminal domain (CTD) of Hsp70, including the EEVD motif, seems to be required [28]. However, quantitative studies performed on the Hop-Hsp70 complex suggest that binding in that system involves additional contacts outside the TPR-EEVD [30]. Further, a recent cryo-EM structure of the Hsp70-Hop-Hsp90 complex also supports the idea that the interaction surface may be more extensive [31].

Here, we quantified the free energy contributions of the major domains in the CHIP-Hsp70 and CHIP-Hsp90 complexes. We report that CHIP binding to the CTD of Hsp70 contributes a majority (~80%) of the interaction energy, while Hsp70 additionally interacts with CHIP via a second contact in its substrate-binding domain (SBD). This extra contact likely accounts for the 2-fold higher affinity for the CHIP-Hsp70 interaction over CHIP-Hsp90. These findings help

clarify how these molecular chaperones cooperate with CHIP to accelerate substrate turnover.

2.2. Results

2.2.1. Design of CHIP and Hsp70 truncations

Pioneering analyses on the Hsp70-CHIP complex were performed by Ballinger *et al* [20], in which they generated a series of truncation mutants of both CHIP and Hsp70 and then qualitatively evaluated the impact of individual domains using pulldowns. To extend that work, we were interested in quantifying the binding affinities of the various domains in an *in vitro* system. Accordingly, we designed a set of deletion constructs including, a CHIP TPR domain deletion (CHIP Δ TPR) and two C-terminal truncations 1-142 and 1-197 (CHIP 1-142 and CHIP 1-197, respectively) (**Figure 2.1**). We also deleted the first 25 amino acids of CHIP, which have been shown to be important in auto-ubiquitination (CHIP Δ 25).

Hsp70 deletions included removal of the EEVD motif (Hsp70- Δ EEVD), the C-terminal “lid” sub-domain (CTD) (Hsp70 1-555) and the entire substrate-binding domain (SBD) of Hsp70 to retain only the nucleotide-binding domain (NBD) (Hsp70-NBD). We also purified the prokaryotic Hsp70, DnaK, which naturally lacks the EEVD motif. Finally, we expressed and purified full length human Hsp90 α (herein referred to as Hsp90) to permit comparisons between the two chaperones. Together, this collection of full length and truncated partners was

expected to provide insight into the contributions of various domains to the affinity of the CHIP-Hsp70 and CHIP-Hsp90 complexes.

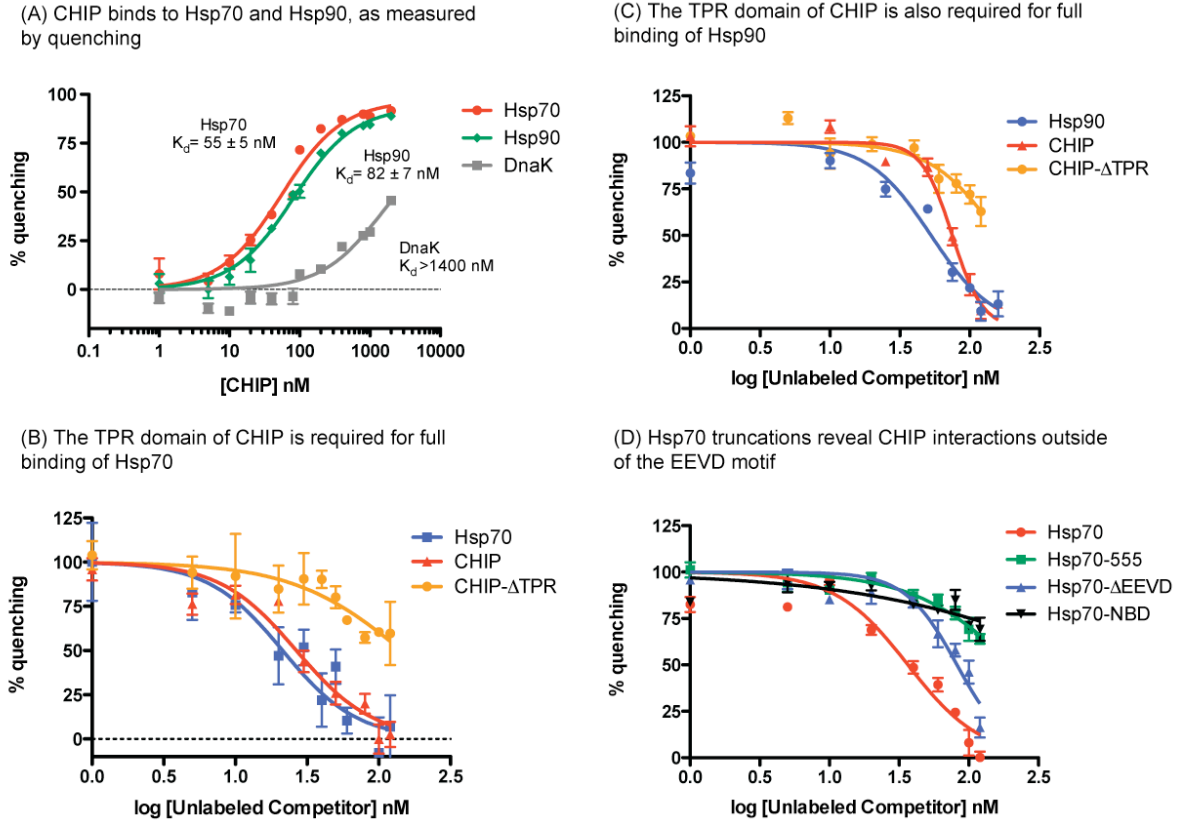


Figure 2.2 Binding of Hsp70/Hsp90 to CHIP by fluorescence quenching. (A) Hsp70, DnaK, and Hsp90 were labeled with Alexa-488 and CHIP with BHQ-10. At 50 nM for all chaperone proteins, the indicated apparent affinities for CHIP are shown. (B-C) At 80 nM Hsp90, and 50 nM Hsp70 or CHIP, the ability for unlabeled protein to compete away the quenching signal was measured. (D) At 50nM Hsp70 and CHIP, the ability of truncations of Hsp70 to compete away the quenching signal was measured. All data points are the average of triplicates and the error bars represent the standard error of the mean (SEM). K_i values for competition experiments are outlined in **Table 2.1**.

2.2.2. Full binding of CHIP to Hsp70 and Hsp90 requires an intact TPR domain, but other regions also contribute

In order to measure the binding affinities of CHIP and Hsp70 or Hsp90, we first developed a homogeneous, solution phase, fluorescence quenching assay.

Briefly, Hsp70 and Hsp90 were labeled on exposed amines with the fluorescent donor AlexaFluor488 (AF488), which has an emission wavelength of 525 nm, and CHIP was similarly labeled with Black Hole Quencher10 (BHQ10), a strong fluorescence acceptor that absorbs at 507 nm. This simple system allows sensitive measurement of protein-protein interaction affinities, which are estimated from the quench in AF488 fluorescence [32, 33]. At a 50 nM concentration for both labeled Hsp70 and Hsp90, increasing concentrations of labeled CHIP produced a dose-dependent quench of the AF488 signal, giving apparent K_d values of ~ 60 nM and 80 nM for Hsp70 and Hsp90, respectively (**Figure 2.2A**). Encouragingly, DnaK, which does not bind CHIP, had a much weaker affinity ($K_d > 1400$ nM; **Figure 2.2A**). Additionally, labeled CHIP is not interacting with chaperone proteins as a substrate, as the synthetic peptide substrate NRLLLTG does not compete for labeled protein interactions in this assay (**Appendix 2.5.1**), suggesting that the interactions are specific.

Next, using unlabeled chaperone protein as a positive control, we tested the ability of either full-length CHIP or CHIP without its TPR domain (CHIP- Δ TPR) to compete for the interaction of labeled protein. Saturating concentrations of the unlabeled competitor should restore the AF488 signal back to baseline fluorescence. In this experiment, both labeled Hsp70 and Hsp90 were at 50 nM, while labeled CHIP was at 50 nM and 80 nM, respectively. Unlabeled CHIP competed with the labeled protein interaction (**Figure 2.2B-C**). Interestingly,

CHIP- Δ TPR retained some ability to compete for binding both Hsp70 and Hsp90 (**Figure 2.2B-C; Table 2.1**), suggesting that regions besides the TPR domain of CHIP contribute to binding chaperone proteins.

Table 2.1 Binding affinities (K_i values in nM), as measured by fluorescence quench.

Construct	CHIP	CHIP- Δ TPR
Hsp90	75 \pm 2.8	161 \pm 31
Hsp70	36 \pm 5.2	145 \pm 51
Hsp70 Δ EEVD	82 \pm 4.2	--
Hsp70 1-555	209 \pm 45	--
Hsp70 NBD	>> 500	--

2.2.3. CHIP binds to Hsp90 with weaker affinity than Hsp70

To confirm and expand upon our results from the fluorescence quenching assay, we developed a secondary, label-free, surface plasmon resonance (SPR)

platform to measure the affinities of Hsp70 and Hsp90 for CHIP. This was important because the difference between the K_i values for unlabeled protein competition (**Table 2.1**) and the K_d values from the quenching assay (**Figure 2.2A**) suggests that the labeling in this assay affects the interaction, making interpretation difficult. Biotinylated Hsp70 was immobilized on a streptavidin Biacore chip (SA), at a density of \sim 1000 response units (RUs). Binding of recombinant CHIP was evaluated by injecting concentrations ranging from 0 to 500 nM at a flow rate of 20 μ L/min. Binding was measured by first subtracting the signal from a control lane in which DnaK was immobilized, but binding to this

control was not significant ($\Delta RU_{\max} < 20$). Binding affinities were then determined using analyses of equilibrium binding values (**Figure 2.3A**). For the binding of full length Hsp70 to CHIP, the apparent K_d was determined to be 190 ± 3.6 nM (**Figure 2.3B**). This observed affinity is 3-fold weaker than that predicted by the fluorescence quenching assay, suggesting that either the SA surface may partially interfere with binding or, as previously observed, affinities in the quenching assay are influenced by labeling. To confirm that the observed interaction was specific, we verified that free Hsp70 competed with CHIP for binding to the surface. This experiment provided a K_i of ~ 340 nM at either of two different concentrations of CHIP (100 nM and 250 nM), suggesting that the interaction is indeed specific (**Figure 2.3C**). We noted that the K_i value was larger than the observed K_d , perhaps because of contributions from multivalent binding at the SA-chip surface.

CHIP has been shown to bind both Hsp90 and Hsp70, guiding triage decisions during protein quality control [28]. Traditionally, Hsp70 is more closely associated with CHIP-mediated degradation, while Hsp90 is considered a stabilizing chaperone [9]. However, other studies have shown that Hsp90, not Hsp70, is more closely linked to degradation of some substrates, such as VHL [34, 35]. To better understand this system, biotinylated Hsp90 (1950 RUs) was immobilized on an SA chip and then full length CHIP was injected at a flow rate of $20 \mu\text{L}/\text{min}$. These studies showed that CHIP bound Hsp90 with a 2-fold weaker affinity ($K_d =$

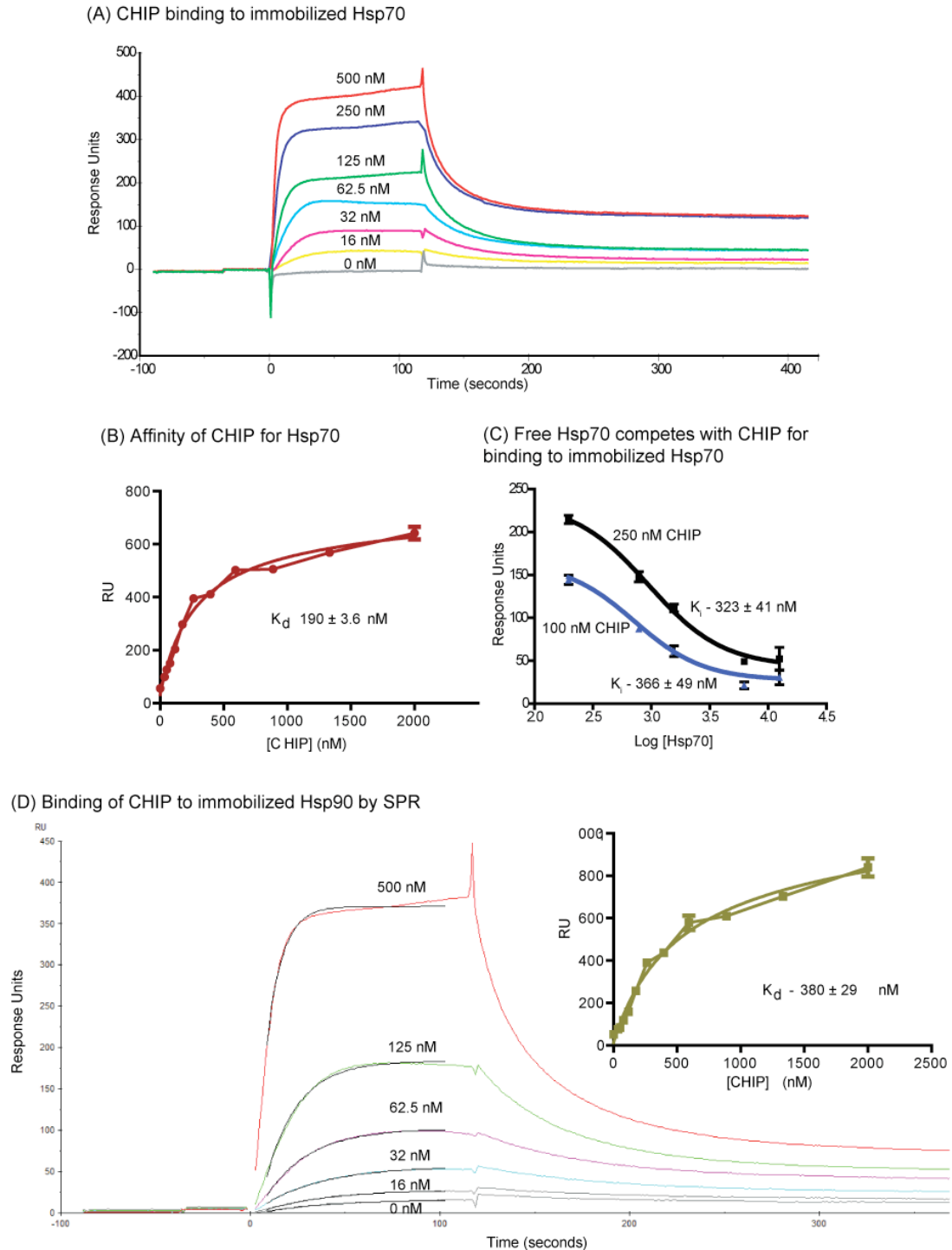


Figure 2.3 Full-length CHIP binds Hsp70 and Hsp90 by surface plasmon resonance (SPR). (A) Raw traces of CHIP binding to immobilized Hsp70 on an SA Biacore chip. Hsp70 was immobilized at ~ 1000 RU. (B) Thermodynamic fit of the SPR results estimates the affinity of CHIP binding to Hsp70. (C) Free Hsp70 added to the CHIP solutions (at two different CHIP concentrations) competes with binding to the Hsp70 surface. (D) Raw sensogram of a representative SPR experiment in which CHIP is bound to immobilized Hsp90. The inset shows the results of fitting the equilibrium binding values to calculate the K_d . All results are the average of two experiments performed in triplicate and errors are SEM.

380 ± 29 nM) than Hsp70 (**Figure 2.3D**). This conclusion was supported by the results of the quenching studies in which labeled Hsp90 bound labeled CHIP with an apparent K_d of 82 ± 7 nM, approximately 1.6-fold weaker than the Hsp70-CHIP interaction (**Figure 2.2A**).

2.2.4. Truncation mutants reveal domains critical for the Hsp70-CHIP interaction

Because interactions between Hsp70 and CHIP seem to be more extensive than what has been previously reported, and Hsp70 binds CHIP with a 2-fold higher affinity over Hsp90, we next focused on the Hsp70-CHIP PPI to investigate what additional contacts outside of the EEVD-TPR interaction could account for these observations. Towards this goal, biotinylated Hsp70 truncations were immobilized on a SA-chip and binding of recombinant CHIP (and its truncations) was measured in a similar fashion as described above. Results from these experiments are summarized in **Table 2.2**. Consistent with the results from the fluorescence quenching assay, the TPR domain of CHIP is important for binding to Hsp70, as deletion of this domain results in a 3-fold loss in affinity ($K_d = 601 \pm 54$ nM). In addition, the coiled-coil region of CHIP also contributes, because CHIP 1-142 had a 30% weaker affinity ($K_d = 247 \pm 36$ nM) than full length. This is an interesting result because this domain is not conserved in other TPR proteins, suggesting that it may help contribute to specificity. The CHIP 1-197 and CHIP Δ 25 proteins had affinities similar to full length CHIP, suggesting that the

deleted regions did not significantly contribute to Hsp70 binding (**Table 2.2**). Deletion of the EEVD region of Hsp70 resulted in a loss of only 2-fold in affinity ($K_d = 430 \pm 36$ nM). The Hsp70 1-555 construct was still able to weakly bind to CHIP ($K_d = 835 \pm 44$ nM), suggesting that regions of the substrate-binding domain (SBD) outside the C-terminal lid also participate in binding CHIP. This interaction likely involves contacts with the TPR and coiled-coil regions of CHIP, because Hsp70 1-555 had no appreciable affinity for either CHIP 1-142 or CHIP- Δ TPR ($K_d > 5 \mu\text{M}$). As expected [20], the NBD did not contribute to the interaction, as the Hsp70-NBD truncation did not have significant affinity ($K_d > 5 \mu\text{M}$).

As shown in **Figure 2.2D** and summarized in **Table 2.1**, the Hsp70 truncation results were consistent across platforms. The quenching assay also revealed that the Hsp70 EEVD motif is important for binding, as the Hsp70 Δ EEVD mutant

Table 2.2 Binding affinities (KD values in nM) for binding of Hsp70 to CHIP, as measured by SPR.

Construct	CHIP	CHIP1-142	CHIP1-197	CHIP Δ 25	CHIP Δ TPR
Hsp70	190 \pm 3.6	247 \pm 36	220 \pm 23	201 \pm 34	601 \pm 54
Hsp70 Δ EEVD	430 \pm 36	520 \pm 46	490 \pm 42	440 \pm 33	990 \pm 65
Hsp70 1-555	835 \pm 44	> 5 μM	920 \pm 56	940 \pm 74	> 5 μM
Hsp70 NBD	> 5 μM	> 5 μM	> 5 μM	> 5 μM	> 5 μM

had a K_i value ~2.5-fold higher than full length ($K_i = 82 \pm 4.2$ nM vs 36.60 ± 5.2 nM). And interestingly, Hsp70 1-555 and Hsp70 NBD displayed progressively weaker binding to CHIP. Calculation of the free energy values from the affinities measured by SPR revealed that ~80% of the binding between CHIP and Hsp70 can be attributed to interactions within the Hsp70 CTD (**Appendix 2.5.5**). This finding once again suggests that some binding energy for the full-length interaction is contained within areas of the SBD outside of the CTD. Taken together, these results show that binding of CHIP to the C-terminus of Hsp70, while certainly a contributor to the PPI, is not sufficient to describe the entire affinity. Additionally, they provide insight into the requirements for forming a complex between Hsp70 and CHIP.

2.2.5. CHIP does not display nucleotide dependence in binding to Hsp70

Since nucleotide binding and hydrolysis result in conformational changes in Hsp70 [36, 37], we wanted to measure the binding affinities for CHIP under different nucleotide states. Nucleotide dependence has already been shown for the TPR-domain co-chaperone, Hop, which binds Hsp70 in the ADP-bound conformation 2-fold better than Hsp70-ATP [38]. In contrast, our results showed that CHIP did not have a preference for Hsp70's nucleotide state; similar affinities of ~ 200 to 240 nM were found for Hsp70 in the ATP, ADP and apo states by SPR (**Figure 2.4A**) and ~ 55 nM for Hsp70 in the presence of either ATP, ADP or AMP-PnP in the fluorescence quench assay (**Figure 2.4B**).

These findings suggest that CHIP does not have a preference for nucleotide states of Hsp70 and, therefore, it might not be expected to have any effect on steady state ATP turnover in the chaperone. To test CHIP in this setting, steady state ATPase assays on full length Hsp70 were performed, showing that CHIP neither increased nor decreased the rate of ATP hydrolysis (**Figure 2.4C**). In contrast, the well-known J domain co-chaperone, DJA2 (DnaJA2), was a potent stimulator of this activity (**Figure 2.4C**). These studies suggest that CHIP binding occurs independent of nucleotide state and that it does not allosterically impact Hsp70 enzymatic activity.

2.2.6. TPR domain is required for the ubiquitination of Hsp70

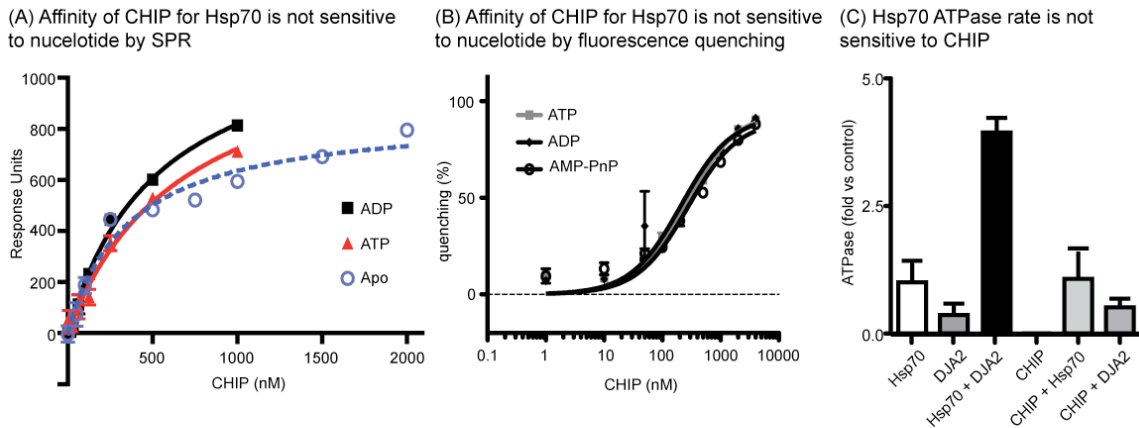


Figure 2.4 CHIP interaction with Hsp70 is independent of nucleotide state. (A) Binding of CHIP to immobilized Hsp70 by SPR. Hsp70 was treated with saturating ADP or ATP. Alternatively, it was dialyzed to the apo-form before being immobilized for binding. Experiments were performed in triplicate. All nucleotides were added at 1 mM. (B) Binding of CHIP-BHQ10 to Hsp70-AF488 in various nucleotide states was performed using the fluorescence quenching assay. All nucleotides were added at 1 mM. (C) CHIP does not effect the steady state ATPase activity of Hsp70. As a control, Hsp70 was stimulated with recombinant, human DJA2. Concentrations are Hsp70 (1 μ M), DJA2 (0.2 μ M), CHIP (1 μ M), ATP (1 mM). Results are the average of triplicates and the error bars represent SEM.

CHIP ubiquitinates Hsp70 in cells and this activity is thought to promote turnover of both the chaperone and its bound substrates [39]. Based on our biochemical studies, we wanted to assess which domains are necessary for this enzymatic function of CHIP. Using *in vitro* ubiquitination assays, CHIP and Hsp70 were incubated with a mixture of components required for the reconstitution of the ubiquitin cycle [14]: ubiquitin (Ub), E1 and E2 enzymes and ATP. Conjugation of ubiquitin to Hsp70 was then measured using Western blot analysis (**Figure 2.5**). Using a series of CHIP truncations, we found that both the ubiquitination domain by itself (Ubox) and CHIP Δ TPR lacked activity. Interestingly, deletion of just the first TPR motif in the CHIP sequence (Δ -TPR-1) also abolished activity. Thus, these studies strongly support a key, functional role for the TPR domains of CHIP in ubiquitination of Hsp70.

2.3. Discussion

2.3.1. The TPR domain in CHIP and the EEVD motif in Hsp70/Hsp90 play important roles in binding but other regions also contribute

CHIP cooperates with the molecular chaperones Hsp70 and Hsp90 to play a central role in protein quality control [40, 41]. Here, we sought to measure the affinities of CHIP for Hsp70/90 and, further, determine which domains contribute to binding. Using SPR and fluorescence proximity assays, we found that the TPR domain in CHIP is important for binding to both Hsp70 and Hsp90, with the coiled-coil region also playing a role in binding Hsp70. On the other side, the

EEVD motif of both chaperones has historically been found to be important for binding [20, 26]. However, our data suggests that this region was not the only one involved in the interaction as the Hsp70 Δ EEVD truncation had only a 2-fold weaker affinity for CHIP. Further, the Hsp70 1-555 truncation retained weak binding affinity, suggesting that regions in the CTD and SBD also interact with CHIP. This result has some interesting parallels with studies on the Hop-Hsp70 interaction [27], in which contacts outside the EEVD-TPR make important, secondary contributions. One result of this additional contact between Hsp70 and CHIP was an approximately 2-fold tighter affinity, compared to CHIP-Hsp90.

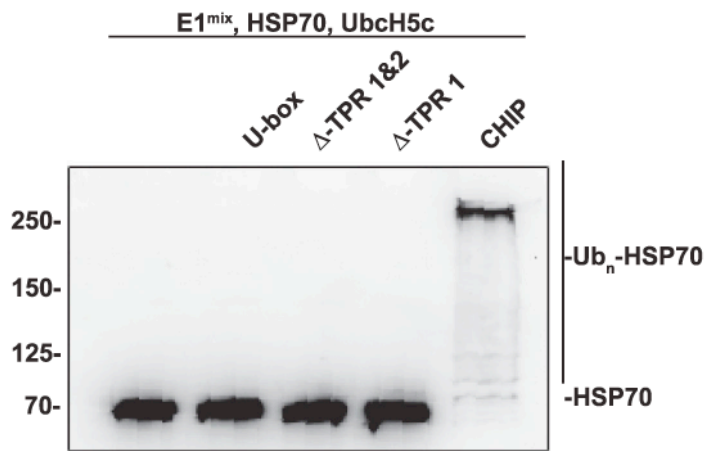


Figure 2.5 Ubiquitination of Hsp70 by CHIP requires the TPR domains. Ubiquitination reactions were carried out at 37C for 1 hour in the presence of Ube1, UbcH5c, and ATP.

Based on these measurements, we conclude that ~80% of the interaction energy from binding of Hsp70 to CHIP arises from interactions between CHIP and the C-terminal “lid” domain of Hsp70,

while the remaining affinity comes from a poorly understood contact in the SBD. This secondary interaction is not due to non-specific binding of CHIP in the substrate binding cleft of Hsp70, because it was not influenced by saturating

levels of a model peptide substrate (see **Appendix 2.5.1**). Rather, we hypothesize that this additional contact might provide the Hsp70-CHIP complex with additional opportunities for fine-tuning the position of the substrate, CHIP and the E2 enzyme. There are many examples of Hsp70 being a critical partner for CHIP-mediated degradation of substrates [9], suggesting that, in some cases, the Hsp70-CHIP interaction may be especially suited for promoting turnover. However, in other cases, Hsp90 has clearly been shown to play a dominant role in chaperone-mediated turnover [35]. Our results suggest that the HSP90-CHIP interaction is only 2-fold weaker than the Hsp70-CHIP contact, supporting the idea that either chaperone can facilitate substrate turnover through the UPS. The ultimate choice of which chaperone partner becomes involved may be dictated by structural topology of the individual substrates, although more studies are certainly required to address this hypothesis.

2.3.2. Nucleotide state does not influence CHIP binding to Hsp70

Another TPR-domain containing co-chaperone, Hop, has been shown to preferentially bind Hsp70 in an ADP bound state [38]. Unexpectedly, the affinity of the CHIP-Hsp70 interaction was nucleotide independent and, further, it had no significant impact on ATP turnover by Hsp70. Thus, we propose that the Hop-Hsp70 and CHIP-Hsp70 contact surface may be different, allowing communication of the nucleotide-specific conformation between Hop and Hsp70,

but not CHIP and Hsp70. More work is required to understand this difference and learn its potential functional significance in protein quality control.

2.4. Materials and methods

2.4.1. Protein purification

All Hsp70 proteins were derived from the human Hsp72 (HSP1A1). The Hsp90 used in these studies was human Hsp90a-1. All Hsp70 truncations were cloned into the pMCSG7 plasmid (Midwest Center for Structural Genomics, Bethesda, MD) by ligation independent cloning and transformed into Rosetta (DE3) cells for expression. To express Hsp70 truncations, 25 mL of overnight (37 °C) LB culture of Rosetta (DE3) culture was poured into 1 L of Terrific Broth. After 3 hours incubation at 37 °C, the culture was cooled down to 28 °C for 2 hours before overnight induction of expression with 200 μ M IPTG overnight, and the cell pellet was stored at -80 °C until use. The wt and Hsp70 truncations were purified using same procedures as described except the addition of the EDTA-free protease inhibitor cocktail (Roche) (1/4 tablet for each sample) in the lysis buffer and the omitting of final Ni-NTA resin clean-up step for Hsp70 truncations. All CHIP truncations were expressed in *E. coli* (BL21 DE3 LysS) and purified on glutathione sepharose resin (GE Healthcare) [42, 43]. All GST tagged proteins were cleaved with Precision protease and purified prior to use. Ubch5c was purified as previously described [43].

2.4.2. Surface plasmon resonance experiments

A streptavidin chip (SA; GE Healthcare) was docked and equilibrated with HBS buffer (10 mM HEPES, 150 mM NaCl, pH 7.4 containing 0.005% Tween-20) overnight at 5 μ L/min. All experiments were performed at 25 °C. Proteins were biotinylated using Sulpho-NHS-LC-Biotin (Invitrogen, catalog B-6353) following the protocol provided by Invitrogen (MP00143). Hsp70's were immobilized in MES buffer (20mM MES, 150 mM NaCl, pH 5.5, 0.01% Tween-20). Average immobilization responses for the various Hsp70 truncations were approximately 1200 RUs. After immobilization of all biotinylated proteins, the chip was equilibrated for at least 4 hours at 5 μ L/min. Varying concentrations of CHIP and its truncations (10 nM to 2 μ M) were prepared in HBS buffer and 40 μ L were injected at 20 μ L/min. For competition experiments, CHIP (100 nM) and unlabeled Hsp70 (50 nM – 10 μ M) were combined in HBS immediately prior to injection. For both direct and competition binding, the binding surface was recovered with regeneration buffer (HBS buffer, 100 mM NaOH, 100 mM MgCl₂), using a pulse injection of 20 μ L until the baseline response was reached. Equilibrium data was fit using the RU values 5 seconds prior to the end of the association phase, followed by non-linear regression analysis using GraphPad Prism software.

2.4.3. Analytical ultracentrifugation

Sedimentation velocity and equilibrium experiments were carried out in a Beckman XL-I ProteomeLab analytical ultracentrifuge with absorbance optics. Samples were prepared in 10 mM HEPES, 150 mM NaCl at pH 7.4. In the sedimentation velocity experiments, 400 μ L of Hsp72 (10 μ M) and CHIP (20 μ M) were loaded into two-sector charcoal-filled epon centerpieces and spun at 48,000 rpm at 20 °C. Data were analyzed using c(s) and c(M) models in SEDFIT.

2.4.4. Gel filtration

Purified protein was pre-incubated on ice in HEPES buffered saline (10 mM HEPES, 100 mM NaCl, pH 7.4) containing 1 mM ADP. Each sample was injected onto an analytical size exclusion column (Superdex 200, GE Healthcare) and run at 0.5 mL/min in HBS buffer. All curves were normalized to the elution peak of free nucleotide. Relative molecular weights were determined by comparison to protein standards.

2.4.5. ATPase assays

The colormetric assay for monitoring steady-state ATP activity has been previously described [44, 45]. Briefly, Hsp70 (1 μ M) plus either a J-domain co-chaperone (DJA2, 0.2 μ M) or CHIP (1 μ M) was prepared in assay buffer (0.02% Triton X-100, 100 mM Tris-HCl, 20 mM KCl, and 6 mM MgCl₂, pH 7.4). Protein samples were aliquoted into 96-well plates containing 1 mM ATP. After 3h at

37°C, malachite green reagent was used to detect liberated phosphate and the signal measured on a SpectraMax M5.

2.4.6. Fluorescence quenching assays

Protein samples were labeled and prepared as previously described [32, 33]. Briefly, amine reactive Alex488 (Invitrogen) was used to label Hsp70 and Hsp90 by mixing the dye and protein at a 10:1 molar ratio in bicarbonate buffer (100 mM NaHCO₃ [pH 8] containing 150mM NaCl). CHIP was similarly labeled using BHQ-10 (Biosearch Technologies) at a molar ratio of 50:1, dye: protein. Excess labels were removed by passage through Zeba desalting columns (Thermo Scientific) equilibrated with HEPES-buffered saline. Using the extinction coefficients supplied by the manufacturer, label concentrations were determined for each protein sample and used to calculate the amount of molar incorporation. MIR values for Hsp70, Hsp90, and CHIP were 3.2, 2.4, and 14.1 respectively. All quenching assays were performed at the indicated protein concentrations in 10 mM HEPES buffer (pH 7.4) containing 150 mM NaCl, and 0.05% Tween-20. Equilibrium binding measurements were taken in a 384-well microplate format using a SpectraMax M5 microplate reader (Molecular Devices). Each sample was excited at 480nm and total fluorescence was read at 525nm with a 515nm cut-off. The average fluorescence intensity of 15 reads was recorded for each sample.

2.4.7. Ubiquitination assays

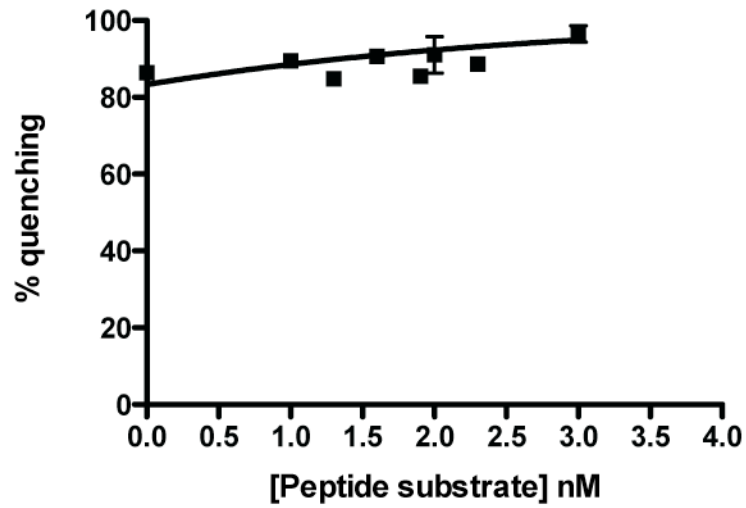
Ubiquitination was typically performed for 1 hr at 37 °C in 10 μ L mixtures containing buffer A (50 mM Tris pH7.5, 50 mM KCl, 0.2 mM DTT), Ubmix (2.5 mM ATP, 5 mM MgCl₂, 50 nM Ube1 (E1 enzyme), and 100 μ M ubiquitin), 1 μ M UbcH5, 1 μ M CHIP, prepared as previously described [46]. Reactions were stopped by addition of SDS-Laemmli buffer and boiling, followed by separation of proteins by SDS-PAGE and visualization by Western blotting with appropriate antibodies. Mouse monoclonal antibody to Hsp70 (Assay Designs) was used to visualize ubiquitin transfer.

Notes

The work in this chapter was a collaborative effort and is in the process of being published under the title “Characterization of the Binding of the E3 Ubiquitin Ligase CHIP to the Molecular Chaperones Hsp70 and Hsp90”. Srikanth Patury, Matthew Smith and Jason Gestwicki designed the experiments. Srikanth Patury and Andrea Thompson performed the SPR experiments. Matthew Smith performed the quenching experiments. And K. Matthew Scaglione ran the ubiquitination assays. Srikanth Patury, Matthew Smith and Jason Gestwicki wrote the manuscript.

2.5. Appendix

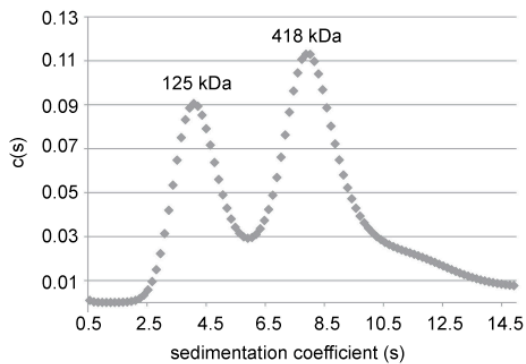
2.5.1. CHIP does not bind Hsp70 as a substrate



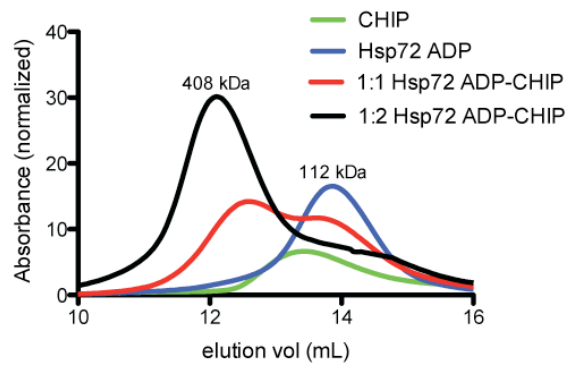
Appendix 2.5.1 Peptide substrate does not compete for the Hsp70-CHIP interaction by fluorescence quenching assay

2.5.2. Hsp70-CHIP complex formation

(A) Analytical ultracentrifugation suggests formation of a 1:1 Hsp70:CHIP complex

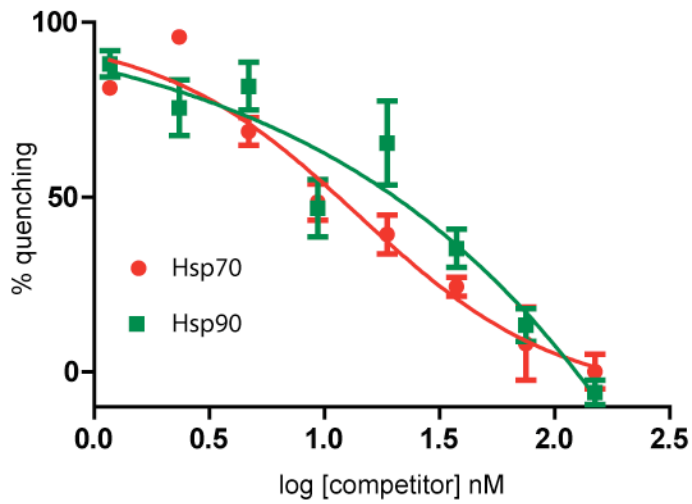


(B) Gel filtration also suggests a 1:1 Hsp70:CHIP complex



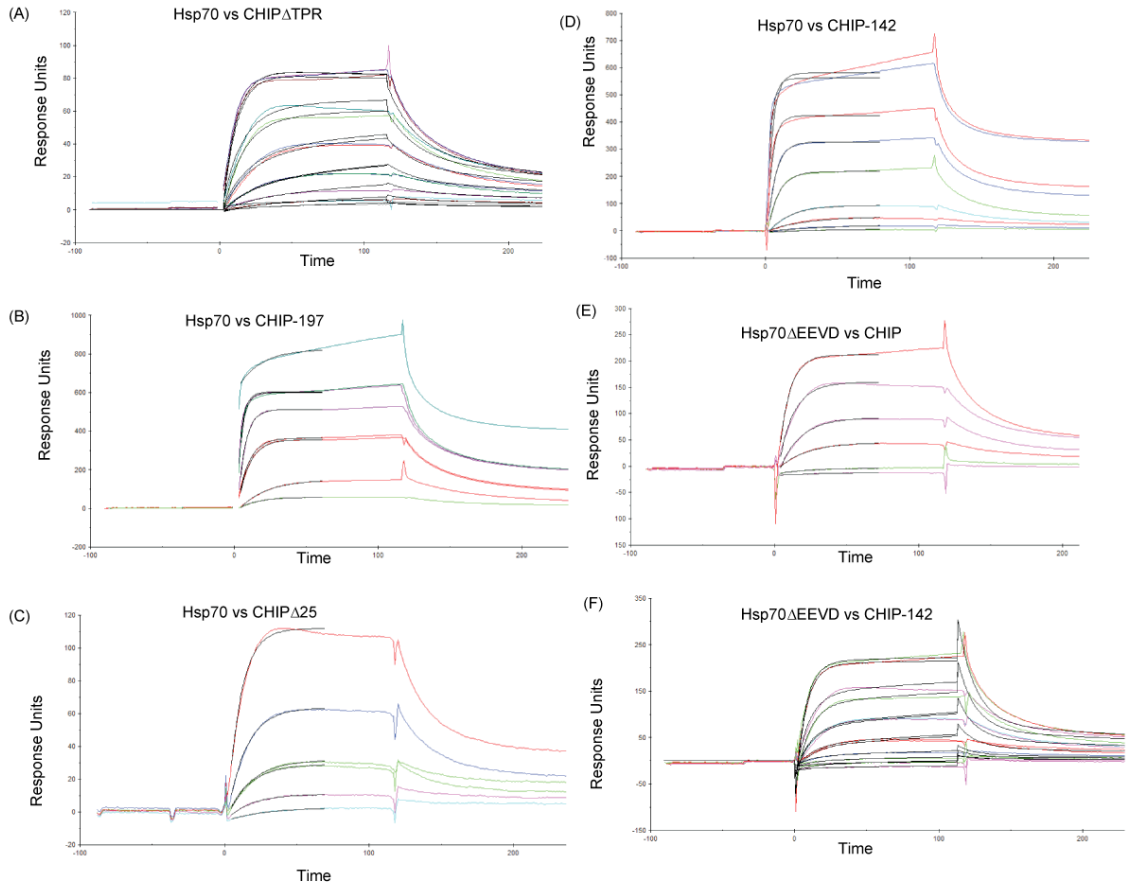
Appendix 2.5.2 CHIP binding to Hsp70 results in mostly a 1:1 complex. (A) Hsp70 (10 μ M) and CHIP (20 μ M) were mixed in vitro and the resulting complexes analyzed by analytical ultracentrifugation. (B) Analysis of the Hsp70-CHIP complex by gel filtration. Molecular weight standards support a complex of ~420 kDa (1:1 Hsp70:CHIP). All complexes were formed in the presence of 1 mM ADP. Results are normalized to the free ADP peak.

2.5.3. Hsp90 can compete with Hsp70 for CHIP binding



Appendix 2.5.3 Hsp90 can compete with binding of Hsp70 to CHIP. The concentrations of Hsp70-AF488 and CHIP-BHQ-10 were 50 nM.

2.5.4. Raw SPR curves



Appendix 2.5.4 Raw binding curves for binding of CHIP and Hsp70 truncations by SPR.

2.5.5. Free energy values calculated from SPR binding affinities

Appendix 2.5.5 Free energy values (kCal/mol) calculated from binding affinities measured by SPR.

Construct	CHIP	CHIP1-142	CHIP1-197	CHIP Δ 25	CHIP Δ TPR
Hsp70	-9.160 ± 0.011	-9.005 ± 0.086	-9.073 ± 0.061	-9.127 ± 0.1	-8.478 ± 0.053
Hsp70 Δ EEVD	-8.677 ± 0.05	-8.564 ± 0.052	-8.599 ± 0.057	-8.663 ± 0.044	-8.183 ± 0.038
Hsp70 1-555	-8.284 ± 0.031	N/A	-8.226 ± 0.036	-8.213 ± 0.046	N/A
Hsp70 NBD	N/A	N/A	N/A	N/A	N/A

2.6. References

1. Pratt, W.B. and D.O. Toft, *Regulation of signaling protein function and trafficking by the hsp90/hsp70-based chaperone machinery*. Exp Biol Med (Maywood), 2003. **228**(2): p. 111-33.
2. Bukau, B., J. Weissman, and A. Horwich, *Molecular chaperones and protein quality control*. Cell, 2006. **125**(3): p. 443-51.
3. Hartl, F.U., *Molecular chaperones in cellular protein folding*. Nature, 1996. **381**(6583): p. 571-9.
4. Krukenberg, K.A., et al., *Conformational dynamics of the molecular chaperone Hsp90*. Q Rev Biophys, 2011. **44**(2): p. 229-55.
5. Frydman, J., *Folding of newly translated proteins in vivo: the role of molecular chaperones*. Annu Rev Biochem, 2001. **70**: p. 603-47.
6. Wegele, H., L. Muller, and J. Buchner, *Hsp70 and Hsp90--a relay team for protein folding*. Rev Physiol Biochem Pharmacol, 2004. **151**: p. 1-44.
7. Pickart, C.M. and D. Fushman, *Polyubiquitin chains: polymeric protein signals*. Curr Opin Chem Biol, 2004. **8**(6): p. 610-6.
8. Goldberg, A.L., *Protein degradation and protection against misfolded or damaged proteins*. Nature, 2003. **426**(6968): p. 895-9.
9. Pratt, W.B., et al., *Proposal for a role of the Hsp90/Hsp70-based chaperone machinery in making triage decisions when proteins undergo oxidative and toxic damage*. Exp Biol Med (Maywood), 2010. **235**(3): p. 278-89.
10. Hohfeld, J., D.M. Cyr, and C. Patterson, *From the cradle to the grave: molecular chaperones that may choose between folding and degradation*. EMBO Rep, 2001. **2**(10): p. 885-90.
11. Kundrat, L. and L. Regan, *Balance between folding and degradation for Hsp90-dependent client proteins: a key role for CHIP*. Biochemistry, 2010. **49**(35): p. 7428-38.
12. Patury, S., Y. Miyata, and J.E. Gestwicki, *Pharmacological targeting of the Hsp70 chaperone*. Curr Top Med Chem, 2009. **9**(15): p. 1337-51.
13. Cyr, D.M., J. Hohfeld, and C. Patterson, *Protein quality control: U-box-containing E3 ubiquitin ligases join the fold*. Trends Biochem Sci, 2002. **27**(7): p. 368-75.
14. Hershko, A. and A. Ciechanover, *The ubiquitin system*. Annu Rev Biochem, 1998. **67**: p. 425-79.
15. Pratt, W.B., et al., *Chaperoning of glucocorticoid receptors*. Handb Exp Pharmacol, 2006(172): p. 111-38.
16. Meacham, G.C., et al., *The Hsc70 co-chaperone CHIP targets immature CFTR for proteasomal degradation*. Nat Cell Biol, 2001. **3**(1): p. 100-5.
17. Dickey, C., et al., *Akt and CHIP coregulate tau degradation through coordinated interactions*. Proc Natl Acad Sci U S A, 2008. **105**(9): p. 3622-7.

18. Zhang, Y., et al., *Parkin functions as an E2-dependent ubiquitin- protein ligase and promotes the degradation of the synaptic vesicle-associated protein, CDCrel-1*. Proc Natl Acad Sci U S A, 2000. **97**(24): p. 13354-9.
19. Tsai, Y.C., et al., *Parkin facilitates the elimination of expanded polyglutamine proteins and leads to preservation of proteasome function*. J Biol Chem, 2003. **278**(24): p. 22044-55.
20. Ballinger, C.A., et al., *Identification of CHIP, a novel tetratricopeptide repeat-containing protein that interacts with heat shock proteins and negatively regulates chaperone functions*. Mol Cell Biol, 1999. **19**(6): p. 4535-45.
21. Jana, N.R., et al., *Co-chaperone CHIP associates with expanded polyglutamine protein and promotes their degradation by proteasomes*. J Biol Chem, 2005. **280**(12): p. 11635-40.
22. Miller, V.M., et al., *CHIP suppresses polyglutamine aggregation and toxicity in vitro and in vivo*. J Neurosci, 2005. **25**(40): p. 9152-61.
23. Morishima, Y., et al., *CHIP deletion reveals functional redundancy of E3 ligases in promoting degradation of both signaling proteins and expanded glutamine proteins*. Hum Mol Genet, 2008. **17**(24): p. 3942-52.
24. Goebel, M. and M. Yanagida, *The TPR snap helix: a novel protein repeat motif from mitosis to transcription*. Trends Biochem Sci, 1991. **16**(5): p. 173-7.
25. Cortajarena, A.L. and L. Regan, *Ligand binding by TPR domains*. Protein Sci, 2006. **15**(5): p. 1193-8.
26. Prodromou, C. and L.H. Pearl, *Structure and functional relationships of Hsp90*. Curr Cancer Drug Targets, 2003. **3**(5): p. 301-23.
27. Scheufler, C., et al., *Structure of TPR domain-peptide complexes: critical elements in the assembly of the Hsp70-Hsp90 multichaperone machine*. Cell, 2000. **101**(2): p. 199-210.
28. Connell, P., et al., *The co-chaperone CHIP regulates protein triage decisions mediated by heat-shock proteins*. Nat Cell Biol, 2001. **3**(1): p. 93-6.
29. Jiang, J., et al., *CHIP is a U-box-dependent E3 ubiquitin ligase: identification of Hsc70 as a target for ubiquitylation*. J Biol Chem, 2001. **276**(46): p. 42938-44.
30. Brinker, A., et al., *Ligand discrimination by TPR domains. Relevance and selectivity of EEVD-recognition in Hsp70 x Hop x Hsp90 complexes*. J Biol Chem, 2002. **277**(22): p. 19265-75.
31. Southworth, D.R. and D.A. Agard, *Client-loading conformation of the Hsp90 molecular chaperone revealed in the cryo-EM structure of the human Hsp90:Hop complex*. Mol Cell, 2011. **42**(6): p. 771-81.
32. Ruan, Q., J.P. Skinner, and S.Y. Tetin, *Using nonfluorescent Forster resonance energy transfer acceptors in protein binding studies*. Anal Biochem, 2009. **393**(2): p. 196-204.

33. Chang, L., et al., *Chemical screens against a reconstituted multiprotein complex: myricetin blocks DnaJ regulation of DnaK through an allosteric mechanism*. Chem Biol, 2011. **18**(2): p. 210-21.
34. Stankiewicz, M., et al., *CHIP participates in protein triage decisions by preferentially ubiquitinating Hsp70-bound substrates*. Febs J, 2010. **277**(16): p. 3353-67.
35. McClellan, A.J., M.D. Scott, and J. Frydman, *Folding and quality control of the VHL tumor suppressor proceed through distinct chaperone pathways*. Cell, 2005. **121**(5): p. 739-48.
36. Swain, J.F., et al., *Hsp70 chaperone ligands control domain association via an allosteric mechanism mediated by the interdomain linker*. Mol Cell, 2007. **26**(1): p. 27-39.
37. Bertelsen, E.B., et al., *Solution conformation of wild-type E. coli Hsp70 (DnaK) chaperone complexed with ADP and substrate*. Proc Natl Acad Sci U S A, 2009. **106**(21): p. 8471-6.
38. Johnson, B.D., et al., *Hop modulates Hsp70/Hsp90 interactions in protein folding*. J Biol Chem, 1998. **273**(6): p. 3679-86.
39. Kundrat, L. and L. Regan, *Identification of residues on Hsp70 and Hsp90 ubiquitinated by the cochaperone CHIP*. J Mol Biol, 2010. **395**(3): p. 587-94.
40. Picard, D., *Heat-shock protein 90, a chaperone for folding and regulation*. Cell Mol Life Sci, 2002. **59**(10): p. 1640-8.
41. Dickey, C.A., et al., *The high-affinity HSP90-CHIP complex recognizes and selectively degrades phosphorylated tau client proteins*. J Clin Invest, 2007. **117**(3): p. 648-58.
42. Scaglione, K.M., et al., *Ube2w and ataxin-3 coordinately regulate the ubiquitin ligase CHIP*. Mol Cell, 2011. **43**(4): p. 599-612.
43. Brzovic, P.S., et al., *A UbcH5/ubiquitin noncovalent complex is required for processive BRCA1-directed ubiquitination*. Mol Cell, 2006. **21**(6): p. 873-80.
44. Miyata, Y., et al., *High-throughput screen for Escherichia coli heat shock protein 70 (Hsp70/DnaK): ATPase assay in low volume by exploiting energy transfer*. J Biomol Screen, 2010. **15**(10): p. 1211-9.
45. Chang, L., et al., *High-throughput screen for small molecules that modulate the ATPase activity of the molecular chaperone DnaK*. Anal Biochem, 2008. **372**: p. 167-176.
46. Sahara, N., et al., *In vivo evidence of CHIP up-regulation attenuating tau aggregation*. J Neurochem, 2005. **94**(5): p. 1254-63.

Chapter 3

Improving the synthesis of 15-deoxyspergualin analogs using the Ugi multicomponent reaction

3.1. Abstract

Spergualin is a natural product that exhibits immunosuppressive, anti-tumor and anti-bacterial activities. Its derivatives, such as 15-deoxyspergualin (15-DSG), have been clinically approved for acute allograft rejection. It binds to the molecular chaperone heat shock protein 70 (Hsp70) with low micromolar affinity and may provide a promising scaffold from which to build modulators of this enzyme. However, with all its promise, the reported syntheses to produce spergualin and its derivatives are cumbersome (> 10 steps) and they suffer from low overall yields (~ 0.3 to 18%). Moreover, spergualin is chemically unstable and it rapidly hydrolyzed in an aqueous environment. To address these problems, we have developed a modified synthetic route with significantly improved overall yield (~31 to 47%). The key transformation is a microwave-accelerated Ugi multi-component reaction that is used to generate the α -acylamino carboxamide core in a single step. Using the products of this route, we found that modifications of the hemiaminal significantly increased chemical

stability. We also determined that these products maintain some of the anti-bacterial activity of the natural product. Thus, we anticipate that this synthetic route will improve access to biologically active spergualin derivatives.

3.1.1. Spergualin and its derivatives are unstable, yet biologically active, polyamines

The natural product spergualin was first isolated from *Bacillus laterosporus*, and it has gathered significant medical interest because of its potent immunosuppressive, anti-tumor and anti-bacterial activities [1-4]. Early

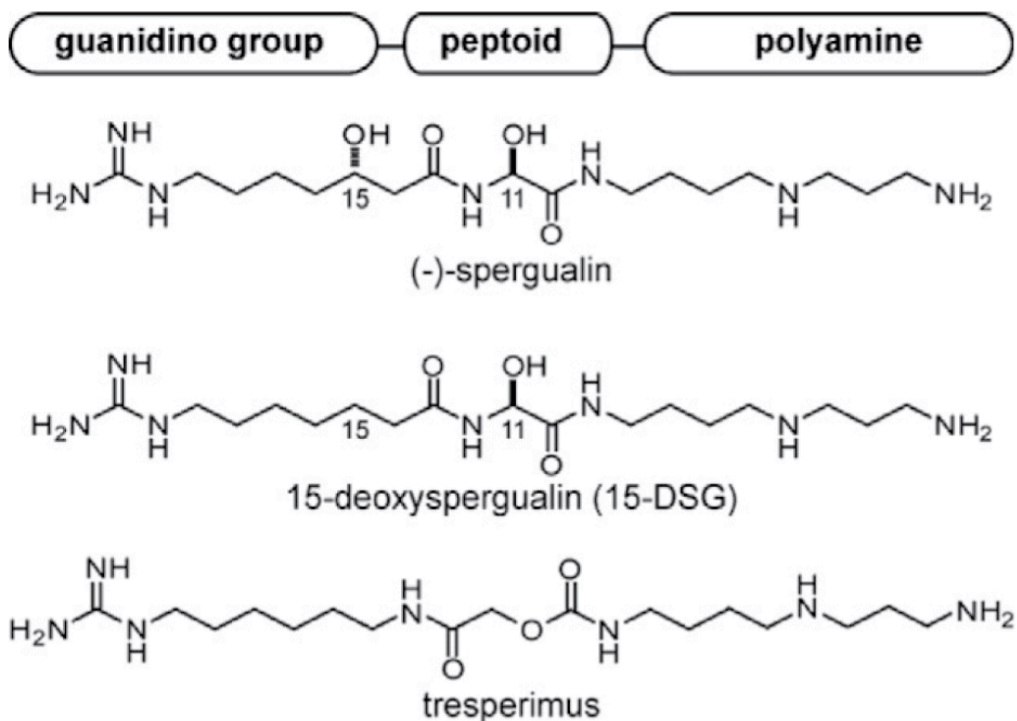


Figure 3.1 Chemical structures of the natural product, spergualin, and two of its derivatives. A schematic of the architecture is shown and the positions of carbons 11 and 15 are indicated.

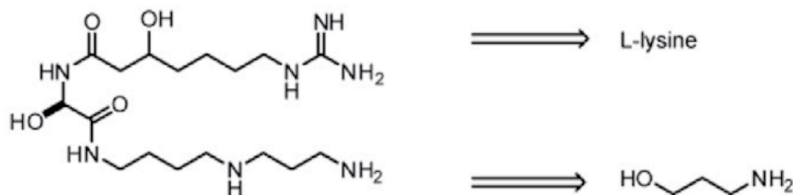
characterization revealed that spergualin is composed of three key regions: an α -acylamino carboxamide (peptoid) core, guanidylated alkyl group and spermidine-derived polyamine (**Figure 3.1**) [5] and each of these modules are thought to be required for biological activity [2, 6, 7]. However, attempts to further characterize the pharmacology of spergualin were complicated by its rapid hydrolysis in aqueous buffers. Thus, a major goal of early synthetic efforts was to modify the most labile regions, such as the hydroxyl at position 15 and produce a more stable analog.

Accordingly, medicinal chemistry studies showed that removing the hydroxyl group at the 15 position on the scaffold produced a more potent analog, likely due to its increased stability [7]. This product, (-)-15-deoxyspergualin (15-DSG) (**Figure 3.1**), was approved for treatment of acute allograft rejection in renal transplant patients [8]. In an effort to understand the mechanism behind the immunosuppressive activity of 15-DSG, Nadler *et al.* demonstrated that the compound binds to the constitutively expressed Hsp70 family member Hsc70 with a dissociation constant (K_d) of 4 μ M [9, 10]. 15-DSG produces an Hsc70-dependent reduction in NF- κ B signaling, [11] and it inhibits CD4⁺ T cell maturation [12].

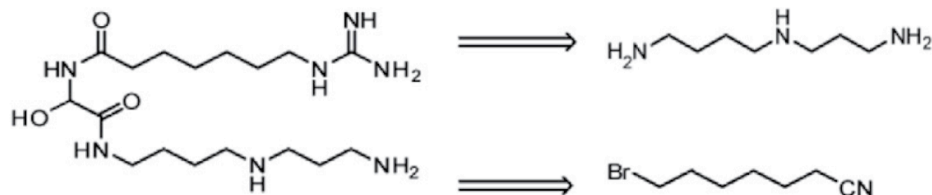
More recent synthetic efforts have yielded additional derivatives of 15-DSG, such as tresperimus (**Figure 3.1**), in which a portion of the unstable peptoid is

replaced with a carbamate [13, 14]. Along with sharing the immunosuppressive activity of 15-DSG, tresperimus has also been shown to bind Hsc70, [15]

(A) Literature precedented route to spergualin



(B) Literature precedented route to 15-DSG



(C) Proposed retrosynthetic analysis of 15-DSG analogs

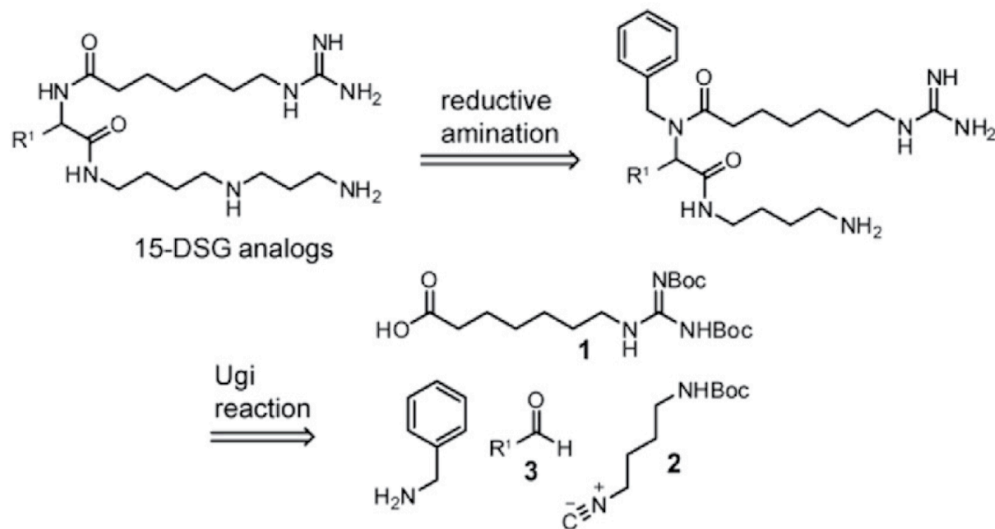


Figure 3.2 Comparison of the retrosynthetic analyzes. Known convergent routes to spergualin (A) and 15-DSG (B) proceed through a series of more than 10 convergent steps. (C) The proposed route employs the Ugi multi-component reaction to generate the peptoid and guanidylated regions in a single step. See the text for references.

supporting the idea that this interaction plays a major role in the activity of spergualin analogs.

Although these derivatives are an improvement on spergualin, they are still relatively unstable, with short half-lives ($t_{1/2}$) in neutral and basic conditions [13]. In addition, they are only weakly orally bioavailable (<5%) and metabolized rapidly, with terminal half-lives of only 1-2 hours [16].

3.1.2. The synthesis of spergualin derivatives remains difficult

One major challenge in the search for improved spergualin derivatives is that the reported synthetic routes are cumbersome and low yielding. For example, the first attempts produced 15-DSG in only 0.3% yield in more than 10 steps, starting from L-lysine and 1-amino-propanol (**Figure 3.2A**) [2, 6, 17]. Later efforts mildly improved the yield of 15-DSG (to ~7% to 18%) by starting with 7-bromoheptanenitrile and a protected spermidine derivative (**Figure 3.2B**), but these convergent routes remain protracted (> 10 steps) and challenging [18-20]. We envisioned an alternative synthetic approach. Specifically, our retrosynthetic analysis employs the Ugi multicomponent reaction to assemble the core of spergualin in a single step (**Figure 3.2C**). The Ugi reaction proceeds through the condensation of a carboxylic acid, amine, isocyanide, and aldehyde (or ketone. [21, 22]. Thus, in addition to the potential advantages gained from the concise creation of the peptoid, this route is also expected to allow access to combinatorial diversity through varying the identity of the four modules, including the guanidinylated amino acid (**1**), protected isocyanide (**2**) and aldehyde (**3**).

3.2. Results

3.2.1. Optimizing the microwave irradiation-assisted Ugi reaction

Many conditions for the Ugi reaction have been reported, with the most recent studies focusing on the use of microwave irradiation to improve yield and reaction times. [23, 24] Guided by these efforts, we first tested the feasibility of the approach using the commercially available isocyanide, 1-isocyanopentane, as a model reactant. Briefly, an equimolar solution of benzylamine, benzaldehyde, 6-guanidinoheptanoic acid, [25] and 1-isocyanopentane was heated in methanol at 120 °C for 20 minutes in a microwave reactor. These conditions yielded the product in good (70%) yield. Encouraged by this observation, we next substituted the simple isocyanide with the desired, tert-butyl (4-isocyanobutyl)carbamate (**2**) [26]. Unfortunately, we found that this change dropped the yield to 11%. To solve this issue, we re-investigated the reaction conditions, focusing on the variables of time, temperature, and solvent (**Table 3.1**). This approach revealed that the yield was particularly sensitive to solvent and that DMF tended to be the best choice (average purified yields between 36-46%).

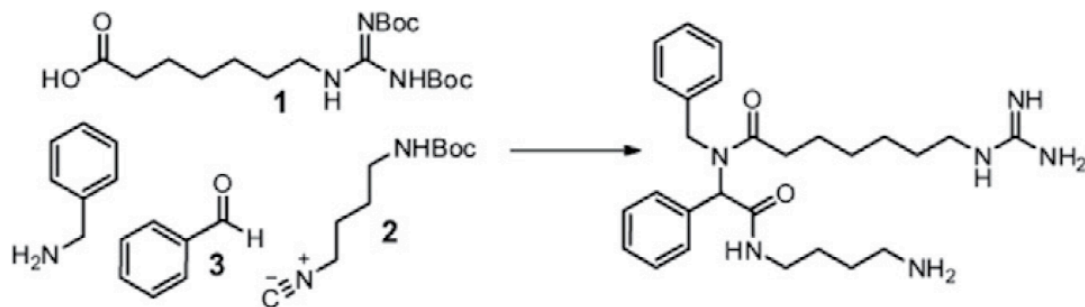
3.2.2. Building a focused library of spergualin analogs

Using the optimized Ugi conditions (DMF, 100 °C, 20 minutes), we then pursued the synthesis of 15-DSG derivatives. Although this reaction is often used in the

assembly of large, combinatorial libraries, our first efforts focused on producing a small number of focused derivatives to test specific issues related to chemical stability (see below). Towards that goal, we combined four aldehydes (**3a-d**) with

Table 3.1

Optimization of the Ugi reaction conditions



Entry	Solvent	Temp (°C)	Time (min)	Yield (%)
1	MeOH	100	20	2–10
2	MeOH	100	30	<2
3	MeOH	90	20	36
4	MeOH	90	30	22
5	MeOH	110	20	<2
6	MeOH	120	10	12
7	MeOH	130	10	nd
8	MeOH	rt	240	35
9	EtOH	90	20	27
10	EtOH	90	40	17
11	DMF	100	20	46
12	DMF	120	20	36
13	DMF	rt	240	43

7-guanidinoheptanoic acid (**1**), benzylamine, and tert-butyl (4-isocyanobutyl)carbamate (**2**) to produce intermediates **4a-d** after Boc deprotection. In the next step, we envisioned using a reductive amination to complete the spermidine module. Towards that goal, we first assembled Fmoc-3-

amino-1-propanal (**5**) from Fmoc- β -alanine, using the method of More and Finney [27]. Then, compound **5** (0.05 mmol, 1 equiv) was reacted with **4a-d** (0.05 mmol, 1 equiv) in 2 mL THF and NaBH(OAc)₃ (0.07 mmol, 1.4 equiv) for 1.5 hours to produce intermediates **6a-d**. Importantly, NaBH(OAc)₃ was chosen for this step because, unlike NaBH₃CN, it does not require low pH. [28] This was an important consideration because of the sensitivity of spergualin analogs to degradation. Following the reductive amination, we sought to remove the final protecting groups. However, we found that common ways of removing Fmoc, such as 20% piperidine in DMF, caused significant hydrolysis. Therefore, we employed the alternative, Tris-amine resin (50 equiv) in CHCl₃ for 20 minutes [29]. Finally, the benzyl group was readily removed under mild conditions using ammonium cerium (IV) nitrate (CAN) [30]. Following a final purification by alumina chromatography, the products **7a-d** were isolated as racemic mixtures in 31 to 47% overall yield (**Figure 3.3**).

3.2.3. Spergualin analogs are significantly more stable than the natural product

Having attained our synthetic goals, we wanted to examine the stability of our generated analogs in aqueous buffers. As mentioned above, one of the biggest challenges in this area is that spergualin and some of its derivatives are prone to hydrolysis. Previous studies had suggested that removal of the labile 15-hydroxyl group could improve stability [14]. However, Lebreton *et al.* found that even the

clinically approved 15-DSG had a $t_{1/2}$ of only ~2 hrs in pH 10 buffer [13]. Under these conditions, degradation occurs via hydrolysis at the labile hemiaminal

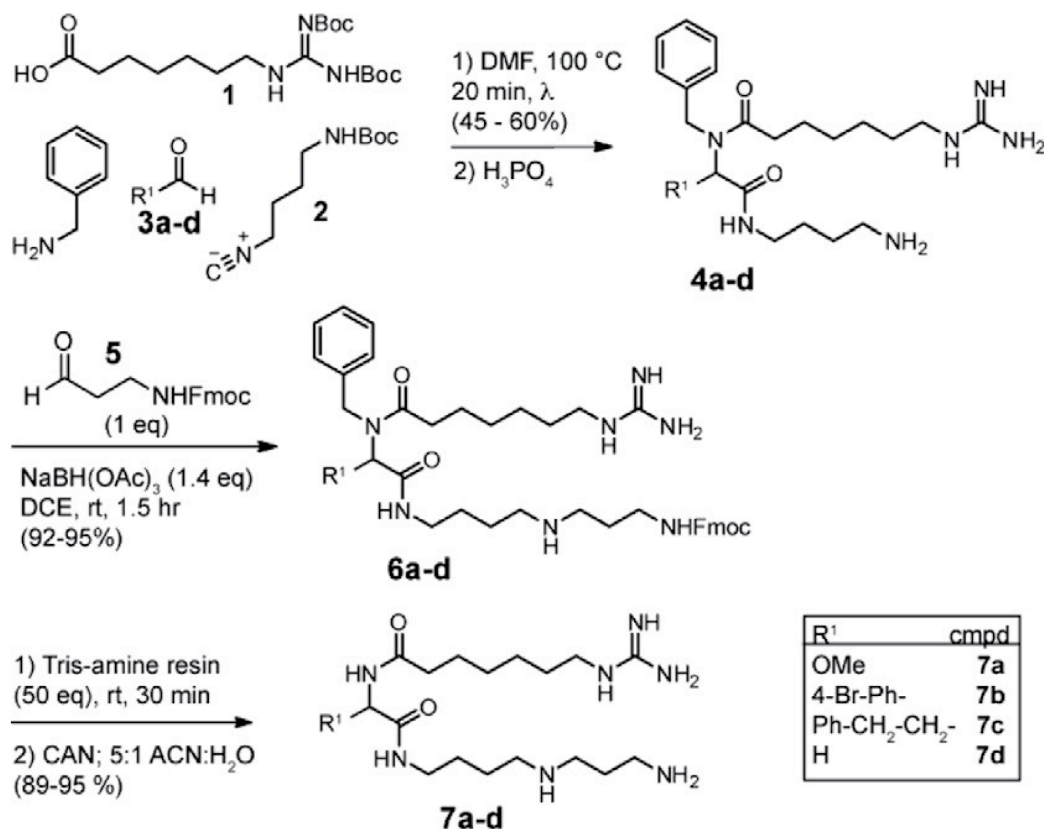


Figure 3.3 Synthesis of spergualin analogs. The Ugi condensation of aldehydes 3a–d, followed by Boc deprotection, produced the intermediates 4a–d in good yield. Reductive amination with the aldehyde 5, followed by deprotection of the final Fmoc and benzyl groups yielded the final products 7a–d in overall, purified yields from 31% to 47%.

(**Figure 3.4C**) [31]. Thus, we reasoned that blocking this degradation route might further improve persistence. To test this idea, we first compared the stability of spergualin and 11-methoxy-15-deoxyspergualin (**7a**) using thin layer chromatography. Consistent with previous findings, the natural product (Sigma Aldrich cat #S5822) is relatively stable under mild acidic conditions (pH 5.0) but it is highly unstable in neutral and basic buffers (**Figure 3.4A**). By comparison,

compound **7b**, with the methoxy substitution at position 11, had significantly improved stability under basic and neutral conditions (**Figure 3.4B**). Next, we quantified the $t_{1/2}$ values of compounds **7a-d** and compared them to those of

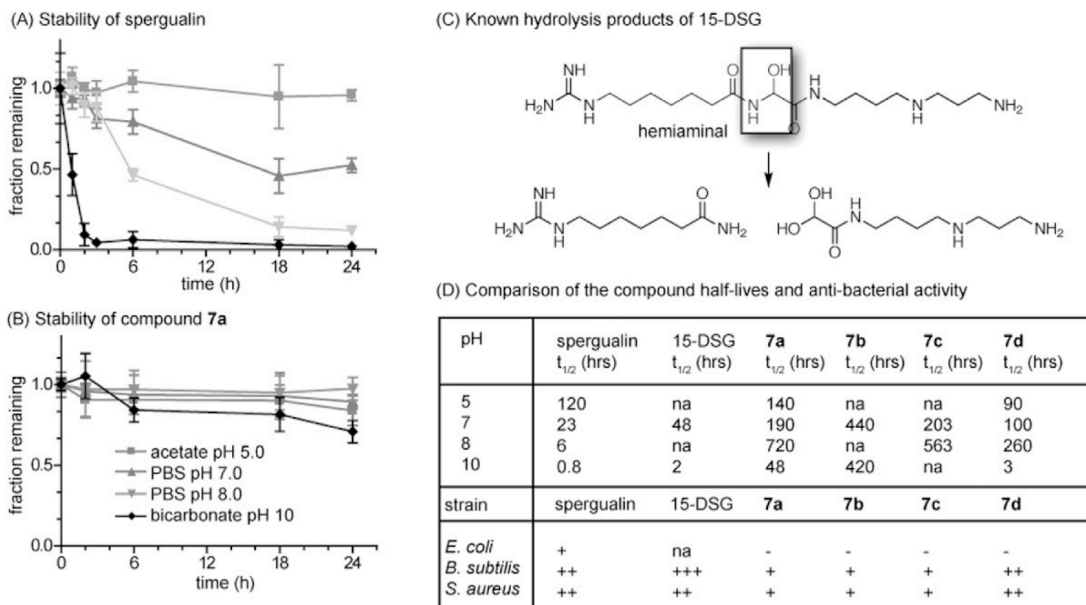


Figure 3.4 Synthetic derivatives of spergualin are more stable than the natural product. (A) The stability of spergualin was tested by thin layer chromatography. The time points were initiated immediately after dissolution in aqueous buffers at the indicated pH. (B) Stability of **7a** under the same conditions. Results are the average of at least independent triplicates and the error bars represent standard error of the mean. (C) Summary of the known hydrolysis products of 15-DSG (D) Table of the stability values for spergualin, 15-DSG and compounds **7a-d**. Also included are the relative anti-bacterial activities (+++MIC <10 lg/mL; ++MIC 10–50 lg/mL; +MIC 50–250 lg/mL; -MIC >250 lg/mL).

spergualin and 15-DSG. In these studies, we found that the $t_{1/2}$ values of compound **7a** at pH 7.0 and 8.0 were 8- and 120-fold greater than spergualin and at least 4-fold greater than 15-DSG (**Figure 3.4D**). More striking, bulky substitutions at position 11, as in compound **7b** and **7c**, markedly improved stability to greater than 2 weeks. Together, these results suggest that multiple types of substitutions at the hemiaminal could provide significant increases in stability under neutral and basic conditions.

3.2.4. Spergualin analogs retain antibacterial activity

To understand whether the introduced substitutions might disrupt bioactivity, we tested compounds **7a–d** in a series of anti-bacterial assays against *Escherichia coli*, *Bacillus subtilis* and *Staphylococcus aureus*. Consistent with previous reports, spergualin and 15-DSG had anti-bacterial activity, especially against the gram-positive strains [32] (**Figure 3.4D**). We found that compounds **7a–d** retained some anti-bacterial activity, although the relative potencies were decreased. Of these compounds, **7d** appeared the most promising, with good activity against *B. subtilis* and *S. aureus*. Additional studies are clearly needed to understand the relevant structure–activity relationships and to improve compound potency. However, these initial efforts show that spergualin analogs with greatly improved chemical stability retain some bioactivity.

3.3. Discussion

3.3.1. The Ugi multicomponent reaction allows increased access to spergualin derivatives

The spergualin scaffold was once seen as a very promising potential therapeutic due to its many biological activities. However a long and difficult synthesis, coupled to a high rate of hydrolysis have since curbed most of these expectations. In part due to spergualins activity towards Hsp70, we wanted to reinvestigate these issues. The main hurdle in our eyes was the established synthetic routes. We rationalized that if we could improve the synthesis and

thereby gain increased access to spergualin derivatives, then tackling hydrolysis would be a much easier task. One of the most successful ways to decrease the steps in a synthetic route and open a scaffold to derivitization is to develop a combinatorial scheme using multicomponent reactions [33]. Applying this method to the case of spergualins leads us to the Ugi reaction and the synthetic scheme outlined above. Using this synthesis, we were able to produce a small library of spergualin analogs with a 2-fold increase in the highest previously published yield. Thus we should now be able to produce large derivative libraries of spergualin in a more rapid and efficient manner than previously possible.

3.3.2. Spergualin analogs are more stable than and maintain biological activity of the natural product

To reduce the likelihood of hydrolysis at the hemiaminal region of spergualin, we synthesized molecules that had the hydroxyl group either masked (**7a**) or replaced with hydrogen (**7d**) or a bulky substitution (**7b-c**) at the 11-position. All of these substitutions lead to an increased stability of the compound in aqueous buffer at a range of pH values. Furthermore, although slightly reduced, *in vivo* anti-bacterial activity persisted in these compounds. Suggesting that these modifications to the scaffold did not completely abolish interactions with the scaffold's biological target, Hsc70.

3.3.3. Conclusions

In this work, an improved method for producing 15-DSG analogs was developed, which increased the overall yields by at least 2-fold and greatly reduced the number of steps. The key transformation is the Ugi reaction to simultaneously generate the peptoid and guanidylated regions. Using this approach, we found that substitutions of the hemiaminal significantly improved chemical stability of these compounds, which is expected to provide a path towards exploration of these compounds as both research probes and therapeutics. Most importantly for this thesis work, the revised synthetic route now, for the first time, makes these spergualin analogs available for testing as potential inhibitors of the protein-protein interactions (PPIs) between Hsp70 and TPR-domain co-chaperones. This concept will be explored in more detail in Chapter 4.

The next steps to making potent, stable and selective spergualin analogs will be to expand upon the library described in the current work, and use these compounds to explore the mechanism behind spergualins *in vivo* activity. Currently, another graduate student in the Gestwicki laboratory is expanding our collection of spergualin analogs and exploring their structure-activity relationships (SAR) in more detail.

3.4. Materials and methods

3.4.1. Reagents and general syntheses

Reagents and solvents were purchased from Sigma and used without further purification. All NMR spectra collected on a Varian 400 MHz system.

The synthesis of the known guanidylated amino acid (**1**) followed a procedure reported by Feichtinger, et al. [25] Briefly, a flame-dried round bottom flask containing **1** mmol of the 1-heptanoic acid was diluted with 8 mL of anhydrous dichloromethane (DCM). Then, N-methyl-N-trimethylsilyl-trifluoroacetamide (2.2 mmol) was added, and the reaction was heated to reflux under an argon atmosphere. Upon clarification of the solution, it was cooled and triethylamine (1.1 mmol) and N,N'-di-Boc-N''-triflylguanidine (1.1 mmol) were added. The reaction was then stirred at room temperature for 4-5 hours, diluted with DCM and washed with brine and water. The organic phase was dried with sodium sulfate, concentrated and the product purified by column chromatography (eluted 50:50 ethyl acetate:hexanes). The purified yields ranged from 74-85%.

The preparation of the known isocyanide intermediate (**2**) followed literature precedent [26]. Briefly, 1, 4-diaminobutane (1, 4-DAB; 7.5 g, 85.08 mmol) was diluted in 30 mL of dioxane. Then, a solution of di-tert-butylidicarbonate (2.4 g, 11 mmol) in 30 mL of dioxane was then added drop- wise over 1.5 hours. This reaction was stirred for 24 hours and the solvent removed under vacuum. To this

mixture, 50 mL of water was added and the resulting insoluble material was removed by filtration. The filtrate was extracted three times with 45 mL of DCM. The organic layers were dried with sodium sulfate and concentrated to give a 56-61% yield. Next, the product (2 mmol) was diluted in 5 mL DCM and formic acid (2 mmol) was added to the stirring reaction. The reaction was then placed into an ice-bath. Once cooled, DIC (2 mmol) was added and the mixture stirred for 4 hours at room temperature. The reaction was filtered and the filtrate washed with saturated sodium bicarbonate. The organic layer was then dried with sodium sulfate and concentrated. The resulting product, tert-butyl (4-aminobutyl)-carbamate, was obtained in 90-92% yield. This product (8.7 mmol) was then diluted with 13 mL of DCM, triethylamine (26.2 mmol) was added and the solution was cooled in an ice-bath. POCl₃ (8.7 mmol) was then added drop-wise. The reaction was stirred for 30 minutes, followed by addition of potassium carbonate (8.7 mmol). The reaction was then stirred for another 30 minutes and the aqueous layer extracted five times with DCM, the organic layers combined, washed with water, dried with sodium sulfate, and concentrated. The final product was purified by flash column chromatography (eluting at 50:50 ethyl acetate: hexanes) giving a 72-76% yield

The synthesis of the known Fmoc-aminopropanal (**5**) followed the procedure of More, and Finney. [27] Briefly, Fmoc- β -alanine (3 mmol, 1 equiv) was added to a flame dried round bottom flask and diluted with 20 mL anhydrous DCM. Then,

triphenylphosphine (6 mmol, 2 equiv) and trichloroacetonitrile (6 mmol, 3 equiv) were added. After the Fmoc- β -alanine appeared to be consumed by TLC, N-O-dimethyl-hydroxylamine hydrochloride (6.3 mmol, 2.1 equiv) and pyridine (15 mmol, 5 equiv) were added at 0 °C. After 1 hour, the reaction was washed with brine and dried over sodium sulfate. After concentration, the product, N-methoxy-N-methyl-3-(Fmoc-amino)-propionamide, was purified by flash column chromatography (eluting at 50:50 ethyl acetate:hexanes) to give a 97% yield. Next, the N-methoxy-N-methyl-3-(Fmoc-amino)-propionamide (1.15 mmol, 1 eq) was dissolved in 10 mL anhydrous THF. The reaction was cooled to -78 °C under argon and 3.45 mL of a 1.0 M solution of diisobutylaluminum hydride (3 equiv) in THF was added drop-wise over 10 minutes. After 5 minutes the reaction was quenched with 5% HCl in EtOH, and allowed to warm to room temperature. This solution was diluted into DCM and washed with brine. The organic layers were dried over sodium sulfate and then concentrated under vacuum. The product was then purified by flash column chromatography (eluting with 50:50 ethyl acetate:hexanes) to afford Fmoc-3-amino-1-propanal in 62% yield. ¹H NMR (CDCl₃): δ 9.83 (1H, s), 7.78 (2H, d), 7.60 (2H, d), 7.33 (4H, m), 5.3 (1H, bs), 4.40 (2H, d), 4.20 (1H, t), 3.52 (2H, t), 2.76 (2H, t). [M+H]⁺ e: 296.12, o: 296.1.

3.4.2. Spergualin analog syntheses

The Ugi reaction was performed by mixing benzylamine (0.1 mmol), an aldehyde (**3a-e**; 0.1 mmol), 6-guanidinohexanoic acid (1; 1.1 mmol), and tert-butyl (4-isocyanobutyl)carbamate (2; 0.1 mmol) in 0.5 mL DMF. This reaction was heated to 100 °C for 20 minutes in a Biotage Initiator EXP microwave reactor. The products were treated with phosphoric acid and purified on silica. Each product (0.05 mmol, 1 equiv) was reacted with compound 5 (0.05 mmol, 1 equiv) in 2 mL THF and NaBH(OAc)₃ (0.07 mmol, 1.4 equiv) for 1.5 hours. The reactions were quenched with saturated sodium bicarbonate, the products extracted into ethyl acetate and purified on basic alumina oxide, eluting with 10:90 methanol:ethyl acetate. The remaining Fmoc groups were removed with 30 equiv of Tris-amine resin (Biotage) at room temperature. Finally, the benzyl group was removed by adding CAN (2.1 equiv) in a solution of 1:5 water:acetonitrile (2 mL). After stirring for 2 hours, the reaction was quenched with saturated sodium bicarbonate, stirred for 10 minutes and extracted with ethyl acetate. The organic layers were combined, dried over sodium sulfate and concentrated under vacuum. The product was then purified on basic alumina oxide (eluting at 10:90 methanol:ethyl acetate) to afford the final products. The overall purified yields ranged from 31-47%.

N-(2-((4-((3-aminopropyl)amino)butyl)amino)-1-methoxy-2-oxoethyl)-7-guanidinoheptanamide (**7a**). ¹³C NMR (100 MHz, methanol-d₆) 174.9, 166.1,

157.1, 91.3, 55.7, 53.0, 51.2, 46.9, 40.4, 39.8, 39.0, 37.3, 32.3, 28.5, 27.3, 26.8, 26.1, 24.7; ¹H NMR (CDCl₃) δ 8.16 (2H, s), 5.84 (1H, s), 4.61-4.38 (2H, d), 4.10-3.75 (2H, d), 3.31 (3H, d), 3.13 (2H, s), 2.70 (6H, s), 2.32-2.03 (8H, m), 1.64-1.51 (10H, m) 1.25-1.14 (4H, m). HPLC purity 90%

N-(2-((4-((3-aminopropyl)amino)butyl)amino)-1-(4-bromophenyl)-2-oxoethyl)-7-guanidinoheptanamide (**7b**). ¹³C NMR (100 MHz, methanol-d₆) 170.5, 168.2, 157.1, 137.8, 133.3, 133.7, 129.9, 129.6, 121.9, 57.9, 53.0, 51.2, 46.9, 40.5, 39.8, 39.5, 37.3, 32.1, 28.5, 27.3, 26.6, 26.1, 24.6; ¹H NMR (CDCl₃) δ 8.16 (2H, s), 7.79 (2H, d), 7.51 (2H, d), 5.82 (1H, s), 4.56-4.18 (4H, m), 4.15 (2H, s), 3.20 (2H, s), 3.05 (2H, s), 1.54-1.49 (6H, m), 1.19 (6H, s), 0.86 (2H, s). HPLC purity 81%

N-(1-((4-((3-aminopropyl)amino)butyl)amino)-1-oxo-4-phenylbutan-2-yl)-7-guanidinoheptanamide (**7c**). ¹H NMR (CDCl₃) δ 8.14 (2H, s), 7.67 (2H, m), 7.29 (2H, m), 7.10 (1H, m), 6.09 (1H, s), 5.82 (2H, s), 4.99 (1 H, s), 4.59 (2H, s), 4.38 (2H, d), 3.32-3.21 (4H, m), 3.12 (2H, d), 2.32 (1H, t), 2.05 (1H, s), 1.62-1.55 (8H, m), 1.52-1.41 (10H, m), 1.25 (2H, s), 1.12 (2H, s), 0.86 (2H, s). HPLC purity 80%

N-(1-((4-((3-aminopropyl)amino)butyl)amino)-1-oxo-4-phenylbutan-2-yl)-7-guanidinoheptanamide (**7d**). ¹³C NMR (100 MHz, methanol-d₆) 175.5, 169.5, 157.1, 52.3, 49.4, 48.6, 46.9, 40.4, 39.5, 38.7, 37.3, 32.3, 28.5, 27.3, 26.8, 26.1,

24.7; ¹H NMR (CDCl₃) δ 5.92 (1H, s), 4.61-4.57 (2H, d), 3.86-3.84 (2H, d), 3.60 (1H, s), 3.16-3.02 (8H, m), 2.38-2.35 (t, 2H), 2.28-2.24 (t, 1H), 1.97 (s, 1H), 1.61-1.53 (6H, m), 1.46-1.17 (8H, m), 0.86 (2H, s). HPLC purity 82%

3.4.3. High performance liquid chromatography

HPLC analysis for purity was performed using a Waters Spherisorb ODS2 analytical column (4.6x250mm), mobile phase: 5-80% ACN in water, sample load: 1 mg in 500 μL DMSO, flow rate: 2 mL/min, detection: 218 nm UV.

3.4.4. Thin-layer chromatography

The chemical stability of the spergualin derivatives was estimated by monitoring the integrity of the products by TLC. We found that this approach was better able to identify certain degradation products than HPLC. Briefly, compounds **7a-d** or spergualin were first suspended in dimethyl sulfoxide at a concentration of 20 mM, then diluted to 1 mM in aqueous buffer. Aliquots (~1 μL) were spotted on silica TLC plates and developed in a solvent mixture of butanol, water, pyridine, and acetic acid (3:2:1:1 v/v). Products were visualized with ninhydrin. The plates were then immediately scanned and the images quantified with NIH Image J. Results are the average of independent triplicates.

Notes

This work has been published as “Improved synthesis of 15-deoxyspergualin analogs using the Ugi multi-component reaction” *Bioorganic & Medicinal Chemistry Letters*, 2011. **21**(9): p. 2587-2590. Chris Evans and Jason Gestwicki designed the revised spergualin synthesis. Chris Evans and Matt Smith performed the experiments. JP Carolan helped with the syntheses and anti-bacterial assays. Chris Evans, Matt Smith and Jason Gestwicki analyzed the results and wrote the manuscript.

3.5. References

1. Takeuchi, T., et al., *A new antitumor antibiotic, spergualin: isolation and antitumor activity*. J Antibiot (Tokyo), 1981. **34**(12): p. 1619-21.
2. Umeda, Y., et al., *Synthesis and antitumor activity of spergualin analogues. I. Chemical modification of 7-guanidino-3-hydroxyacyl moiety*. J Antibiot (Tokyo), 1985. **38**(7): p. 886-98.
3. Thomas, F.T., et al., *15-Deoxyspergualin: a novel immunosuppressive drug with clinical potential*. Ann N Y Acad Sci, 1993. **685**: p. 175-92.
4. Evans, C.G., L. Chang, and J.E. Gestwicki, *Heat Shock Protein 70 (Hsp70) as an Emerging Drug Target*. Journal of Medicinal Chemistry, 2010. **53**(12): p. 4585-4602.
5. Umezawa, H., et al., *Structure of an antitumor antibiotic, spergualin*. J Antibiot (Tokyo), 1981. **34**(12): p. 1622-4.
6. Umeda, Y., et al., *Synthesis and antitumor activity of spergualin analogues. II. Chemical modification of the spermidine moiety*. J Antibiot (Tokyo), 1987. **40**(9): p. 1303-15.
7. Umeda, Y., et al., *Synthesis and antitumor activity of spergualin analogues. III. Novel method for synthesis of optically active 15-deoxyspergualin and 15-deoxy-11-O-methylspergualin*. J Antibiot (Tokyo), 1987. **40**(9): p. 1316-24.
8. Kaufman, D.B., *15-Deoxyspergualin in experimental transplant models: a review*. Transplant Proc, 1996. **28**(2): p. 868-70.
9. Nadler, S.G., et al., *Interaction of the immunosuppressant deoxyspergualin with a member of the Hsp70 family of heat shock proteins*. Science, 1992. **258**(5081): p. 484-6.
10. Nadeau, K., et al., *Quantitation of the interaction of the immunosuppressant deoxyspergualin and analogs with Hsc70 and Hsp90*. Biochemistry, 1994. **33**(9): p. 2561-7.
11. Nadler, S.G., et al., *Elucidating the mechanism of action of the immunosuppressant 15-deoxyspergualin*. Ther Drug Monit, 1995. **17**(6): p. 700-3.
12. Asano, K., et al., *Inhibitory action of deoxyspergualin on effector/memory T cell generation during Hymenolepis nana infection in mice*. Immunology Letters, 1996. **53**(1): p. 51-57.
13. Lebreton, L., et al., *Structure-immunosuppressive activity relationships of new analogues of 15-deoxyspergualin. 1. Structural modifications of the hydroxyglycine moiety*. J Med Chem, 1999. **42**(2): p. 277-90.
14. Lebreton, L., et al., *Structure-immunosuppressive activity relationships of new analogues of 15-deoxyspergualin. 2. Structural modifications of the spermidine moiety*. J Med Chem, 1999. **42**(23): p. 4749-63.
15. Simpson, D., *Tresperimus: a new agent for transplant tolerance induction*. Expert Opin Investig Drugs, 2001. **10**(7): p. 1381-6.

16. Ohlman, S., et al., *Pharmacokinetics of 15-deoxyspergualin studied in renal transplant patients receiving the drug during graft rejection*. *Transpl Int*, 1994. **7**(1): p. 5-10.
17. Kondo, S., et al., *The total synthesis of spergualin, an antitumor antibiotic*. *J Antibiot (Tokyo)*, 1981. **34**(12): p. 1625-7.
18. Bergeron, R.J.a.M., J.S., *Total Synthesis of 15-Deoxyspergualin*. *J Org Chem*, 1987. **52**(9): p. 1700-03.
19. Durand, P., Richard, P., and Renaut, P., *(-)-15-Deoxyspergualin: A New and Efficient Enantioselective Synthesis Which Allows the Definitive Assignment of the Absolute Configuration*. *J Org Chem*, 1998. **63**(26): p. 9723-27.
20. Durand, P., P. Peralba, and P. Renaut, *A new efficient synthesis of the immunosuppressive agent (±)-15-deoxyspergualin*. *Tetrahedron*, 2001. **57**(14): p. 2757-2760.
21. Marcaccini, S. and T. Torroba, *The use of the Ugi four-component condensation*. *Nat Protoc*, 2007. **2**(3): p. 632-9.
22. Wang, W. and A. Domling, *Efficient synthesis of arrays of amino acid derived Ugi products with subsequent amidation*. *J Comb Chem*, 2009. **11**(3): p. 403-9.
23. Lew, A., et al., *Increasing rates of reaction: microwave-assisted organic synthesis for combinatorial chemistry*. *J Comb Chem*, 2002. **4**(2): p. 95-105.
24. Ugi, I. and S. Heck, *The multicomponent reactions and their libraries for natural and preparative chemistry*. *Comb Chem High Throughput Screen*, 2001. **4**(1): p. 1-34.
25. Feichtinger, K., Zapf, C., Sings, H.L., and Goodman, M., *Diprotected Triflylguanidines: A New Class of Guanidinylation Reagents*. *J Org Chem*, 1998. **63**(12): p. 3804-05.
26. Xu, P.Z., Ting; Wang, Wenhao; Zou, Xiaomin; Zhang, Xin; Fu, Yiqiu, *Synthesis of PNA Monomers and Dimers by Ugi Four-Component Reaction*. *Synthesis*, 2003. **2003**(8): p. 1171-76.
27. More, J.D. and N.S. Finney, *A Simple and Advantageous Protocol for the Oxidation of Alcohols with o-Iodoxybenzoic Acid (IBX)*. *Org Lett*, 2002. **4**(17): p. 3001-3003.
28. Abdel-Magid, A.F., et al., *Reductive Amination of Aldehydes and Ketones with Sodium Triacetoxyborohydride. Studies on Direct and Indirect Reductive Amination Procedures(1)*. *J Org Chem*, 1996. **61**(11): p. 3849-3862.
29. Carpino, L.A., Sadat-Aalae, D., and Beyermann, M., *Tris(2-aminoethyl)amine as a Substitute for 4-(Aminomethyl)piperidine in the Fmoc/Polyamine Approach to Rapid Peptide Synthesis*. *J Org Chem*, 1990. **55**(5): p. 1673-1675.
30. Bull, S.D., Davies, S.G., Fenton, G., Mulvaney, A.W., Prasad, R.S., and Smith, A.D., *Chemoselective debenzoylation of N-benzyl tertiary amines*

with ceric ammonium nitrate. J Chem Soc, Perkin Trans I, 2000. **2000**(22): p. 3765-3774.

31. Nishizawa, R., et al., *Synthesis and biological activity of spergualin analogues. I.* J Antibiot (Tokyo), 1988. **41**(11): p. 1629-43.
32. Hibasami, H., et al., *Bactericidal effect of 15-deoxyspergualin on Staphylococcus aureus.* Chemotherapy, 1991. **37**(3): p. 202-5.
33. Dömling, A. and I. Ugi, *Multicomponent Reactions with Isocyanides.* Angewandte Chemie International Edition, 2000. **39**(18): p. 3168-3210.

Chapter 4

Spergualin analogs as novel inhibitors of the Hsp70/CHIP protein-protein interaction

4.1. Abstract

The molecular chaperone Hsp70 sits at a critical junction in protein homeostasis. Through concerted interactions with a number of co-chaperones, Hsp70 can promote either the stability or degradation of its client proteins. There is growing interest in using chemical probes to better understand the specific roles played by Hsp70's co-chaperones. Here, we describe an analog of the natural product spergualin that inhibits binding of Hsc70 to the co-chaperone, C-terminus of Hsc70 interacting protein (CHIP), an E3 ubiquitin ligase involved in degradation of Hsc70 clients. This compound directly blocked the protein-protein interaction between Hsc70 and CHIP *in vitro* and it caused accumulation of the Hsc70 client protein, tau, in cells. This work provides the first small molecule inhibitor of the Hsc70-CHIP interaction and provides insight into the role of this complex in protein homeostasis.

4.1.1. Protein-protein interactions in the Hsp70 system

As discussed briefly in Chapter 1, Heat-shock protein 70 (Hsp70) is an essential and ubiquitous molecular chaperone that protects the proteome by binding to exposed hydrophobic regions in unfolded proteins [1, 2]. In this task, Hsp70 relies on a number of co-chaperone proteins, which are divided into three classes based on their functionality and mode of binding to Hsp70. Members of the J-domain superfamily of co-chaperones have the dual function of presenting protein substrates to Hsp70 and facilitating hydrolysis of ATP, thereby increasing affinity for substrate [3]. Nucleotide exchange factors (NEFs) potentiate the release of ADP and subsequent substrate release [4, 5]. Finally, tetratricopeptide repeat (TPR) domain-containing proteins are thought to bind to Hsp70 and dictate the fate of the bound substrate, facilitating either protein refolding or degradation [6, 7]. Though recent studies have elucidated how these TPR proteins bind Hsp70 [8], the mechanism of how they arbitrate between these two very important but dichotomous paths remains completely unresolved.

4.1.2. The C-terminus of Hsp70 acts as a hub for TPR protein binding

The TPR domain is a common motif that facilitates protein-protein interactions in a wide range of organisms, from bacteria to humans [9]. The structure of the domain consists of multiple repeats of a degenerate 34 amino acid consensus sequence that forms a basic helix-turn-helix fold [8]. These repeats assemble into anti-parallel α helices with an overall super-helical structure and ligands typically

bind to the concave surface of this super-helix. These ligands of TPR domains are often short, elongated peptide sequences [10]. For example, the last four amino acids of Hsp70 (EEVD) have been shown to bind to the TPR domain of the co-chaperone Hop (Hsp70/90-organizing protein) [8]. And, as mentioned in Chapter 2, the EEVD motif has been shown by our group to account for ~80% of the binding affinity for the Hsp70-CHIP interaction.

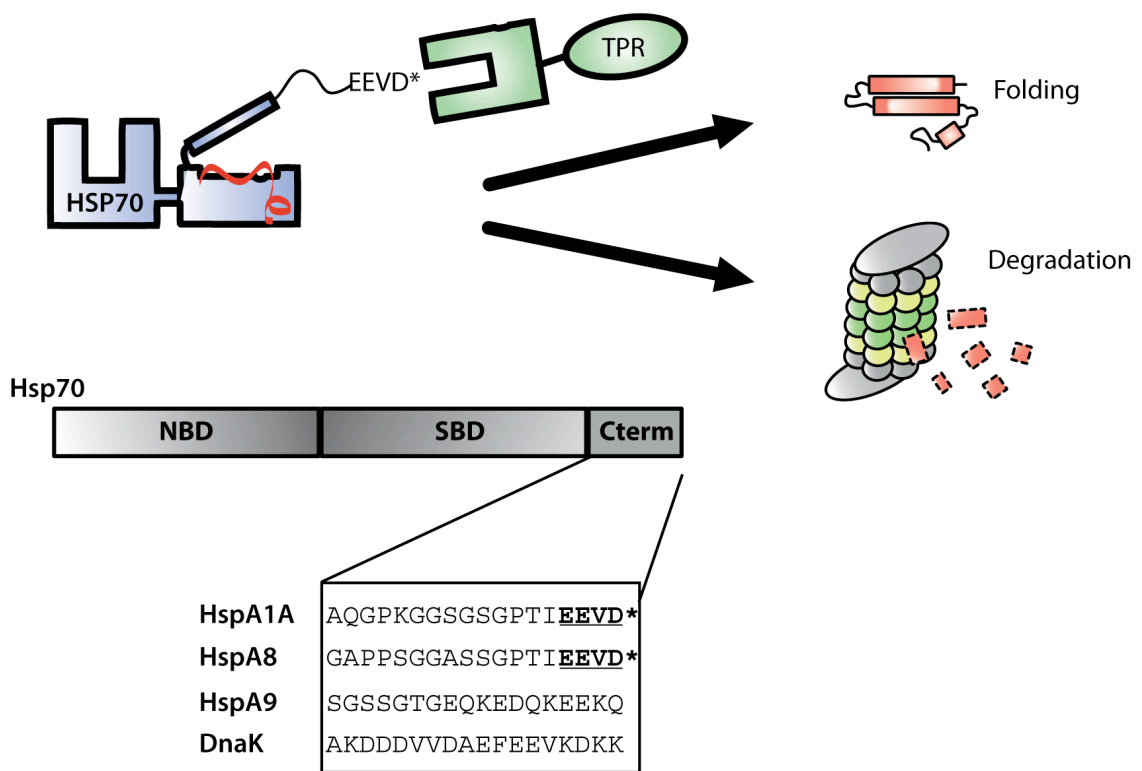


Figure 4.1 TPR-proteins coordinate substrate fate. The extreme C-terminal EEVD sequence of Hsp70 (HspA1A) and Hsc70 (HspA8) facilitate binding to TPR domain containing co-chaperones like HOP and CHIP which facilitate folding or degradation, respectively. Notably, mitochondrial Hsp70 (HspA9) or the prokaryotic Hsp70 (DnaK) do not bind TPR domains using this C-terminal motif.

Through this EEVD-TPR interaction, Hsp70 recruits TPR-domain co-chaperones that are essential for carrying out chaperone functions. For example, CHIP links

Hsp70 and its substrates to the proteasome, while HOP allows for the transfer of substrates to the Hsp90 system for further folding (**Figure 4.1**) [11]. Furthermore, it has been well established that only one TPR-domain co-chaperone can bind to Hsp70 at a time [6, 7, 12] suggesting that this interaction may represent a critical step in the triage decision process. Because this protein-protein interaction (PPI) is a nexus for Hsp70 biology, it has drawn considerable interest among chemical biologists as a point for chemical intervention [13, 14]. However, there are few small molecule inhibitors of the TPR interaction and their mechanisms remain unclear. The goal of this Chapter is to determine whether spergualin analogs might serve as a new chemical scaffold for building inhibitors of this important PPI.

4.1.3. Spergualin analogs bind to the C-terminus of Hsp70

Spergualin is a natural product produced by *Bacillus laterosporus*, which was originally found to have antitumor and antibiotic activity [15]. Early structural efforts revealed that spergualin is a polyamine-derived natural product [16] and structure-activity studies produced 15-deoxyspergualin (15-DSG) [17], which has superior stability. Subsequent efforts showed that 15-DSG has potent immunosuppressive activity [18], and this compound was granted clinical approval for the treatment of acute allograft rejection in Japan [19]. Target identification studies suggested that 15-DSG binds to Hsp70 [20] and further mass spectrometry and crosslinking studies suggested that the likely binding site

is in the C-terminal EEVD motif [21]. Because of the importance of the EEVD motif in binding TPR domain proteins (Chapter 2), we considered it possible that this compound might block the protein-protein interaction (PPI) between Hsp70 and its TPR co-chaperones. To allow these inquiries, we described (in Chapter 3) an improved synthesis of spergualin analogs. In this Chapter, we deploy these analogs to test whether this scaffold inhibits the Hsp70-CHIP interaction.

4.2. Results

4.2.1. A spergualin analog inhibits binding of Hsp70 to CHIP

In a previous study (Chapter 2), we developed a fluorescence-quenching assay to characterize the interaction between CHIP and Hsc70 (the constitutively expressed isoform of the Hsp70 family). In this assay, the quenching of a fluorophore is measured upon mixing of labeled Hsc70 and CHIP (**Figure 4.2**). The apparent K_d for the Hsc70-CHIP interaction was calculated to be 76 ± 11 nM (**Figure 4.2A**). We therefore used this assay to test spergualin analogs for the ability to inhibit this PPI. As a first test of this idea, we incubated labeled Hsc70 ($0.05 \mu\text{M}$) and CHIP ($0.08 \mu\text{M}$) with compound **1**, a spergualin analog that has been reported to bind Hsc70 [22]. This compound weakly ($\text{IC}_{50} = 131 \pm 13 \mu\text{M}$) inhibited the Hsc70-CHIP interaction (**Figure 4.2B**), suggesting for the first time, that spergualin analogs can inhibit the binding of Hsc70 to a TPR co-chaperone.

Next, we tested which regions of spergualin might be important for this activity.

Previous attempts to acquire structure-activity relationships (SAR) in the spergualin series relied primarily on data from murine models, such that pharmacokinetics and metabolic stability would contribute to the apparent SAR. We wanted to re-explore this issue using our *in vitro* assay to generate SAR

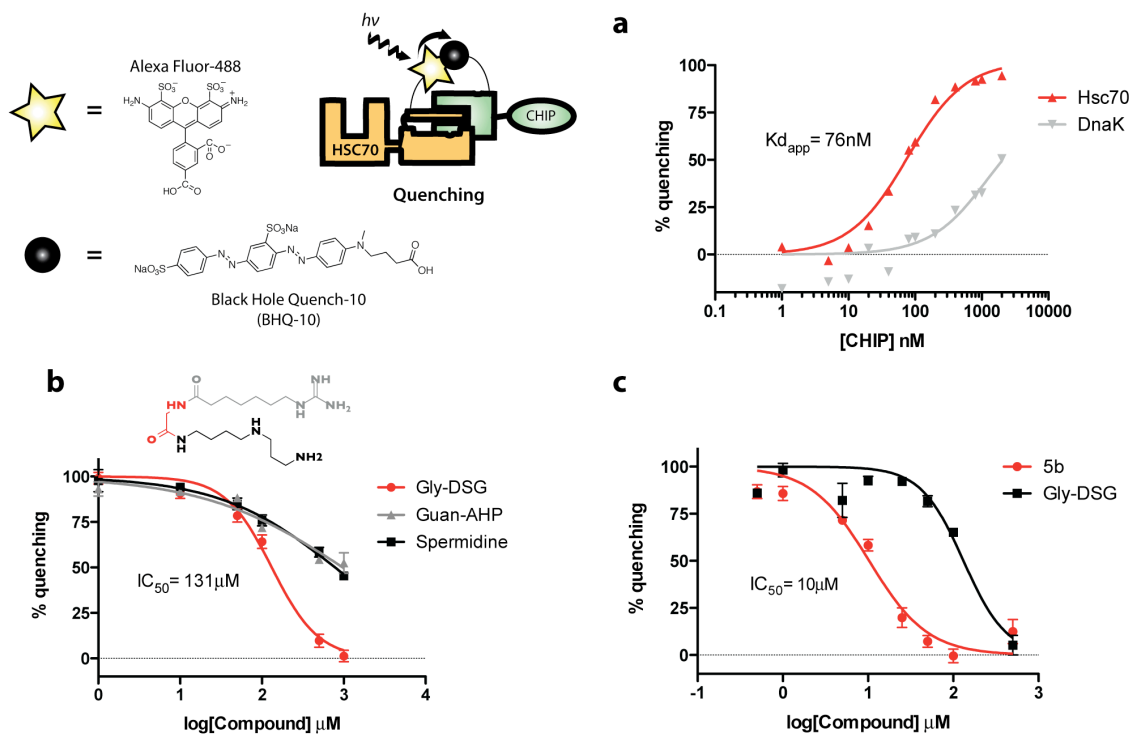
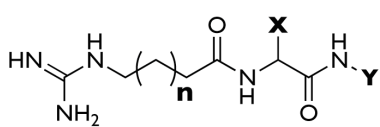
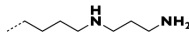
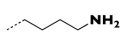


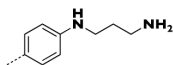
Figure 4.2 Spergualin analogs inhibit the Hsc70-CHIP PPI by FRET. A quenching assay was developed to monitor the interaction between Hsc70 and CHIP. (a). At 50 nM Hsc70, CHIP has an apparent K_d of ~80 nM. DnaK, which doesn't bind to CHIP shows a much lower affinity in this assay, with an estimated K_d in the low micromolar. (b). At 50 nM Hsc70 and 80 nM CHIP, the spergualin derivative Gly-DSG (1) inhibited this PPI with an IC_{50} of ~130 μM . Both ends of the molecule are necessary for binding as guanidylated amino acid (grey) or spermidine (black) had no effect. (c). Screening a small library of analogs revealed an inhibitor with an IC_{50} 10x higher than the literary compound (1). Each data point is the average of triplicates and the error bars represent the standard error of the mean (SEM).

focused more directly on the inhibition of the Hsc70-CHIP PPI. Our initial studies revealed that the α -acylamino carboxamide core is essential for activity, as neither side of the core, 7-gaunidinoheptanoic acid nor spermidine, in isolation, show significant inhibition (IC_{50} 's $\gg 500 \mu M$; **Figure 4.2B**).

Table 4.1 Characterization of compound effect in fluorescence quenching assay


$Y_1 =$


$Y_2 =$


$Y_3 =$


compd	n	X	Y	FRET IC ₅₀ (μM)
1/Gly-DSG	4	H	1	132 ± 13
2a	1	-CH ₃	1	74 ± 18
2b	3	-CH ₃	1	48 ± 13
2c	4	-CH ₃	1	85 ± 25
3a	1	-(CH ₂) ₂ -phenyl	1	29 ± 6
3b	3	-(CH ₂) ₂ -phenyl	1	179 ± 61
3c	4	-(CH ₂) ₂ -phenyl	1	76 ± 16
4a	1	-OMe	1	172 ± 52
4b	3	-OMe	1	265 ± 49
4d	3	-OMe	2	>500
4e	3	-OMe	3	184 ± 32
5a	1	-(4-Br)-phenyl	1	62 ± 7
5b	3	-(4-Br)-phenyl	1	10 ± 1
5d	3	-(4-Br)-phenyl	2	11 ± 3
5e	3	-(4-Br)-phenyl	3	74 ± 15
6	3	-sec-butyl	1	253 ± 47
7	3	-(3-OH)-phenyl	1	>500
8	3	-(3,5-OMe)-phenyl	1	48 ± 8
9	3	-(4-BnO)-phenyl	1	22 ± 4
Guan-AHP	--	--	--	>500
Spermidine	--	--	--	>500

4.2.2. Screen of spergualin library reveals a potent inhibitor

Guided by these initial findings, we expanded the chemical series of spergualin

analogues and tested them in the fluorescence assay (**Table 4.1**). We focused this series on varying the 11-position and varying the lengths of the regions adjacent to the carboxamide core, because early studies suggested that these positions are important for *in vivo* activity. From the IC₅₀ values of the compounds in this series, it appears that adding bulk to the 11-position (compounds **5a-e** and **9**) significantly increased potency. Further, with these bulky substitutions, the full spermidine moiety was dispensable for activity (compare compounds **4b**, **4d** to **5b**, **5d**). The most potent compounds were **5b** and **5d**, which both have the 11-position (4-Bromo)-phenyl substitution and an IC₅₀ value of ~10 μM. These compounds were approximately 10-fold more potent than the initial compound **1** (**Figure 4.2C**). Thus, we decided to use compound **5b** to further explore the mechanism of spergualin activity on the Hsc70-CHIP interaction.

4.2.3. Spergualin analog disrupts the Hsc70-CHIP interaction by size-exclusion chromatography

To confirm the inhibitory activity seen in the quenching assay, we explored whether compound **5b** could disrupt the Hsc70-CHIP complex by gel filtration. The elution pattern of Hsc70 alone, and in complex with CHIP is shown in **Figure 4.3A**. At a 2:1 molar ratio for Hsc70:CHIP, approximately half of the Hsc70 was in complex with CHIP, and so we used this molar ratio to characterize compound administration. Because the protein concentration in the gel filtration platform is 40 fold higher than what was used in the fluorescence quenching assay, we

increased the compound concentration to 500 μ M and tested for inhibition. Compound **5b** showed a clear decrease in the amount of complex formation when compared to a DMSO control or administration of a negative control compound spermidine (**Figure 4.3B**). Compound **5d** showed a very similar effect at the same concentration (**Figure 4.3C**). Taken together, these data confirm that spergualin analogs inhibit binding of Hsc70 to CHIP.

4.2.4. The effect of Spergualin analogs on other Hsp70 PPIs

Spergualin analogs have been shown to modestly inhibit single-turnover ATP hydrolysis of Hsc70 in the presence of a J domain co-chaperone [23]. Thus, we wanted to test whether compound **5b** might disrupt the binding of a J protein. Using our quenching assay to monitor the interaction of the prokaryotic Hsp70, DnaK, to its J protein co-chaperone, DnaJ, (**Appendix 4.5.1**), we found that compound 5b had no effect on this PPI ($IC_{50} > 500 \mu$ M; **Figure 4.4A**). In contrast, the small molecule myricetin, has been shown to be a potent inhibitor of DnaK-DnaJ interactions in this assay [24].

Next, we tested whether spergualin analogs would impact the ATPase activity of Hsp70 using a well known malachite green (MG) assay [25, 26]. This assay measures the stimulation of Hsc70 ATPase activity by J protein co-chaperones. Consistent with previous reports of 15-DSG's activity towards Hsc70 [23], none of the compounds tested had any effect on the ATPase activity of Hsc70 stimulated

by a purified J domain (**Figure 4.4B**). These data suggest that spergualin analogs block the Hsc70-CHIP interaction but they do not effect ATP turnover or

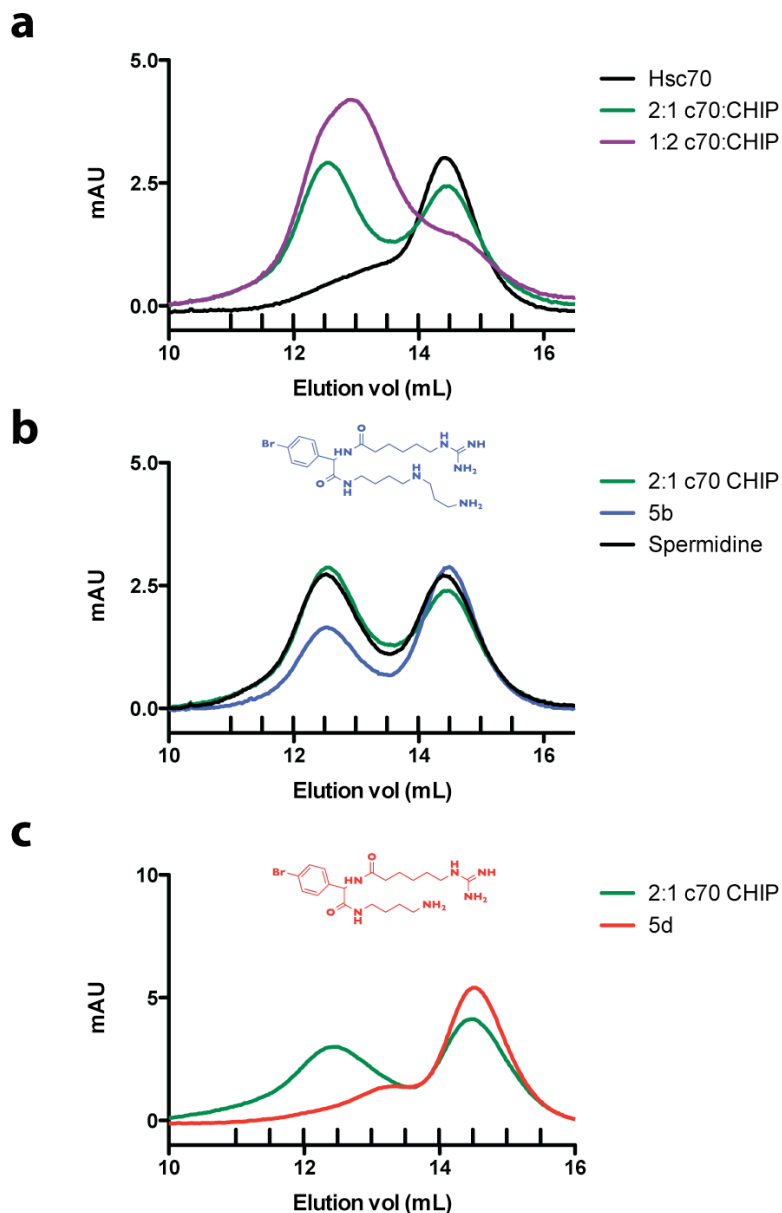


Figure 4.3 Inhibitory effect of compound seen by gel filtration. (a). Elution pattern of Hsc70 alone, a 2:1, or a 1:2 molar ratio of Hsc70 to CHIP. The 2:1 ratio (green) shows both proteins in complex and Hsc70 alone. (b). Addition of 500 μ M compound **5b** shows a reduction in the amount of Hsc70 and CHIP in complex (blue). (c) Addition of 500 μ M compound **5d** shows a similar effect.

interactions with J proteins.

Due to the mutually exclusive manner in which TPR proteins have been shown bind to Hsc70, we decided to investigate whether compound **5b** might disrupt other Hsc70-TPR interactions. In order to accomplish this, we adapted the fluorescence quench assay to monitor the binding between Hsc70 and Hop (Hsp70-90 organizing protein) and the immunophilin FKBP51. Both proteins show moderate affinity for Hsc70 having similar apparent K_d 's ($\sim 140 \mu\text{M}$) (**Appendix 4.5.1**). Compound **5b** inhibited both interactions, with IC_{50} values in the mid-micromolar (22 ± 1.0 and $18 \pm 2.0 \mu\text{M}$ respectively; **Figure 4.4C-D**). This is very similar to the potency of this compound towards inhibiting Hsc70-CHIP, suggesting that it is a pan-inhibitor of Hsc70-TPR PPIs.

4.2.5. Spergualin binds the C-terminus of Hsc70

To gain further mechanistic information about how spergualin analogs might block the EEVD-TPR interaction, we explored the binding of compound **5b** to Hsc70 by NMR. Guided by the previous studies using mass spectrometry, we focused on the C-terminal region of Hsc70 (residues 391 to 647). This region includes the beta-sandwich domain, which binds to Hsc70 substrates and the "lid" region, which contains the EEVD motif. ^{15}N TROESY NMR spectra were recorded of this construct in phosphate buffer (150 mM NaCl, 50 mM sodium phosphate, pH = 7) at $200 \mu\text{M}$. Assignment of this construct is still ongoing, but we observed a clearly defined region consistent with the beta sandwich domain and a more flexible region consistent with the lid. Titration of compound **5b** into

this system revealed a number of discrete chemical shift perturbations (data not shown), with the most dramatic shifts in the lid and a few shifts in the beta-sandwich. Although definition of this binding site awaits assignment of the spectra, these results strongly support the idea that the spergualin scaffold binds to the C-terminus of Hsc70.

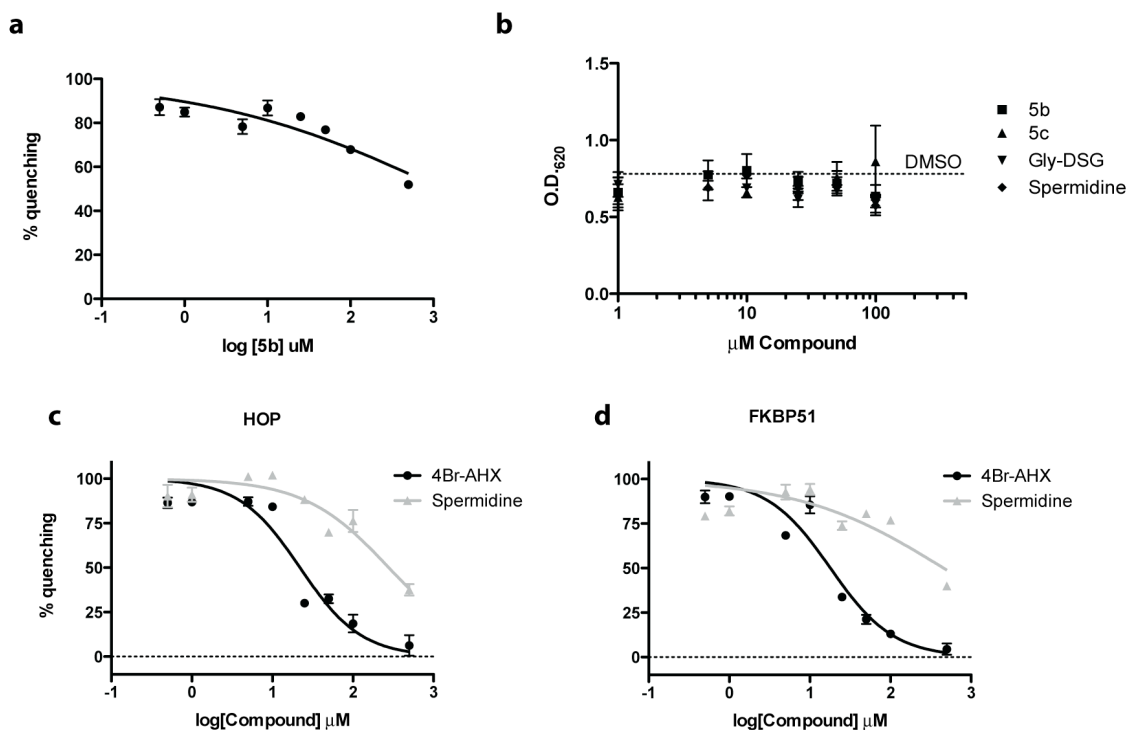


Figure 4.4 Compound effect on Hsc70 PPIs. (a). At 50 nM Alexa-488 DnaK and 2 μ M BHQ-10 DnaJ, compound **5b** shows no inhibitory effect towards this interaction. (b). All compounds tested showed no modulation of the J-mediated steady-state ATPase rate of Hsc70. (c-d). At 50 nM Hsc70, compound **5b**, but not spermidine shows an inhibitory effect towards both HOP and FKBP51 (both at 150 nM) with an IC₅₀ of 18 and 22 μ M, respectively. Each data point is the average of triplicates and the error bars represent the standard error of the mean (SEM).

4.2.6. Spergualin analog inhibits the Hsp70-TPR interactions in cells

Having established that compound **5b** inhibited Hsc70-TPR interactions *in vitro*, we next wanted to investigate whether this effect was maintained in the more complex environment of the cell. To test this idea, we transiently transfected

HeLa cells with HA-tagged constructs of either CHIP, HOP or FKBP51 (**Figure 4.5A**). We then performed co-immunoprecipitation experiments using Sepharose-immobilized anti-HA antibody and probed for the presence of Hsc70 (**Figure**

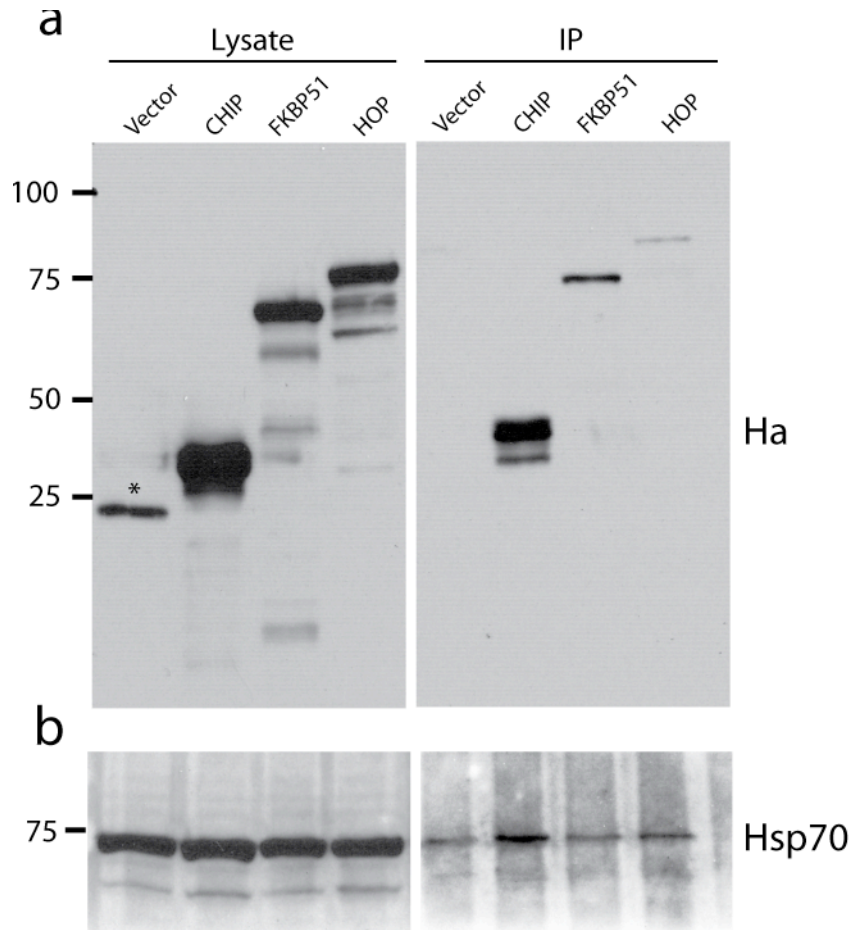


Figure 4.5 The cellular disruption of Hsc70 PPIs by compound 5b. (a) HeLa cells were transiently transfected with Ha-tagged CHIP, FKBP51 and HOP. Immunoprecipitation with 3 mg total lysate using Ha-Sepharose shows enrichment for Ha-proteins over vector control. *Nonspecific band. (b). Hsp70 is pulled down with TPR proteins CHIP, HOP and FKBP51.

4.5B). This experiment confirmed that Hsc70 binds these TPR co-chaperones in HeLa cells. Tests using the spergualin analogs are ongoing, but we expect that they will reduce the levels of precipitated Hsc70, which would confirm inhibition of

the Hsc70-TPR interaction.

4.2.7. Inhibition of the Hsc70-CHIP interaction in cells causes Tau accumulation

One of the important cellular targets of the Hsc70-CHIP complex is the microtubule-associated protein tau (MAPT; tau) [27]. For example, depletion of CHIP elevates tau levels in both a HeLa cell model of tau overexpression and mouse brain homogenates [27, 28]. Thus, we reasoned that spergualin analogs might elevate tau levels in cells, if they block CHIP function by inhibiting the Hsc70-CHIP PPI. Consistent with this idea, compound **5b** increased tau levels in these cells with an EC₅₀ value of approximately 5 μ M (**Figure 4.6A**), Compound **1** also showed modest activity in this assay (**Appendix 4.5.2**), whereas spermidine had no effect (**Figure 4.6C**). Interestingly, compound **5d**, which lacks the full polyamine portion of the molecule, also did not have any activity in the cell culture model (**Figure 4.6B**). Because this compound had activity *in vitro*, this result suggests that the spermidine moiety may be required for membrane permeability [29]. These studies suggest that spergualin analogs capable of blocking the Hsc70-CHIP interaction will be useful probes of this important chaperone PPI.

4.3. Discussion

4.3.1. Rational design of a novel Hsc70 inhibitor

Due to its central role in Hsc70 substrate processing, the Hsc70-TPR PPI has become a promising target for modulating chaperone activity. However, progress towards inhibitors of this interaction is in its early stages. One promising scaffold

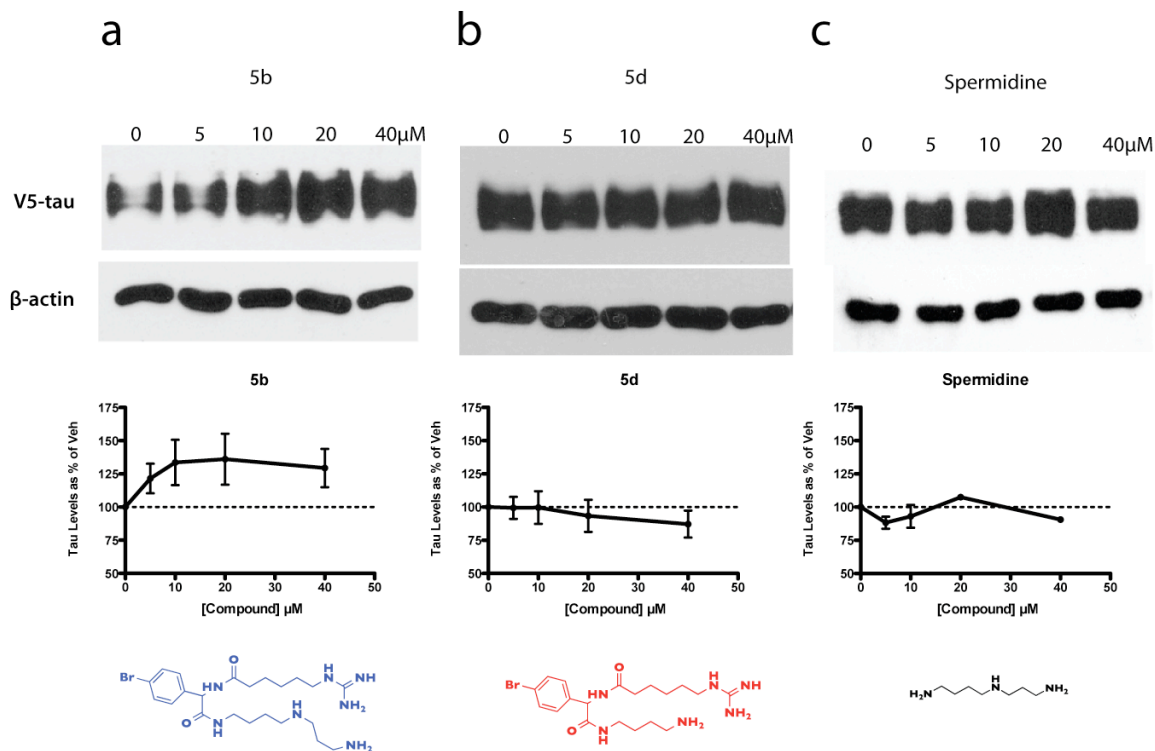


Figure 4.6 Compound administration causes tau accumulation. (a) Administration of compound **5b** to HeLa cells expressing MAPT (tau) produced a significant increase in tau burden. This effect was not seen with either compound **5d** (b) or spermidine (c). Each data point is the average of triplicates and the error bars represent the standard error of the mean (SEM).

is 15-DSG, because spergualin analogs have been shown to bind the EEVD motif of Hsc70 and this compound targets the Hsc70 complex [30]. Using a newly developed synthetic route, we produced a small library of spergualin analogs and found that they could indeed inhibit the interaction between Hsc70 and CHIP, using either a fluorescence assay, gel filtration or an NMR experiment. In this chemical series, we found that substituting the 11-position with significant bulk

significantly improved potency, resulting in compounds **5b** and **5d**. These compounds appear to block the Hsc70-TPR interaction in cells, because compound **5b** caused the accumulation of the Hsc70-CHIP client protein, tau.

Taken together, these data suggest that spergualin derivatives are promising inhibitors of the PPI between Hsc70 and TPR co-chaperones. Notably, this inhibitory effect is not limited to CHIP. Rather, interactions with both HOP and FKBP51 were also sensitive. An interesting future direction will be building selectivity into the spergualin scaffold, a task that will be made much more amenable once binding site information is available.

4.3.2. Re-investigating a promising chemical scaffold

One of the other interesting conclusions of this study is that spergualins might possess biological activity, in part, due to their activity at the Hsp70-TPR interface. It has been over 20 years since the first successful clinical trial involving the spergualin derivative 15-DSG was published [19, 31]. And yet, there has been surprisingly little mechanistic understanding as to how 15-DSG functions at a biochemical level. Spergualin analogs have been reported to have anti-tumor, immunosuppressive, anti-infective and anti-malarial activity [15, 32-34]. How can this compound impact so many different systems? One possibility is that some or all of these biological responses might arise from inhibition of Hsp70 PPIs. This speculative model remains untested. However, the studies

provided here, in combination with the results in Chapter 2 and 3, provide a framework for developing potent inhibitors of Hsp70-TPR interactions.

4.3.3. Conclusions

This work describes the discovery of the first well-characterized inhibitor of the Hsc70-TPR interaction and establishes the framework for using the spergualin scaffold to probe the roles of this PPI in protein homeostasis. Even with the lack

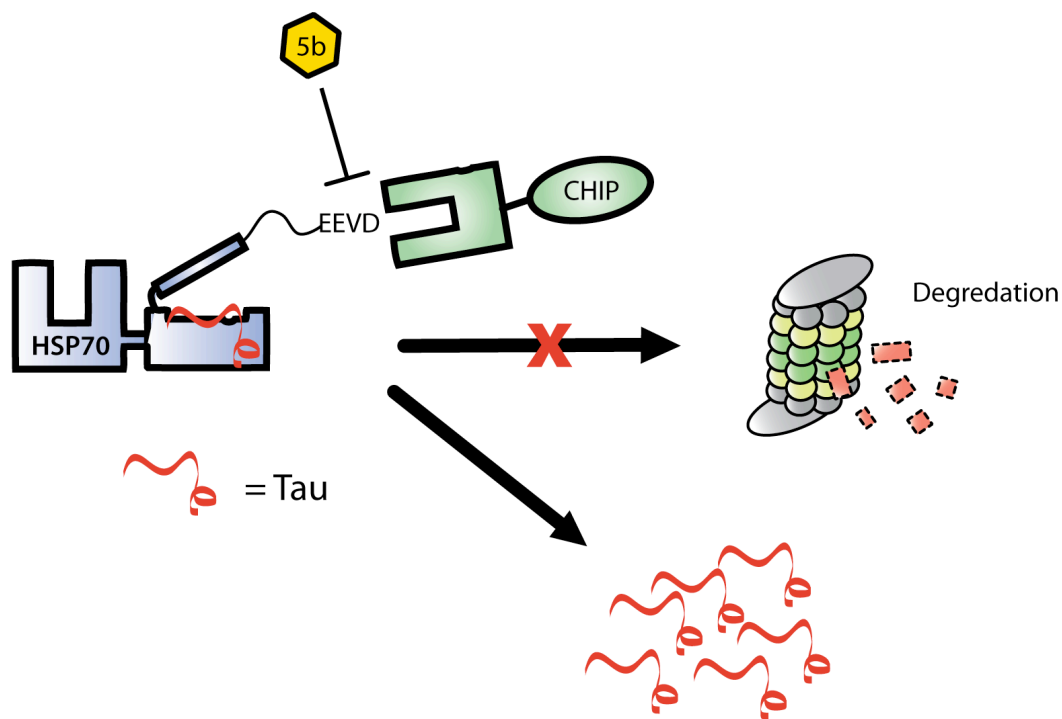


Figure 4.7 Model of compound 5b activity. Certain substrates of Hsc70, such as MAPT (tau) may have dedicated TPR proteins that preferentially dictate the fate of the protein. Tau is preferentially degraded by CHIP and blockade of the Hsc70-CHIP interaction inhibits this degradation leading to tau accumulation in cells.

of specificity, compound administration caused the accumulation of the client protein, tau, in cellular assays. This remarkable result suggests that some Hsc70

clients (i.e. tau) may have dedicated TPR proteins (i.e. CHIP) that preferentially mediate their fate (**Figure 4.7**). Thus, the current study provides a foundation from which to build more selective and potent inhibitors to continue to probe this important PPI. Strategies for achieving this goal are discussed in detail in Chapter 5.

4.4. Materials and methods

4.4.1. Reagents and general syntheses

Reagents and solvents were purchased from Sigma-Aldrich and used without further purification. All NMR spectra were collected on a Varian 400 MHz system. The syntheses for all starting materials have been previously described [35]. Briefly, guanidylated amino acid was prepared from the condensation of either (1 mmol) 1-aminoheptanoic, 1-aminohexanoic, or 1-aminobutanoic acid and (1.1 mmol) N,N'-di-Boc-N''-triflylguanidine, followed by purification by flash chromatography [36]. The isocyanide intermediate was made via reduction of the carbamate moiety generated from either 1,4-diaminobutane or p-phenylenediamine using 1 equivalent POCl₃ in dry dichloromethane [37] and subsequent purification via flash chromatography. Finally, the synthesis of the known Fmoc-aminopropanal followed the procedure of More and Finney [38]. This synthesis is accomplished by the reduction of Fmoc-β-alanine to its corresponding aldehyde using diisobutylaluminum hydride and purification by flash chromatography.

4.4.2. Spergualin analog syntheses

Full details of the spergualin synthesis has been published elsewhere [35]. For the molecules described in this study, the Ugi reaction was performed by mixing benzylamine (0.1 mmol), an appropriate aldehyde (0.1 mmol), guanidylated amino acid (1.1 mmol), and tert-butyl (4-isocyanobutyl)carbamate or tert-butyl (4-isocyanophenyl)carbamate (0.1 mmol) in 0.5 mL DMF. This reaction was heated to 100 °C for 20 minutes in a Biotage Initiator EXP microwave reactor. The products were deprotected with phosphoric acid, followed by neutralization to pH 7 with 10% NaOH and purification on basic alumina oxide. Each product (0.05 mmol, 1 equiv) was either reacted with Fmoc-aminopropanal (0.05 mmol, 1 equiv) in 2 mL THF and NaBH(OAc)₃ (0.07 mmol, 1.4 equiv) for 1.5 hours or deprotected completely to the final product. The reactions were quenched with saturated sodium bicarbonate, the products extracted into ethyl acetate and purified on basic alumina oxide, eluting with 10:90 methanol:ethyl acetate. The remaining Fmoc groups were removed with 30 equiv of Tris-amine resin (Biotage) at room temperature. Finally, the benzyl group was removed by adding Ceric ammonium nitrate (2.1 equiv) in a solution of 1:5 water:acetonitrile (2 mL). After stirring for 2 hours, the reaction was quenched with saturated sodium bicarbonate, stirred for 10 minutes and extracted with ethyl acetate. The organic layers were combined, dried over sodium sulfate and concentrated under vacuum. The product was then purified on basic alumina oxide (eluting at 10:90

methanol:ethyl acetate) to afford the final products. The overall purified yields ranged from 31-47%.

4.4.3. Characterization of spergualin analogs

N-(1-((4-((3-aminopropyl)amino)butyl)amino)-1-oxo-4-phenylbutan-2-yl)-7-guanidinoheptanamide (**1**). ¹³C NMR (100 MHz, methanol-d₆) 175.5, 169.5, 157.1, 52.3, 49.4, 48.6, 46.9, 40.4, 39.5, 38.7, 37.3, 32.3, 28.5, 27.3, 26.8, 26.1, 24.7; ¹H NMR (CDCl₃) δ 5.92 (1H, s), 4.61-4.57 (2H, d), 3.86-3.84 (2H, d), 3.60 (1H, s), 3.16-3.02 (8H, m), 2.38-2.35 (2H, m), 2.28-2.24 (1H, s), 1.97 (1H, s), 1.61-1.53 (6H, m), 1.46-1.17 (8H, m), 0.86 (2H, s).

N-(1-((4-((3-aminopropyl)amino)butyl)amino)-1-oxopropan-2-yl)-4-guanidinobutanamide (**2a**). ¹H NMR (CDCl₃) δ 8.15 (2H, s), 6.06 (1H, s), 4.58 (2H, s), 4.22 (2H, s), 3.33 (4H, d), 3.11 (6H, s), 2.72-2.46 (5H, m), 1.52 (4H, s), 1.45 (5H, d), 1.11 (2H, d).

N-(1-((4-((3-aminopropyl)amino)butyl)amino)-1-oxopropan-2-yl)-6-guanidinohexanamide (**2b**): ¹H NMR (CDCl₃) δ 8.16 (2H, s), 5.82 (1H, s), 4.60 (2H, s), 4.38 (2H, s), 3.31 (4H, d), 3.13 (6H, s), 2.67-2.52 (5H, m), 1.65-1.53 (6H, m), 1.14 (4H, d), 0.83 (5H, d).

N-(1-((4-((3-aminopropyl)amino)butyl)amino)-1-oxopropan-2-yl)-7-guanidinoheptanamide (**2c**): ¹H NMR (CDCl₃) δ 8.03 (2H, s), 5.11 (1H, s), 4.77 (2H, s), 4.51 (2H, s), 3.20 (4H, d), 2.87-2.55 (8H, s), 2.05 (3H, m), 1.85-1.69 (8H, m), 1.14 (4H, d), 0.83 (5H, d).

N-(4-((3-aminopropyl)amino)butyl)-2-(4-guanidinobutanamido)-4-phenylbutanamide (**3a**): ¹H NMR (CDCl₃) δ 8.13 (2H, s), 7.36 (2H, m), 7.24-7.17 (3H, m), 6.06 (1H, s), 4.67 (3H, m), 3.31 (4H, d), 3.11 (4H, d), 2.55-2.46 (8H, m), 1.52 (4H, m), 1.39-1.11 (8H, m).

N-(1-((4-((3-aminopropyl)amino)butyl)amino)-1-oxo-4-phenylbutan-2-yl)-6-guanidinohexanamide (**3b**): ¹H NMR (CDCl₃) δ 8.02 (2H, s), 7.51 (2H, m), 7.34-7.29 (3H, m), 6.19 (1H, s), 4.83 (3H, m), 3.52 (4H, d), 3.22 (4H, d), 2.67-2.51 (8H, m), 1.67 (4H, m), 1.41-1.29 (12H, m).

N-(1-((4-((3-aminopropyl)amino)butyl)amino)-1-oxo-4-phenylbutan-2-yl)-7-guanidinoheptanamide (**3c**): ¹H NMR (CDCl₃) δ 8.19 (2H, s), 7.42 (2H, m), 7.29-7.14 (3H, m), 6.08 (1H, s), 4.56 (3H, m), 3.23 (4H, d), 3.15 (4H, d), 2.54-2.46 (8H, m), 1.79 (4H, m), 1.52-1.41 (10H, m).

N-(2-((4-((3-aminopropyl)amino)butyl)amino)-1-methoxy-2-oxoethyl)-4-guanidinobutanamide (**4a**): ¹H NMR (CDCl₃) δ 8.16 (2H, s), 5.87 (1H, s), 3.32 (3H, s), 3.13 (2H, s), 1.54 (8H, m), 1.49 (10H, s).

N-(2-((4-((3-aminopropyl)amino)butyl)amino)-1-methoxy-2-oxoethyl)-6-guanidinohexanamide (**4b**): ¹H NMR (CDCl₃) δ 8.21 (2H, s), 5.89 (1H, s), 4.43 (1H, d), 4.32 (2H, d), 3.25 (2H, m), 3.03 (3H, s), 1.47 (12H, m), 1.18 (10H, m).

N-(2-((4-aminobutyl)amino)-1-methoxy-2-oxoethyl)-6-guanidinohexanamide (**4d**): ¹H NMR (CDCl₃) δ 8.09 (2H, s), 5.88 (1H, s), 4.32 (3H, d), 3.41-3.06 (6H, d), 2.26 (2H, s), 1.41 (6H, m), 1.19-1.06 (4H, m).

N-(2-((4-((3-aminopropyl)amino)phenyl)amino)-1-methoxy-2-oxoethyl)-6-

guanidinohexanamide (**4e**): ¹H NMR (CDCl₃) δ 8.28 (2H, s), 7.47 (2H, d), 7.34-7.30 (2H, d), 5.82 (1H, s), 4.50 (2H, d), 3.49 (2H, m), 2.04 (1H, s), 1.74 (4H, m), 1.51 (4H, d), 1.26 (4H, s), 0.84 (2H, d).

N-(2-((4-((3-aminopropyl)amino)butyl)amino)-1-(4-bromophenyl)-2-oxoethyl)-4-guanidinobutanamide (**5a**): ¹H NMR (CDCl₃) δ 8.17 (2H, s), 7.77-7.58 (2H, d), 7.40-7.31 (2H, d), 5.87 (1H, s), 4.63 (2H, s), 3.33 (2H, s), 3.14 (2H, s), 1.55 (4H, s), 1.44 (10H, s), 1.15 (2H, d).

N-(2-((4-((3-aminopropyl)amino)butyl)amino)-1-(4-bromophenyl)-2-oxoethyl)-6-guanidinohexanamide (**5b**): ¹H NMR (CDCl₃) δ 8.16 (2H, s), 7.34-6.98 (4H, m), 5.67 (1H, s), 4.68-4.52 (2H, m), 4.49 (2H, s), 3.31-3.06 (4H, dd), 2.43 (2H, m), 2.03 (2H, s), 1.70 (4H, s), 1.48-1.41 (10H, m), 1.13 (4H, d).

N-(2-((4-aminobutyl)amino)-1-(4-bromophenyl)-2-oxoethyl)-6-guanidinohexanamide (**5d**): ¹H NMR (CDCl₃) δ 8.03 (2H, s), 7.81-7.69 (2H, d), 7.63-7.57 (2H, d), 5.82 (1H, s), 4.42 (2H, s), 4.04 (2H, s), 3.41-2.98 (4H, m), 2.25-2.17 (2H, m), 1.97 (2H, s), 1.42 (4H, m), 1.20 (4H, m), 0.86 (2H, d).

N-(2-((4-((3-aminopropyl)amino)phenyl)amino)-1-(4-bromophenyl)-2-oxoethyl)-6-guanidinohexanamide (**5e**): ¹H NMR (CDCl₃) δ 8.28 (2H, s), 7.43-7.39 (4H, d), 7.34-7.30 (2H, d), 6.68 (2H, d), 5.12 (1H, s), 4.39 (2H, d), 3.35 (2H, m), 2.65 (2H, s), 1.83 (4H, m), 1.52 (2H, d), 1.29 (4H, s).

N-(2-((4-((3-aminopropyl)amino)butyl)amino)-1-(3,5-dimethoxyphenyl)-2-oxoethyl)-6-guanidinohexanamide (**6**): ¹H NMR (CDCl₃) δ 8.16 (2H, s), 7.34-6.98

(4H, m), 5.67 (1H, s), 4.68-4.52 (2H, m), 4.49 (2H, s), 3.31-3.06 (4H, d), 2.43 (2H, m), 2.03 (2H, s), 1.70 (4H, s), 1.48-1.41 (10H, m), 1.13 (4H, d).

N-(2-((4-((3-aminopropyl)amino)butyl)amino)-1-(3-hydroxyphenyl)-2-oxoethyl)-6-guanidinohexanamide (**7**): ¹H NMR (CDCl₃) δ 8.03 (2H, s), 7.71 (1H, s), 7.36-7.26 (2H, m), 6.83 (1H, s), 5.82 (1H, s), 4.31-4.22 (2H, d), 3.30 (2H, m), 3.09-2.92 (4H, d), 2.55 (10H, s), 1.41 (14H, s), 1.27 (2H, s).

N-(2-((4-((3-aminopropyl)amino)butyl)amino)-1-(3,5-dimethoxyphenyl)-2-oxoethyl)-6-guanidinohexanamide (**8**): ¹H NMR (CDCl₃) δ 8.16 (2H, s), 7.53-7.06 (3H, s), 5.88 H NMR (CDCl₃) δ 8.16 (2H, s), 7.34-6.98 (4H, m), 5.67 (1H, s), 4.68-4.52 (2H, m), 4.49 (2H, s), 3.31-3.06 (4H, d), 2.43 (2H, m), 2.03 (2H, s), 1.70 (4H, s), 1.48-1.41 (10H, m), 1.13 (4H, d).

N-(2-((4-((3-aminopropyl)amino)butyl)amino)-1-(4-(benzyloxy)phenyl)-2-oxoethyl)-6-guanidinohexanamide (**9**): ¹H NMR (CDCl₃) δ 8.13 (2H, 2), 7.47-7.32 (4H, m), 7.21 (2H, d), 7.01 (2H, d), 6.08 (1H, s), 5.52 (2H, s), 4.57 (2H, s), 3.21 (2H, d), 3.14 (4H, d), 2.13 (4H, m), 1.72 (2H, d), 1.56-1.44 (10H, m), 1.08 (4H, d).

4.4.4 Protein purification

All Hsc70 proteins were derived from the human Hsc70 (HSPA8). All Hsc70, Hsc70 SBD truncations, DnaK, HOP, FKBP51, DnaJ, and J-domain sequences were cloned into the pMCSG7 plasmid (Midwest Center for Structural Genomics, Bethesda, MD) by ligation independent cloning and transformed into Rosetta

(DE3) cells for expression. For expression, 25 mL of overnight (37 °C) LB culture of Rosetta (DE3) culture was poured into 1 L of Terrific Broth. After 3 hours incubation at 37 °C, the culture was cooled down to 16-28 °C for 2 hours before overnight induction of expression with 200-500 μ M IPTG, and the cell pellet was stored at -80 °C until use. For 15 N labeling of Hsc70 SBD, the 25 mL overnight LB starter culture was first rinsed twice with M9 media (minimal media supplemented with 1 g/L 15 N labeled NH_4Cl) before being inoculated into the same media. All proteins were purified on Ni-NTA resin (Qiagen), the His-tag removed by TEV protease cleavage, followed by further purification. CHIP protein was expressed in *E. coli* (BL21 DE3 LysS) and purified on glutathione sepharose resin (GE Healthcare) [39, 40]. The GST-tag was cleaved using PreScission protease (GE Healthcare) and purified prior to use.

4.4.5. Fluorescence quenching assay

Protein samples were labeled and prepared as previously described [24, 41]. Briefly, amine reactive Alex488 (Invitrogen) was used to label Hsp70 and DnaK by mixing the dye and protein at a 10:1 molar ratio in bicarbonate buffer (100 mM NaHCO_3 [pH 8] containing 150mM NaCl). CHIP, HOP, DnaJ, and FKBP51 were similarly labeled using BHQ-10 (Biosearch Technologies) at a molar ratio of 50:1, dye: protein. Excess labels were removed by passage through ZebaTM desalting columns (Thermo Scientific) equilibrated with HEPES-buffered saline (25 mM HEPES, 150 mM NaCl [pH 7.4]). Using the extinction coefficients supplied by the

manufacturer, label concentrations were determined for each protein sample and used to calculate the amount of molar incorporation. MIR values for Hsp70, DnaK, HOP, FKBP51, DnaJ and CHIP were 3.2, 2.5, 7.2, 12.1, 17.4 and 14.1 respectively. All quenching assays were performed at the indicated protein concentrations in 50 mM HEPES buffer (pH 7.4) containing 75 mM NaCl, and 0.05% Tween-20 in a 384-well microplate. Compound or DMSO control was administered directly to each well at the indicated concentrations, and the plate was incubated at 25°C for 2 hours. Equilibrium binding measurements were taken using a SpectraMax M5 microplate reader (Molecular Devices). Each sample was excited at 480nm and total fluorescence was read at 525nm with a 515nm cut-off. The average fluorescence intensity of 15 reads was recorded for each sample. In all of these experiments the effect of compound on fluorophore fluorescence is controlled for, and compound causes no appreciable change in the absorbance spectra of the BHQ-10 quencher (**Appendix 4.5.3**).

4.4.6. Gel filtration assays

Purified protein was pre-incubated on ice in HEPES buffered saline (10 mM HEPES, 100 mM NaCl, pH 7.4) containing 1 mM ADP and either 500 μ M compound or DMSO control. Each sample was injected onto an analytical size exclusion column (Superdex 200, GE Healthcare) and run at 0.5 mL/min in HEPES buffer. All curves were normalized to the elution peak of free nucleotide using GraphPad Prism 4.0.

4.4.7. ATPase assays

The colorimetric assay for monitoring steady-state ATP activity has been previously described [25, 26]. Briefly, Hsc70 (1 μ M) and the J-domain of DnaJ (0.2 μ M) were prepared in assay buffer (0.02% Triton X-100, 100 mM Tris-HCl, 20 mM KCl, and 6 mM MgCl₂ [pH 7.4]). Protein samples were aliquoted into 96-well plates containing 1 mM ATP and either compound at the indicated concentrations or DMSO control. After 3h at 37°C, malachite green reagent was used to detect liberated phosphate and the signal measured on a SpectraMax M5.

4.4.8. Plasmids, transfections and co-immunoprecipitation

The sequences for full length human CHIP (STUB1) HOP (STI1) and FKBP51 (FKBP5) were cloned into the pKH3 plasmid (kind gift from the Allen Saltiel Lab, Michigan). HeLa Cells were seeded at a density of 10,000/cm² on 10x100 mm plates and grown to 80% confluence (3 days). Overnight transfections were carried out using Lipofectamine 2000 reagent (Invitrogen) in Opti-MEM media (Gibco). Cells were lysed at 4°C with lysis buffer (25 mM Tris, 100mM NaCl, 1mM EDTA, 1% NP-40, 5% Glycerol, 10mM phenylmethanesulfonylfluoride (PMSF) and protease inhibitor cocktail [pH 7.4]). Cleared lysates (3 mg/condition) were incubated with Ha-Sepharose (Thermo Fisher) at 4°C overnight. Resin was washed twice with TBS (25 mM Tris, 100mM NaCl [pH 7.4]) and eluted with

100mM Glycine, pH 2.4 at 25°C for 10 min. Standard western blotting procedures were followed to probe for proteins using antibodies towards the Ha-tag and Hsc70 (Santa Cruz Biotechnology).

4.4.9. MAPT stability assays

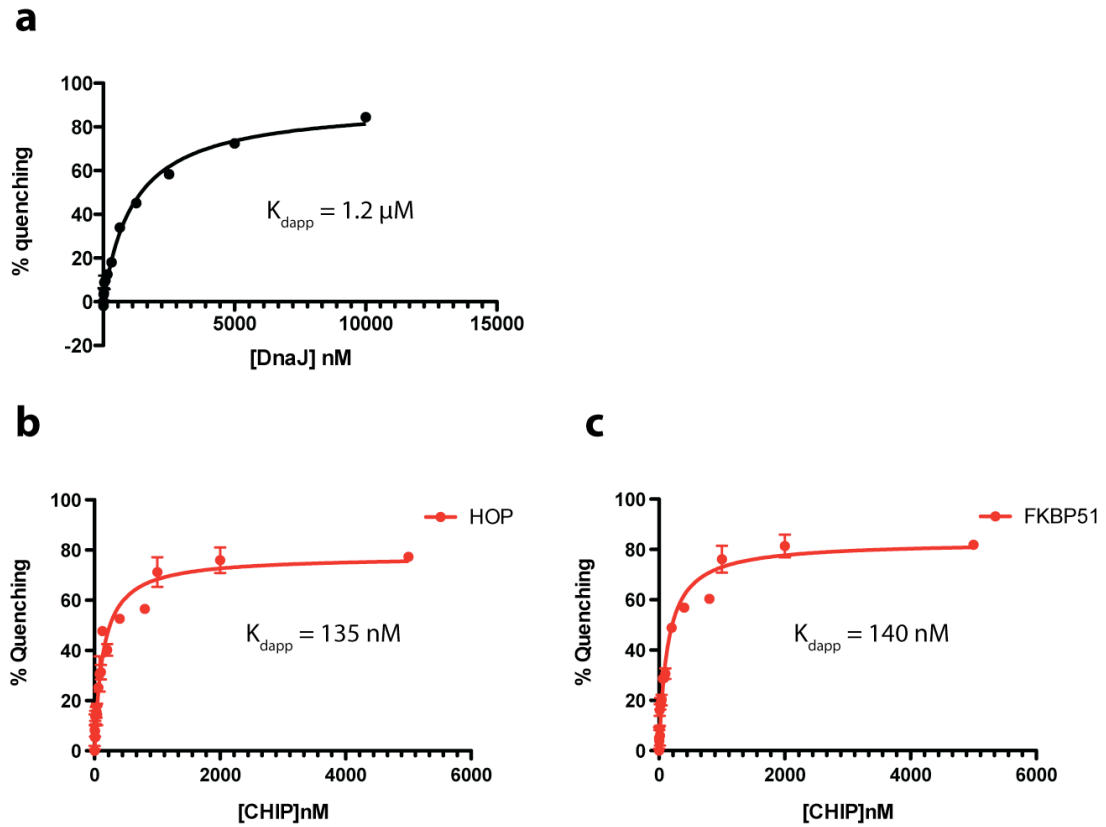
HeLa cells stably expressing V5-tagged tau (kind gift from Chad Dickey Lab, USF [27]) were seeded in 6-well plates at a density of 100,000/well and grown to 60% confluence (2 days). On the morning of the 2nd day, cells were treated with the indicated concentration of compound, or a DMSO control and incubated at 37°C for 5 hours. Cells were lysed at 4°C with M-PER lysis buffer (Thermo Scientific) containing 1mM PMSF and protease inhibitor cocktail. Standard western blotting procedures were used to probe proteins using antibodies towards β -actin (Santa Cruz Biotechnology) and the V5-tag (Sigma Aldrich).

Notes

The work in this chapter was a collaborative effort, and is in preparation to be published under the title “Spergualin analogs as novel inhibitors of the Hsp70/CHIP protein-protein interaction”. Matthew Smith and Jason Gestwicki designed the experiments. Matthew Smith and Chris Evans synthesized all compounds. Matthew Smith performed the experiments. And Matthew Smith and Jason Gestwicki wrote the manuscript.

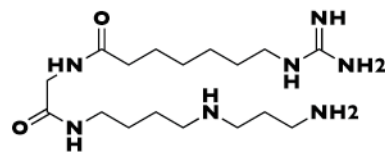
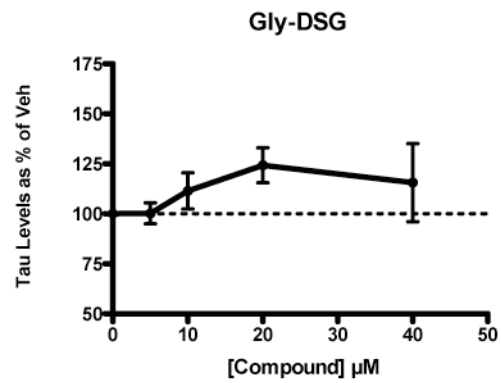
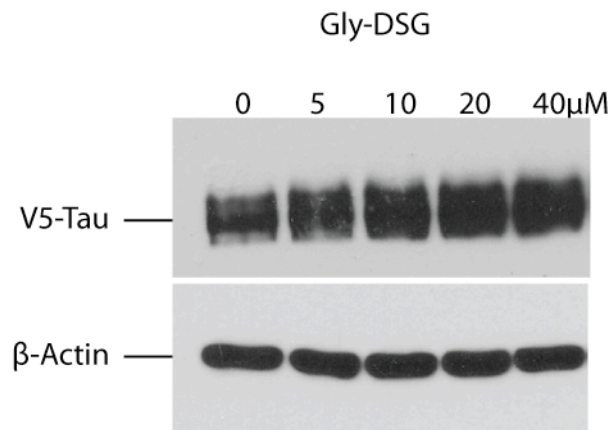
4.5. Appendix

4.5.1. Characterizing Hsc70 PPIs by fluorescence-quenching assay



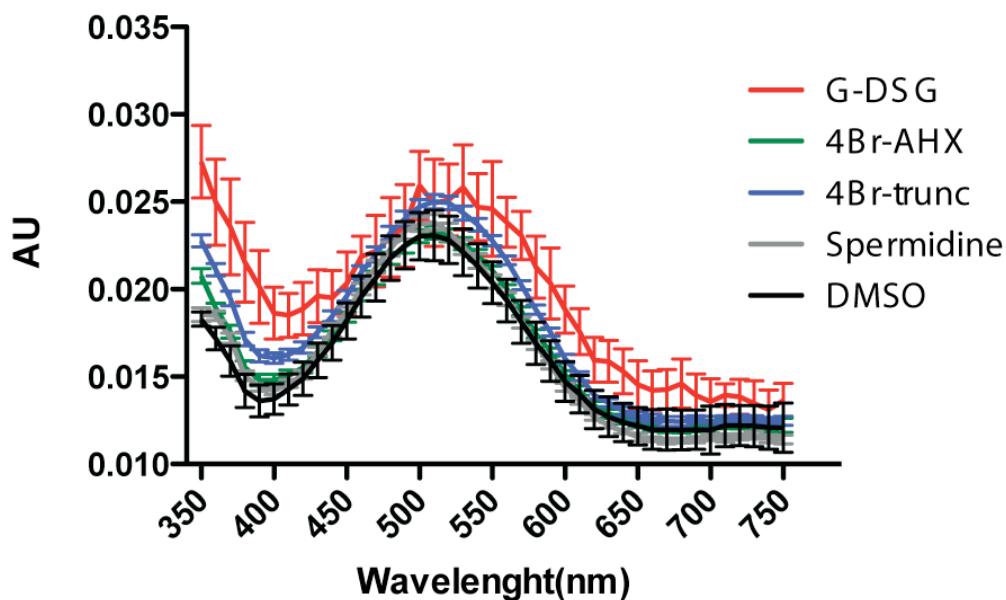
Appendix 4.5.1 Characterization of Hsc70 PPIs by FRET. (a). Alexa-488 labeled DnaK at 50nM gives an apparent K_d for BHQ-10 labeled DnaJ of 1.2 μM . (b-c) Alexa-488 Hsc70 has an apparent K_d for BHQ-10 HOP or FKBP51 of 135 nM and 140 nM respectively. Each data point is the average of triplicates and the error bars represent the standard error of the mean (SEM).

4.5.2 Gly-DSG (1) has a modest effect on tau burden



Appendix 4.5.2 Compound 1 has a modest effect on tau levels. Administration of compound 1 to HeLa cell expressing MAPT (tau) shows a modest increase in tau burden.

4.5.3 Administration of spergualins does not effect BHQ-10 absorbance



Appendix 4.5.3 Compound administration does not alter BHQ-10 absorbance. Compounds (1 mM) were incubated with 80 nM BHQ-10 labeled CHIP for 2 hours and the absorbance spectra were read from 350-750 nm at 10 nm intervals. No change in the absorbance maximum can be detected. Each data point is the average of triplicates and the error bars represent the standard error of the mean (SEM).

4.6 References

1. Rudiger, S., et al., *Substrate specificity of the DnaK chaperone determined by screening cellulose-bound peptide libraries*. EMBO J, 1997. **16**(7): p. 1501-1507.
2. Mayer, M. and B. Bukau, *Hsp70 chaperones: Cellular functions and molecular mechanism*. Cellular and Molecular Life Sciences, 2005. **62**(6): p. 670-684.
3. Kampinga, H.H. and E.A. Craig, *The HSP70 chaperone machinery: J proteins as drivers of functional specificity*. Nature Reviews Molecular Cell Biology, 2010. **11**(8): p. 579-592.
4. Szabo, A., et al., *The ATP hydrolysis-dependent reaction cycle of the Escherichia coli Hsp70 system DnaK, DnaJ, and GrpE*. Proceedings of the National Academy of Sciences, 1994. **91**(22): p. 10345-10349.
5. McCarty, J.S., et al., *The Role of ATP in the Functional Cycle of the DnaK Chaperone System*. Journal of Molecular Biology, 1995. **249**(1): p. 126-137.
6. Allan, R.K. and T. Ratajczak, *Versatile TPR domains accommodate different modes of target protein recognition and function*. Cell Stress & Chaperones, 2011. **16**(4): p. 353-367.
7. Ketterer, N., et al., *Chaperone-assisted degradation: multiple paths to destruction*. Biological Chemistry, 2011. **391**(5): p. 481-489.
8. Scheufler, C., et al., *Structure of TPR Domain-Peptide Complexes: Critical Elements in the Assembly of the Hsp70-Hsp90 Multichaperone Machine*. Cell, 2000. **101**(2): p. 199-210.
9. Zeytuni, N. and R. Zarivach, *Structural and Functional Discussion of the Tetra-Trico-Peptide Repeat, a Protein Interaction Module*. Structure, 2012. **20**(3): p. 397-405.
10. Grove, T.Z., A.L. Cortajarena, and L. Regan, *Ligand binding by repeat proteins: natural and designed*. Current Opinion in Structural Biology, 2008. **18**(4): p. 507-515.
11. Miyata, Y., et al., *Molecular chaperones and regulation of tau quality control: strategies for drug discovery in tauopathies*. Future Medicinal Chemistry, 2011. **3**(12): p. 1523-1537.
12. Kundrat, L. and L. Regan, *Balance between Folding and Degradation for Hsp90-Dependent Client Proteins: A Key Role for CHIP*. Biochemistry, 2010. **49**(35): p. 7428-7438.
13. Yi, F. and L. Regan, *A Novel Class of Small Molecule Inhibitors of Hsp90*. Acs Chemical Biology, 2008. **3**(10): p. 645-654.
14. Ardi, V.C., et al., *Macrocycles That Inhibit the Binding between Heat Shock Protein 90 and TPR-Containing Proteins*. Acs Chemical Biology, 2011. **6**(12): p. 1357-1366.
15. Takeuchi, T., et al., *A new antitumor antibiotic, spergualin: isolation and antitumor activity*. J Antibiot (Tokyo), 1981. **34**(12): p. 1619-21.

16. Umezawa, H., et al., *Structure of an antitumor antibiotic, spergualin*. J Antibiot (Tokyo), 1981. **34**(12): p. 1622-4.
17. Iwasawa, H., et al., *Synthesis of (-)-15-deoxyspergualin and (-)-spergualin-15-phosphate*. J Antibiot (Tokyo), 1982. **35**(12): p. 1665-9.
18. Dickneite, G., et al., *15-deoxyspergualin: from cytostasis to immunosuppression*. Behring Inst Mitt, 1988(82): p. 231-9.
19. Amemiya, H., et al., *A NOVEL RESCUE DRUG, 15-DEOXYSPERGUALIN - 1ST CLINICAL-TRIALS FOR RECURRENT GRAFT-REJECTION IN RENAL RECIPIENTS*. Transplantation, 1990. **49**(2): p. 337-343.
20. Nadler, S., et al., *Interaction of the immunosuppressant deoxyspergualin with a member of the Hsp70 family of heat shock proteins*. Science, 1992. **258**(5081): p. 484-6.
21. Nadler, S., et al., *Identification of a binding site on Hsc70 for the immunosuppressant 15-deoxyspergualin*. Biochem Biophys Res Commun, 1998. **253**(1): p. 176-80.
22. Nadeau, K., et al., *Quantitation of the interaction of the immunosuppressant deoxyspergualin and analogs with Hsc70 and Hsp90*. Biochemistry, 1994. **33**(9): p. 2561-7.
23. Brodsky, J., *Selectivity of the molecular chaperone-specific immunosuppressive agent 15-deoxyspergualin: modulation of Hsc70 ATPase activity without compromising DnaJ chaperone interactions*. Biochem Pharmacol, 1999. **57**(8): p. 877-80.
24. Chang, L., et al., *Chemical Screens against a Reconstituted Multiprotein Complex: Myricetin Blocks DnaJ Regulation of DnaK through an Allosteric Mechanism*. Chemistry & Biology, 2011. **18**(2): p. 210-221.
25. Miyata, Y., et al., *High-Throughput Screen for Escherichia coli Heat Shock Protein 70 (Hsp70/DnaK): ATPase Assay in Low Volume by Exploiting Energy Transfer*. Journal of Biomolecular Screening, 2010. **15**(10): p. 1211-1219.
26. Chang, L., et al., *High-throughput screen for small molecules that modulate the ATPase activity of the molecular chaperone DnaK*. Analytical Biochemistry, 2008. **372**(2): p. 167-176.
27. Dickey, C., et al., *Akt and CHIP coregulate tau degradation through coordinated interactions*. Proc Natl Acad Sci U S A, 2008. **105**(9): p. 3622-7.
28. Dickey, C., et al., *The high-affinity HSP90-CHIP complex recognizes and selectively degrades phosphorylated tau client proteins*. J Clin Invest, 2007. **117**(3): p. 648-58.
29. Umeda, Y., et al., *Synthesis and antitumor activity of spergualin analogues. II. Chemical modification of the spermidine moiety*. J Antibiot (Tokyo), 1987. **40**(9): p. 1303-15.
30. Kamiguchi, K., et al., *Disruption of the association of 73 kDa heat shock cognate protein with transporters associated with antigen processing (TAP) decreases TAP-dependent translocation of antigenic peptides into*

- the endoplasmic reticulum*. Microbiology and Immunology, 2008. **52**(2): p. 94-106.
31. Amemiya, H., et al., *MULTICENTER CLINICAL-TRIAL OF ANTIREJECTION PULSE THERAPY WITH DEOXYSPERGUALIN IN KIDNEY-TRANSPLANT PATIENTS*. International Journal of Clinical Pharmacology Research, 1991. **11**(4): p. 175-182.
 32. Yutaka, M., H. Quazi Manjurul, and N. Shusuke, *Inhibition of Malaria-Infected Erythrocytes by Deoxyspergualin: Effect on in vitro Growth of Malarial Cultures*. Chemotherapy, 1998. **44**(6): p. 409.
 33. Nishikawa, K., et al., *Antitumor activity of spergualin, a novel antitumor antibiotic*. J Antibiot (Tokyo), 1986. **39**(10): p. 1461-6.
 34. Umezawa, K. and T. Takeuchi, *Spergualin: a new antitumour antibiotic*. Biomed Pharmacother, 1987. **41**(5): p. 227-32.
 35. Evans, C., et al., *Improved synthesis of 15-deoxyspergualin analogs using the Ugi multi-component reaction*. Bioorg Med Chem Lett, 2011.
 36. Feichtinger, K., Zapf, C., Sings, H.L., and Goodman, M., *Diprotected Triflylguanidines: A New Class of Guanidinylation Reagents*. J Org Chem, 1998. **63**(12): p. 3804-05.
 37. Xu, P.Z., Ting; Wang, Wenhao; Zou, Xiaomin; Zhang, Xin; Fu, Yiqiu, *Synthesis of PNA Monomers and Dimers by Ugi Four-Component Reaction*. Synthesis, 2003. **2003**(8): p. 1171-76.
 38. More, J.D. and N.S. Finney, *A Simple and Advantageous Protocol for the Oxidation of Alcohols with o-Iodoxybenzoic Acid (IBX)*. Org Lett, 2002. **4**(17): p. 3001-3003.
 39. Scaglione, K.M., et al., *Ube2w and Ataxin-3 Coordinately Regulate the Ubiquitin Ligase CHIP*. Molecular Cell, 2011. **43**(4): p. 599-612.
 40. Brzovic, P.S., et al., *A Ubch5/ubiquitin noncovalent complex is required for processive BRCA1-directed ubiquitination*. Molecular Cell, 2006. **21**(6): p. 873-880.
 41. Ruan, Q., J. Skinner, and S. Tetin, *Using nonfluorescent Forster resonance energy transfer acceptors in protein binding studies*. Anal Biochem, 2009. **393**(2): p. 196-204.

Chapter 5

Conclusions and future directions

5.1. Abstract

There are an estimated 600,000 protein-protein interactions (PPIs) in any given cell, which help to facilitate virtually every cellular function. From a therapeutic perspective, this observation presents a massive untapped opportunity for novel intervention in previously intractable diseases, such as some types of cancer and neurodegeneration. As discussed in Chapter 1, the challenges of developing small molecule modulators of these PPIs are significant, but they can sometimes be surmounted with the right tools and strategies. PPIs in protein quality control have been of particular interest to chemical biologists and, in this thesis, I have described one successful example of targeting a critical quality control PPI. The rational design approach we took is one of many avenues available for advancing a drug target campaign against a PPI. In this chapter, I expand upon the possible uses for the spergualin analogs that have already been characterized, as well as provide a framework for further improvement of these compounds, both in terms of selectivity and potency.

5.2. Conclusions

5.2.1. Targeting protein quality control using small molecules: Rationale for targeting the Hsp70-CHIP interface

The Lasker Prize in 2011 was awarded to Hartl and Horwich for their work on the discovery that many cellular proteins require the assistance of molecular chaperones to be properly folded [1]. Most molecular chaperones drive this process using ATP hydrolysis. For example, heat shock protein 70 (Hsp70) uses ATPase activity to regulate its binding to hydrophobic residues in substrate proteins (**Figure 5.1**). Through these activities, Hsp70 is well positioned as a key component of protein quality control [2]. As discussed extensively in this thesis, protein-protein interactions (PPIs) between Hsp70 and the superfamily of co-chaperones are now believed to be central to guiding the fate of Hsp70-bound substrates [3-5] (**Figure 5.1**). However, to date there are few examples of small molecules that are able to manipulate PPIs in the Hsp70 complex. It is likely that a more complete series of such chemical probes would be invaluable in better understanding chaperone biology and its roles in disease.

In Chapter 2, I described the characterization of the PPI between Hsp70 and the TPR (tetratricopeptide repeat) co-chaperone CHIP (C-terminus of Hsc70 interacting protein). There we reported that the interaction between the TPR of CHIP and the C-terminal domain from Hsp70 constitute ~80% of the binding affinity for these two proteins. With so much of the binding energy focused on this

discrete interaction, we hypothesized that a small molecule binding to this region would be able to inhibit this PPI. Additionally, since CHIP essentially links Hsp70 and its clients to the proteasome by its ubiquitin ligase activity [6], modulation of the Hsp70-CHIP interaction could have wide ranging effects on protein quality control within the cell.

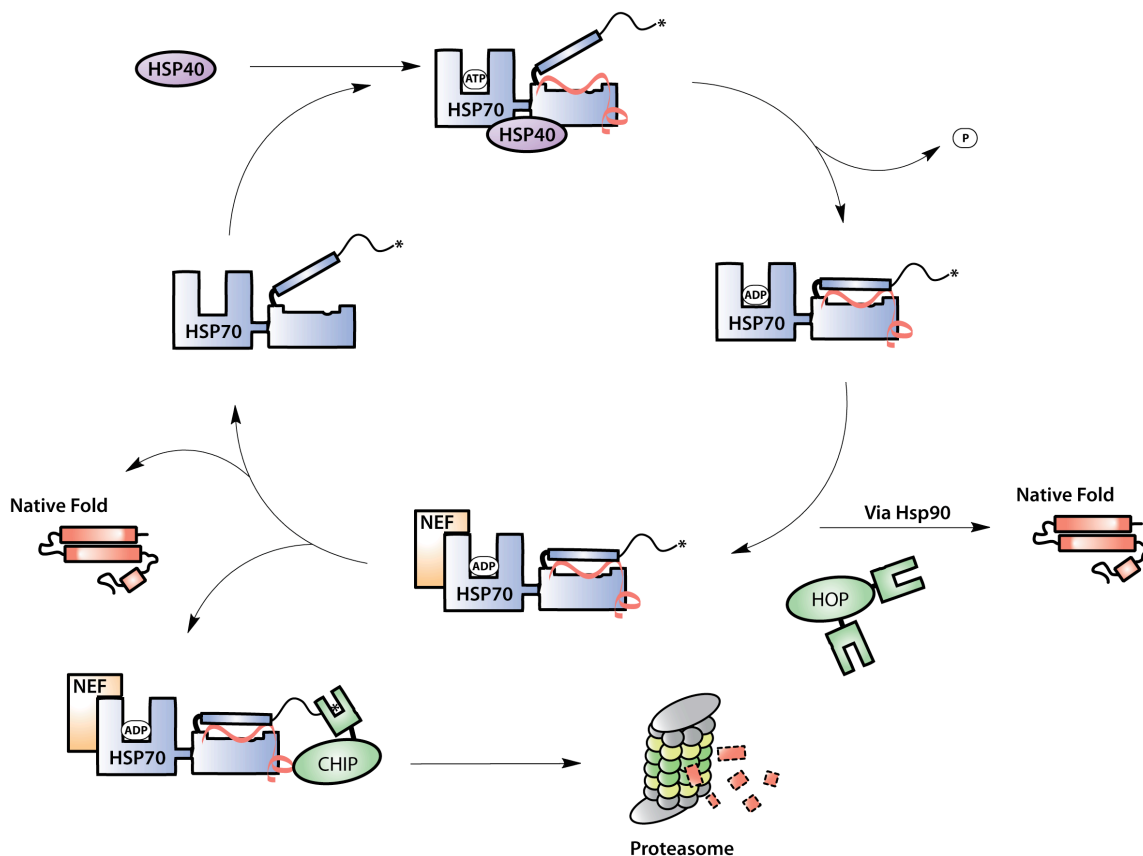


Figure 5.1 The co-chaperone mediated activity of Hsp70. ATP hydrolysis facilitated by J-domain proteins (Hsp40) produces a high-affinity Hsp70-substrate complex. TPR proteins such as HOP and CHIP help triage the bound substrate by assisting in folding via Hsp90 or proteasomal degradation, respectively. NEF's reset the cycle by mediating nucleotide release. * indicates EEVD motif. Abbreviations: Heat shock protein 40, Hsp40; Heat shock protein 70, Hsp70; Nucleotide exchange factor, NEF; Heat shock protein 70/90 organizing protein, HOP; C-terminus of Hsc70 interacting protein, CHIP.

5.2.2. Summary of major advances and characterization of spergualin analogs as inhibitors of the Hsp70-CHIP PPI

In Chapter 3, I describe work aimed at expanding access to an interesting class

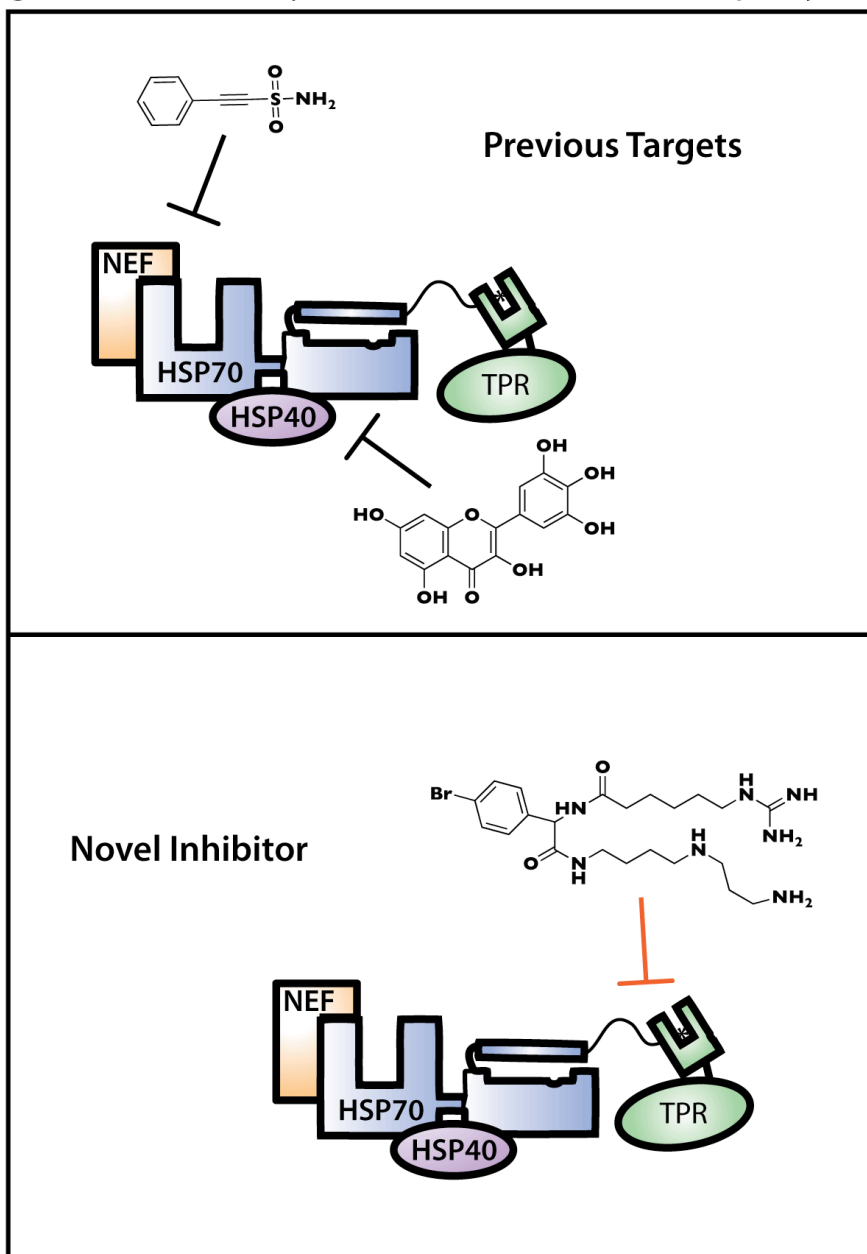
of compounds based on the natural product, spergualin. This scaffold was suggested to bind to the C-terminus of the constitutively expressed Hsc70 [7]. The rationale for redesigning the synthesis was to gain improved access to this compound and its derivatives, in order to test whether they inhibit the Hsp70-CHIP PPI. The resulting synthetic route had an ~5-fold better overall yield compared to the previously published routes [8], constituting a major advance in the synthesis of these compounds. Moreover, due to the modular nature of our synthetic scheme, we were able to rapidly assemble new analogs.

Using our improved synthesis, we designed a small library of spergualin derivatives with a focus on modification at the 11-position [9]. And, in Chapter 4, I provide the first evidence that these compounds inhibit the PPI between Hsp70 and TPR proteins (**Figure 5.2**). Furthermore, we found that these compounds increased the levels of the Hsp70-CHIP client, tau, suggesting that spergualin analogs could indeed alter cellular quality control. This novel activity for the spergualin scaffold provides an exciting, new tool for exploring the biology of Hsp70-TPR protein interactions. For example, recent evidence suggests that CHIP may play a role in peptide presentation by the major histocompatibility complex (MHC) class 1 [10]. These results may help explain why spergualin analogs have immunosuppressive activity.

The work described here provides important new insight into the nature of the

Hsp70-CHIP interaction and produced the first chemical probes of this contact. However, there are a number of important questions related to the mechanism of action of these compounds. Answers to these questions will be important in further advancing this chemical series for use as research reagents and,

Figure 5.2 The discovery of a novel PPI inhibitor of the Hsp70 system.



potentially, as therapeutics.

5.3. Future directions

5.3.1. Improving potency and building selectivity

As discussed in Chapter 3, the most likely binding site for spergualin is the Hsc70 EEVD motif [11]. However, there is little characterization of this possible binding mode. In Chapter 4, I describe our efforts to re-investigate the mechanism of binding for our spergualin derivatives using NMR, but these studies are in their preliminary stages. Once the binding site is mapped, molecular modeling can be used to predict the key regions of the spergualin scaffold that are important. With this information, structure-guided medicinal chemistry might be used to optimize the ligand binding efficiency and increase its affinity. In the absence of binding information, a large-scale spergualin library, with enough variability, could potentially lead us to a more potent compound, and a mixture of these two approaches will likely be the most efficient way forward. Questions of particular interest include: is the polyamine required for membrane permeability? How much steric bulk is tolerated at the 11 position? Which areas of the molecule remain as major metabolic liabilities and how can these be fixed?

The next major question facing this project is whether the spergualin scaffold can be adjusted to gain selectivity for different members of the TPR co-chaperone superfamily. This is an important goal because different TPR proteins, such as

CHIP and HOP, produce opposing outcomes for some Hsp70 substrates. However, the spergualin analogs produced thus far do not distinguish between these TPR domains. The best chance of building selectivity might be to

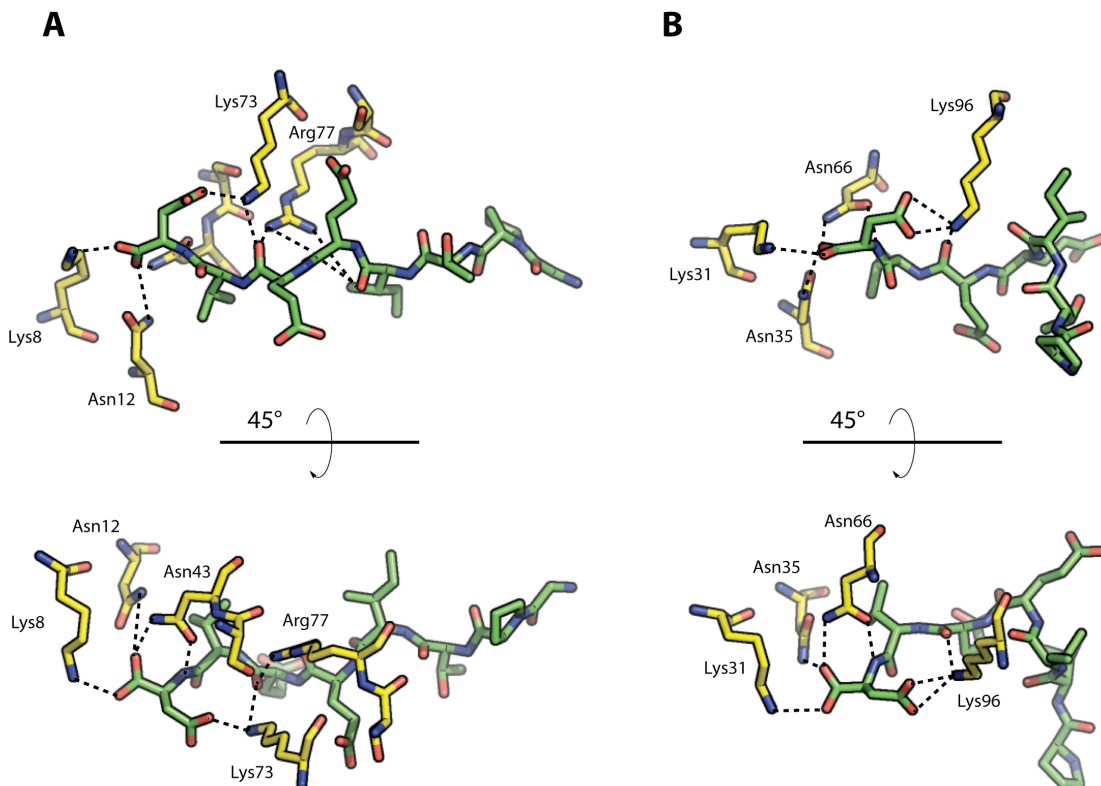


Figure 5.3 Structural differences between Hsp70-TPR interactions. The crystal structures of the Hsp70 C-terminal peptide (green) and hydrogen bonding residues from TPR domains (yellow) of HOP (A) or CHIP (B) are depicted. Asparagine 43, Lysine 73 and Arginine 77 of HOP all make direct backbone contacts with the Hsp70 peptide that are not present in the CHIP binding interface.

determine the binding mode, so that we could take advantage of structural differences that exist between the different TPR domains [12, 13]. For instance, a brief analysis reveals that there are interactions in the Hsp70-HOP complex that are not present between Hsp70-CHIP (**Figure 5.3**). We may be able to gain selectivity by building substitutions within the spergualin scaffold that are sensitive to these differences.

A related concern arises from the fact that Hsp90 uses the same C-terminal EEVD motif to bind to TPR proteins [12]. Since spergualin has been characterized as binding Hsp90 as well [14], this suggests that spergualin analogs may also inhibit the Hsp90-TPR PPI (**Appendix 5.4.1**). In a similar fashion to installing selectivity between TPR proteins of the Hsp70 interaction, we could take advantage of the structural differences between Hsp70 and Hsp90 binding to the TPR. These differences are well illustrated by HOP, where the chaperones bind to separate TPR domains of the same protein, using distinct binding modes [12].

5.3.2. Re-exploring the therapeutic potential of spergualins

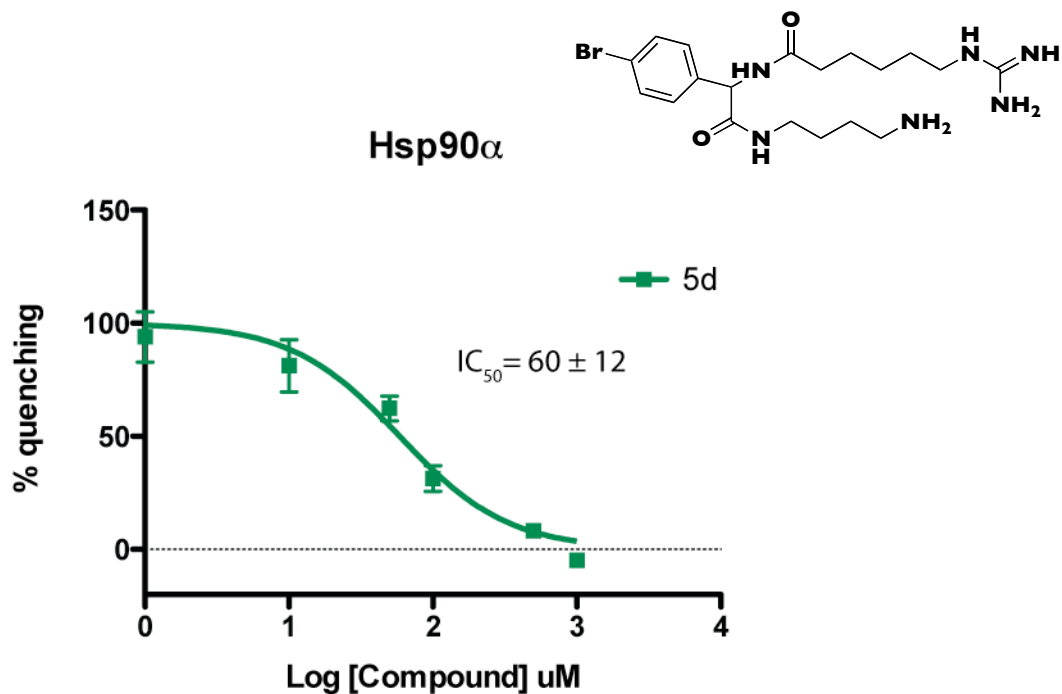
Like many natural products, spergualin was first characterized as having a number of different biological activities. Originally, the molecule was labeled as an antitumor antibiotic [15], owing to its activity against both gram-positive and gram-negative bacterial strains [16]. In addition, these compounds have anti-proliferative activity in tumor models [17]. Soon after, the potent immunosuppressive activity of the scaffold was discovered and the analog, 15-DSG, was approved for acute allograft rejection in Japan [18, 19]. More recently, spergualin has been shown to be effective in treating the more chronic condition of graft versus host disease (GVHD) [20], and it also shows activity in

suppressing malarial infection [21]. One looming, fundamental question is how this simple molecule could achieve such divergent, and often potent, activities.

One possible explanation may be found in spergualin's target molecule. Hsp70 has been shown to play critical roles across cellular pathways and it has been implicated in many different diseases. Thus, the spergualin scaffold may provide an unbiased chemical probe for better understanding the link between Hsp70 and the diseases mentioned here. In this search, combining spergualins with proteomic techniques, such as mass spectral analysis, might be used to monitor changes in genome-wide protein stability. This type of analysis would provide a roadmap to understanding how this molecule broadly effects Hsp70-TPR-substrate multi-protein complexes within the cell, and would allow us to retrospectively piece together a mechanistic understanding of spergualin's effect in disease mitigation.

5.4. Appendix

5.4.1. Spergualin effect on the Hsp90-CHIP interaction



Appendix 5.4.1 Spergualin analog 5d inhibits the Hsp90-CHIP interaction. Alexa-488 labeled Hsp90 α (50 nM) and BHQ-10 labeled CHIP (80 nM) were incubated for 2 hrs with the indicated concentration of compound 5d. Fluorescence readings show the dose-dependent reduction in quenching signal with compound administration, with an IC₅₀ ~60 μ M. Each data point is the mean of duplicated triplicates and the error bars represent the standard error of the mean (SEM).

5.5. References

1. Ostermann, J., et al., *Protein folding in mitochondria requires complex formation with hsp60 and ATP hydrolysis*. *Nature*, 1989. 341(6238): p. 125-130.
2. Hartl, F.U., *Molecular chaperones in cellular protein folding*. *Nature*, 1996. 381(6583): p. 571-9.
3. Miyata, Y., et al., *Molecular chaperones and regulation of tau quality control: strategies for drug discovery in tauopathies*. *Future Medicinal Chemistry*, 2011. 3(12): p. 1523-1537.
4. Connell, P., et al., *The co-chaperone CHIP regulates protein triage decisions mediated by heat-shock proteins*. *Nat Cell Biol*, 2001. 3(1): p. 93-6.
5. Meimaridou, E., S.B. Gooljar, and J.P. Chapple, *From hatching to dispatching: the multiple cellular roles of the Hsp70 molecular chaperone machinery*. *Journal of Molecular Endocrinology*, 2009. 42(1-2): p. 1-9.
6. Stankiewicz, M., et al., *CHIP participates in protein triage decisions by preferentially ubiquitinating Hsp70-bound substrates*. *FEBS Journal*, 2010. 277(16): p. 3353-3367.
7. Nadler, S., et al., *Interaction of the immunosuppressant deoxyspergualin with a member of the Hsp70 family of heat shock proteins*. *Science*, 1992. 258(5081): p. 484-6.
8. Evans, C., et al., *Improved synthesis of 15-deoxyspergualin analogs using the Ugi multi-component reaction*. *Bioorg Med Chem Lett*, 2011.
9. Umeda, Y., et al., *Synthesis and antitumor activity of spergualin analogues. I. Chemical modification of 7-guanidino-3-hydroxyacyl moiety*. *J Antibiot (Tokyo)*, 1985. 38(7): p. 886-98.
10. Kettern, N., et al., *The Hsc/Hsp70 Co-Chaperone Network Controls Antigen Aggregation and Presentation during Maturation of Professional Antigen Presenting Cells*. *PLoS ONE*, 2012. 6(1): p. 11.
11. Nadler, S., et al., *Identification of a binding site on Hsc70 for the immunosuppressant 15-deoxyspergualin*. *Biochem Biophys Res Commun*, 1998. 253(1): p. 176-80.
12. Scheufler, C., et al., *Structure of TPR Domain-Peptide Complexes: Critical Elements in the Assembly of the Hsp70-Hsp90 Multichaperone Machine*. *Cell*, 2000. 101(2): p. 199-210.
13. Wang, L., et al., *Molecular Mechanism of the Negative Regulation of Smad1/5 Protein by Carboxyl Terminus of Hsc70-interacting Protein (CHIP)*. *Journal of Biological Chemistry*, 2011. 286(18): p. 15883-15894.
14. Nadeau, K., et al., *Quantitation of the interaction of the immunosuppressant deoxyspergualin and analogs with Hsc70 and Hsp90*. *Biochemistry*, 1994. 33(9): p. 2561-7.
15. Takeuchi, T., et al., *A new antitumor antibiotic, spergualin: isolation and antitumor activity*. *J Antibiot (Tokyo)*, 1981. 34(12): p. 1619-21.

16. Hibasami, H., et al., *Bactericidal effect of 15-deoxyspergualin on Staphylococcus aureus*. *Chemotherapy*, 1991. 37(3): p. 202-5.
17. Nishikawa, K., et al., *Antitumor activity of spergualin, a novel antitumor antibiotic*. *J Antibiot (Tokyo)*, 1986. 39(10): p. 1461-6.
18. Amemiya, H., et al., *A NOVEL RESCUE DRUG, 15-DEOXYSPERGUALIN - 1ST CLINICAL-TRIALS FOR RECURRENT GRAFT-REJECTION IN RENAL RECIPIENTS*. *Transplantation*, 1990. 49(2): p. 337-343.
19. Fujii, H., et al., *Deoxyspergualin, a novel immunosuppressant, markedly inhibits human mixed lymphocyte reaction and cytotoxic T-lymphocyte activity in vitro*. *Int J Immunopharmacol*, 1992. 14(4): p. 731-7.
20. Makabe, M., K. Orita, and S. Tanaka, *The effect of deoxyspergualin (DSG) on rejection and graft-versus-host disease (GVHD) after small bowel transplantation*. *Transplant International*, 1994. 7: p. 449-452.
21. Yutaka, M., H. Quazi Manjurul, and N. Shusuke, *Inhibition of Malaria-Infected Erythrocytes by Deoxyspergualin: Effect on in vitro Growth of Malarial Cultures*. *Chemotherapy*, 1998. 44(6): p. 409.

Appendix

A chemical biology approach to exploring protein-protein interactions in neurodegeneration

A.1. Abstract

Neurodegenerative disorders such as Alzheimer's and Huntington's disease, all display the hallmark aggregation of misfolded proteins. Yet it remains unknown how this aggregation process contributes to disease. Recent studies suggest that the sequestration of small aggregates into larger, centralized deposits (aggresomes) may be a novel mechanism in protein quality control (PQC). In this Appendix, I focus on one of the key components of PQC, heat shock protein 70 (Hsp70) and explore how protein-protein interactions in the Hsp70 system effect *in vivo* protein aggregation and aggresome formation in the model organism *Saccharomyces cerevisiae*. Our preliminary results suggest that aggresome formation increases the longevity of cells harboring a heavy aggregate burden. Furthermore, inhibition of this process, either by stimulating the Hsp70-Hsp40 interaction or inhibiting interactions between Hsp70 and tetratricopeptide repeat (TPR) proteins, has a negative effect on longevity. These data provide support

for the role aggresome formation plays in PQC and suggest that aggresomes may be a mechanism by which cells cope with misfolded protein in neurodegeneration.

A.1.1. Protein aggregation in neurodegeneration

Research into neurodegeneration started over 100 years ago when Alois Alzheimer described a proteinaceous deposition in and around neurons of patients suffering from dementia [1, 2]. Since then, scientists have uncovered several diseases that are symptomatically distinct from Alzheimer's case, yet share this characteristic protein aggregation in neuronal cells [3]. Why proteins preferentially aggregate in these disease states and how this aggregation process contributes to the degeneration of neurons are key questions in the field. Recent studies have advanced the notion that small, soluble oligomers of misfolded protein represent a toxic aggregation species, while larger, insoluble deposits are relatively benign [4-6]. This is supported by the observation that protein deposition in humans does not correlate with disease severity [7]. Interestingly, Ron Kopito and colleagues have recently identified a form of aggregation that is facilitated by the cell, essentially sequestering distal aggregates into a large, centralized deposit that can be cleared through autophagy [8-11]. These deposits have been termed aggresomes and may represent a novel mechanism for eliminating misfolded protein from the cytosol

[12, 13]. However, to what extent is this novel process integrated into the well established protein quality control (PQC) system? Additionally, what role might aggresomes play in neurodegeneration? In this Appendix, I explore these questions using *Saccharomyces cerevisiae* as an *in vivo* model of protein aggregation.

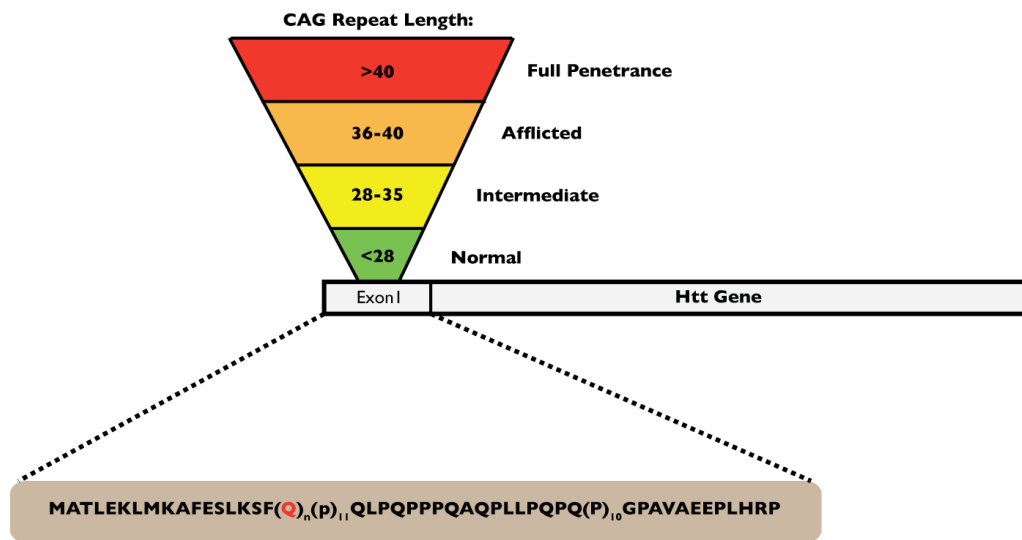


Figure A.1 Characterization of the Huntingtin gene. Exon 1 of Huntingtin contains a CAG repeat region that codes for glutamine. Increasing repeats cause larger stretches of consecutive glutamines in the ensuing protein and is correlated with increased disease severity. Huntington’s disease reaches full penetrance in humans with 40 or more CAG repeats.

A.1.2. Aggresome formation and protein quality control

As discussed previously in my thesis, major components of the PQC system include heat shock protein 70 (Hsp70), Hsp90, Hsp40, nucleotide exchange factors (NEFs), and tetratricopeptide repeat (TPR) domain proteins [14]. Protein-protein interactions (PPIs) within this system facilitate the folding or degradation of misfolded substrates in an ATP-dependent manner [14]. Both Hsp70 and

Hsp90, along with several other PQC components, have been shown to co-localize to the aggresome by immunofluorescent staining [15]. Also, as in the process of proteasomal degradation, ubiquitination appears to be an essential initiator of aggresome formation [13, 16]. In fact, proteasomal inhibition increases aggresome formation in cells expressing misfolded proteins [17, 18], suggesting that aggresomes may compensate for decreased proteasome function. Finally, once formed, aggresomes are engulfed by autophagosomes and cleared from the cytosol [10, 11]. Based on these data, we hypothesize that aggresomes are an integrated part of PQC, allowing misfolded proteins to be detoxified through sequestration into a benign deposit and eventually removed from the cell by autophagy. The preliminary results presented in this appendix provide a basis for speculation on the connection between aggresome formation and PQC and generate hypotheses for future study.

A.2. Results

A.2.1. A *Saccharomyces cerevisiae* model of aggresome formation

Exon 1 of the Huntingtin (Htt) gene harbors a CAG repeat region that encodes a string of consecutive glutamines in the resulting protein [19]. Longer repeat regions lead to higher instability of the protein, the increased propensity for aggregation and a greater severity and earlier onset of symptoms of Huntington's disease (**Figure A.1**). Huntingtin expression causes the formation of aggresomes

in eukaryotic cells [20], and the concomitant inhibition of proteasomal degradation [21, 22], as seen in the disease. Baker's yeast (*Saccharomyces cerevisiae*) offers a convenient way to model the expression of huntingtin

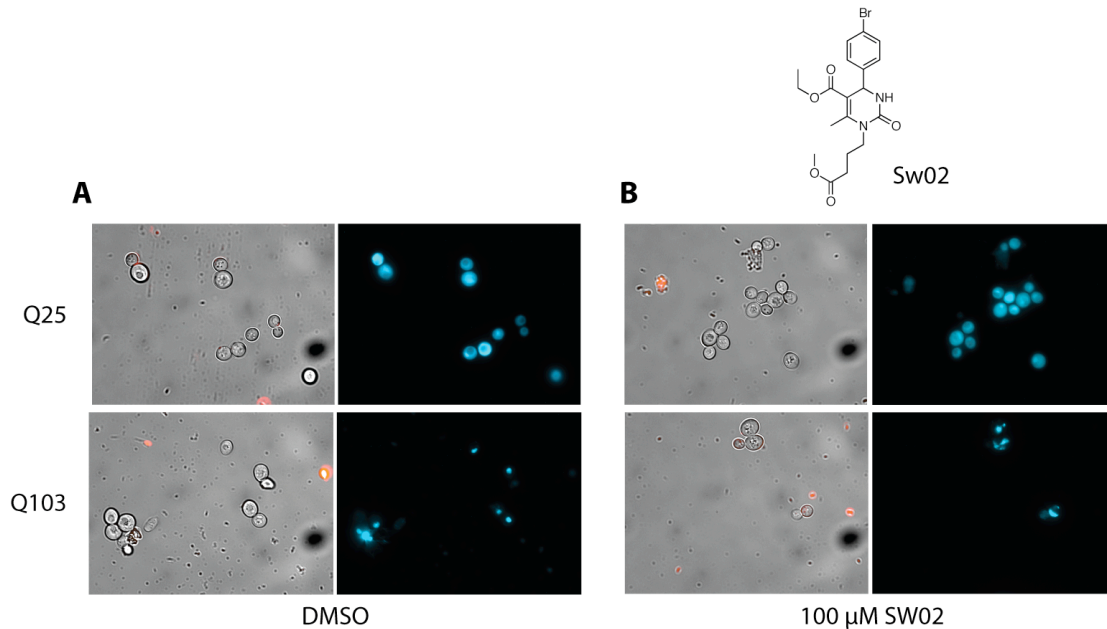


Figure A.2 SW02 causes the inhibition of aggresome formation. (A) Representative micrographs of live cells treated with DMSO control for the first 24 hours post induction. Images depict cells expressing soluble Q25 (top) or aggregated Q103 (bottom). Brightfield images are on the left and are overlaid with TRITC images of propidium iodide (PI) positive cells (dead/dying). CFP fluorescence images are on the right. The majority of Q103 cells harbor single puncta, indicative of aggresome formation. (B) Representative micrographs of live cells treated with 100 μM SW02 on the same timescale. There is a reduction in the number of Q103 cells harboring single puncta.

aggresome formation *in vivo* [23, 24]. In this study we use yeast harboring chromosomal insertions of CFP (cyan fluorescent protein)-fused human Htt exon 1 with 103 (Q103) glutamine repeats, which is prone to rapid aggregation. and soluble CFP-fused human Htt exon 1 containing 25 glutamine repeats (Q25) as a control [25]. Both insertions were made under the GAL promoter and thus expression of the transgene is sensitive to the yeast carbon source.

A.2.2. Modulation of the Hsp70-Hsp40 interaction inhibits aggresome formation

Twenty-four hours after induction, the majority of yeast expressing Q103 form aggresomes (represented by a single, intracellular puncta; **Figure A.2A**). In cells expressing Q25, the mutant protein remains soluble. The dihydropyrimidine SW02 has been shown to selectively stabilize the interaction between Hsp70 and the J-domain of Hsp40, leading to the stimulation of ATPase activity [26]. As the first step in recognition of misfolded proteins is likely binding to Hsp70, we used this compound to test whether modification of the Hsp70-Hsp40 PPI affects aggresomes. Yeast treated with SW02 during the first 24 hours of Q103 induction show a marked decrease in aggresome formation, as measured by the number of cells that form these single puncta (**Figure A.2A**). Conversely, addition of SW02 after aggresome formation, has no effect (data not shown). This finding suggests that aggresome formation is dependent on PPIs within the PQC system, and can therefore be considered as part of PQC.

A.2.3. The pharmacological inhibition of aggresome formation is persistent over time

We next wanted to see how aggregation is manifest in the yeast cell over time. Cells were left to grow for the indicated times in induction media and then imaged for expression of mutant CFP-Htt protein. Interestingly, as the culture aged, the

number of Q103 cells that formed aggresomes increased as a function of the total number of live cells (**Appendix A.5.1**). This suggests that aggresome formation may give the cell a competitive advantage for survival. Treatment with

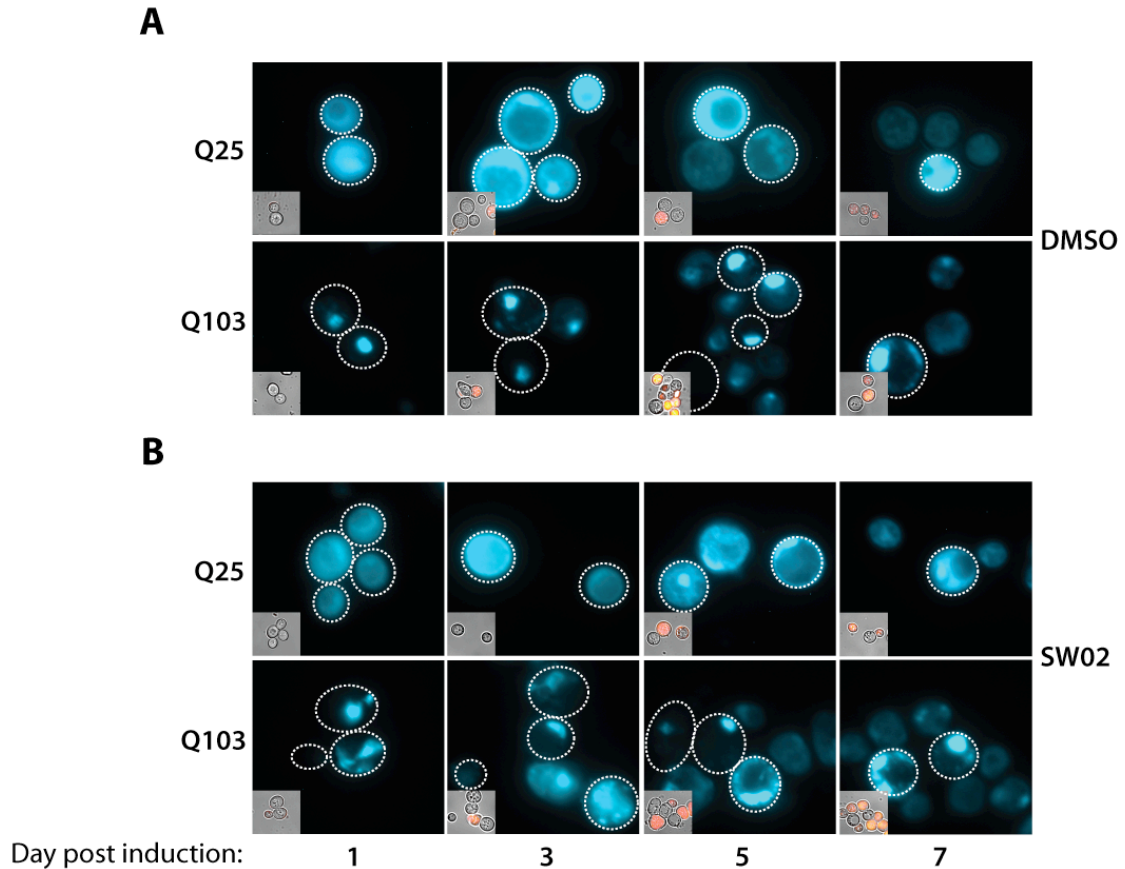


Figure A.3 The inhibition of aggresome formation is persistent over time. (A) Representative micrographs of live cells treated with DMSO control at the start of induction and imaged at the indicated time-point. CFP fluorescence images depict cells expressing soluble Q25 (top) or aggregated Q103 (bottom). Inserts are Brightfield images overlaid with TRITC images of PI positive cells (dead/dying). The majority of Q103 cells harbor single puncta throughout the course of the experiment. (B) Representative micrographs of live cells treated with 100 μ M SW02 on the timescale and imaged at the same time-points. More cells display multiple aggregates after drug treatment.

SW02 during the first 24 hours of induction had a sustained inhibitory effect on the formation of aggresomes (compare **Figure A.3A** and **B**). The carbon source

is likely exhausted within the first 24 hours, so the aggregation pattern shown in these results is likely due the initial inhibition of aggresome formation, and not a persistent effect of the compound, as no new Q103 Htt is produced.

A.2.4. Inhibiting aggresome formation decreases cellular longevity

Since cells treated with SW02 in the first 24 hours do not seem to regain the ability to sequester mutant Q103 Htt into an aggresome, we next sought to determine the effect this might have on cell survival. In order to do this, we took advantage of the stationary phase model of yeast aging. In these experiments, liquid cultures are maintained in a non-fermenting state, past logarithmic growth. A known number of yeast are periodically removed from liquid culture and re-grown on solid media. Survival is measured as the number of individual colonies produced as a function of time. To our surprise, yeast expressing Q103 protein tended to have a significantly more robust lifespan compared to their counterparts expressing the soluble Q25 (**Figure A.4A**). This effect can also be seen by taking yeast at the end of the lifespan curve (Day 12) and inoculating fresh liquid media. Q103 cells show higher levels of growth than Q25 at this late time-point (**Figure A.4B**), suggesting that there are more live cells in Q103 available to inoculate the culture. One possible confounding explanation for this is that expression of Q103 Htt reduces the metabolism in these cells [27], and thereby causes an increase in longevity. Regardless, treatment with SW02 during

the first 24 hours of induction negates this beneficial effect on longevity,

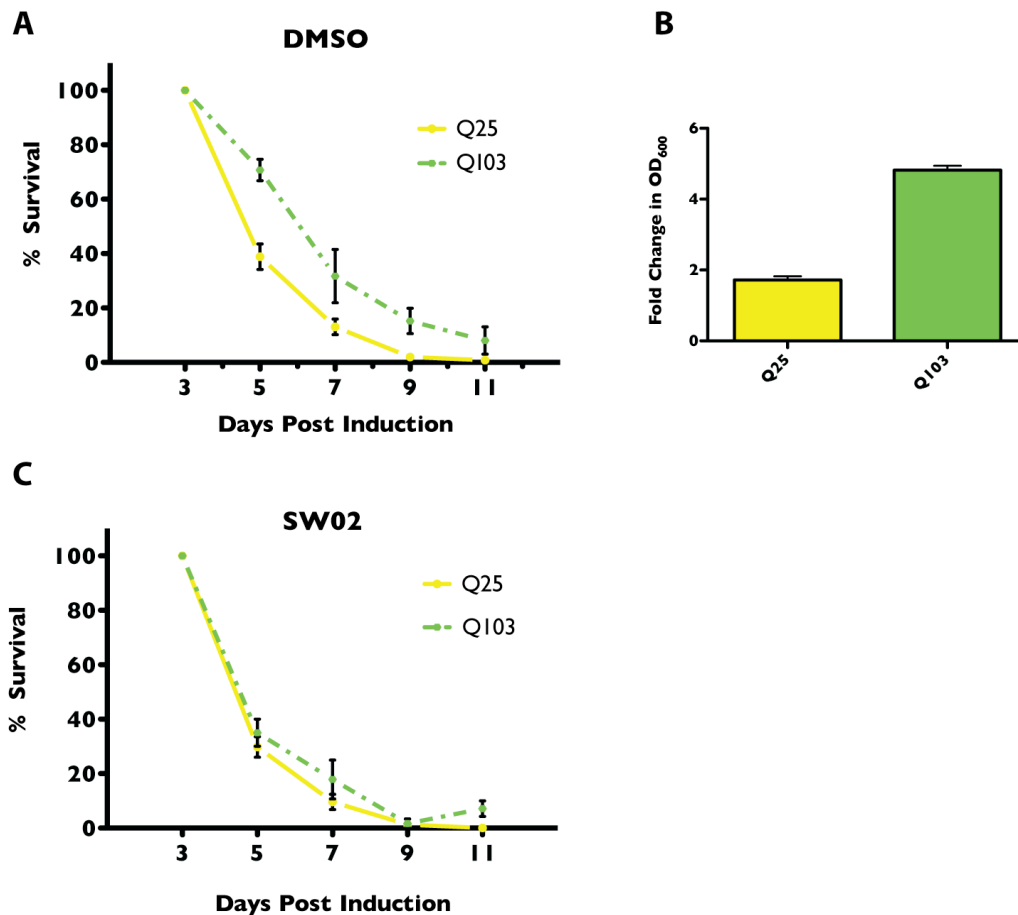


Figure A.4 Inhibiting aggresome formation causes toxicity. (A) Lifespan curves of Q25 and Q103 cells treated with DMSO control. Q103 cells show a significant increase in longevity, but no change in maximum lifespan. (B) Fold change in OD₆₀₀ values upon inoculation of aged cells into fresh liquid SD media. Q103 cultures have more live cells available to re-start a fresh culture. (C) Lifespan curves of cells treated with 100 μ M SW02 during induction. There no longer a difference between Q25 and Q103 expressing cells, suggesting a toxic effect related to the inhibition of aggresome formation. Experiments were performed in triplicate with each data point representing the mean. Error bars are standard error of the mean (SEM).

producing no difference between the survival of Q25 and Q103 treated cells (Figure A.4C). This result suggests that inhibiting aggresome formation is toxic to cells, and is supportive of the literary notion that aggresomes are beneficial. An interesting aside for this thesis is that the spergualin analog MeDSG, described in

Chapter 3, also causes a decrease in aggresome formation (**Figure A.5**). This result implicates a potential role for TPR proteins in the initiation of aggresomes.

A.3. Conclusions

A.3.1. Aggresome formation facilitates cell survival during high misfolded protein burden

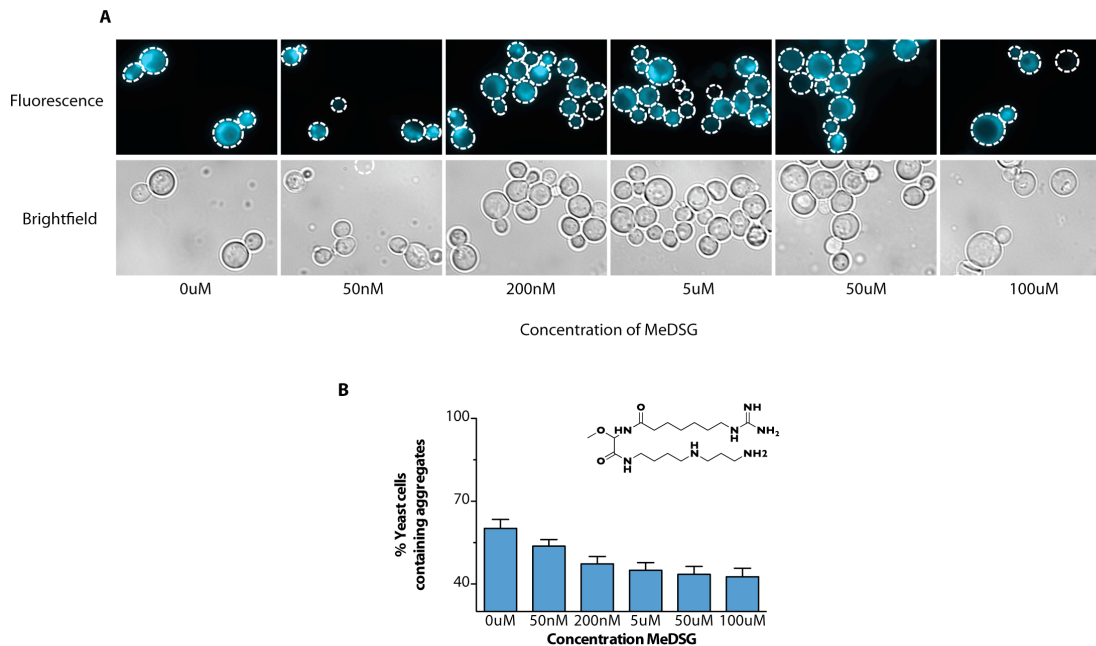


Figure A.5 Spergualin analog administration also inhibits aggresome formation. (A) Representative micrographs of live cells treated with the indicated concentration of spergualin analog MeDSG for 5 hours post induction. DMSO was used as the vehicle control. All images depict cells expressing aggregation prone Q103. CFP fluorescence images are on top, brightfield images below. (B) Quantification of the number of yeast expressing aggregates at the indicated concentrations of MeDSG.

Several studies have characterized the presence of aggresomes in various models of neurodegeneration [20, 28-32]. The current view is that these structures are a staging area to both accumulate misfolded protein, thereby sequestering it away from the rest of the proteome, and eventually dispose of it

[8]. Our data are supportive of this hypothesis, as we found that long-lived cells expressing misfolded protein tend to harbor aggresomes and acute inhibition of aggresome formation has a toxic effect on the longevity of these cells.

A.3.2 Protein quality control directs the formation of aggresomes

One way to identify aggresomes and to distinguish them from other forms of protein aggregates is to monitor co-localization with a number of PQC components [13, 22, 29, 33, 34]. This, together with genetic studies showing the importance of Hsp70 and Hsp90 in aggresome formation [35] led us to the hypothesis that aggresomes may be controlled by the PQC system. The data presented here suggest that this may be the case, since stimulating the Hsp70-Hsp40 interaction causes a reduction in aggresomes. Interestingly, Hsp40-mediated ATP hydrolysis causes Hsp70 to bind substrate proteins with high affinity. This high affinity Hsp70-substrate complex also shows resistance to clearance through the proteasome [36], perhaps representing a situation in which substrates are transiently “stuck” in the Hsp70 binding cycle. Although our results begin to suggest a mechanism of how Hsp70 may help regulate aggresome formation, more work needs to be done to build a comprehensive model.

A.4. Materials and methods

A.4.1. General materials

All yeast strains expressing the Huntingtin fusions were a kind gift from the Martin Duennwald lab (Boston Biomedical Research Institute). SW02 [26] and MeDSG (Chapter 3) were synthesized in-house according to previously described procedures.

A.4.2. Yeast growth and induction

All cells were routinely cultured at 30°C on selective SD medium before being transferred to liquid SG medium (containing drug or DMSO control) for induction of Q25 or Q103 expression.

For live-dead analysis of yeast by microscopy, 50 µL of cells was harvested from liquid culture, washed with phosphate buffered saline [pH 7] (PBS) and incubated with 0.05 mg/mL of propidium iodide (Sigma Aldrich) in PBS for 10 min at room temperature. Live cells were then immobilized on Concanavalin A coated coverslips, mounted on slides and imaged.

A.4.3. Yeast aging assay

Standard protocols for measuring chronological aging in stationary phase yeast

cultures were employed throughout this study [37]. Briefly, single colonies were inoculated into SD media and grown overnight. Total liquid cultures were then washed with sterile PBS and inoculated into 20 mL SG media to a normalized OD_{600} value of 0.2 (media contains either the indicated concentration of compound or DMSO as a control). Yeast were grown at 30°C with 200 rpm shaking and at the indicated time-points, 10 μ L of the liquid culture was diluted to reach 1:10⁴ dilution in sterile water. 10 μ L of this dilution was plated onto solid SD media and grown for 2 days. Single colonies formed were counted, with the number recorded at the first time-point representing 100% survival.

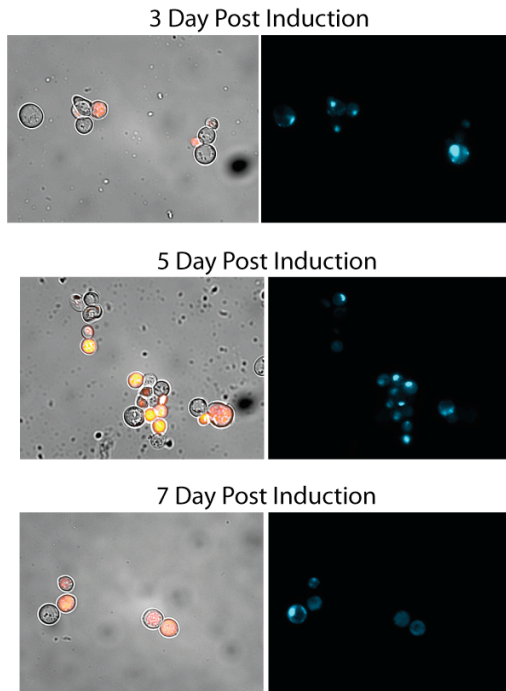
A.4.4. Fluorescence microscopy

Microscopy was performed using an Eclipse 80i system (Nikon Corporation) with DIC, CFP and TRITC filters. All images were processed using Metamorph analysis software (Molecular Devices).

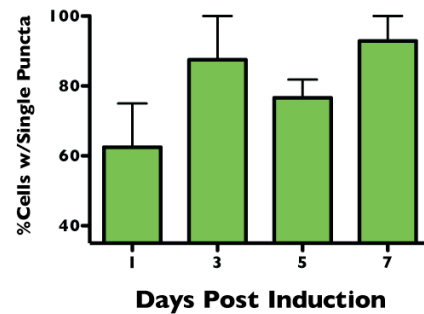
A.5. Appendix

A.5.1 Live cells harboring aggresomes accumulate with age

A



B



Appendix A.5.1 Live cells harboring aggresomes accumulate with age. (A) Fluorescent micrographs showing representative images of yeast expressing Q103 Htt for the indicated number of days. Brightfield images are on the left and are overlaid with TRITC images of propidium iodide (PI) positive cells (dead/dying). CFP fluorescence images are on the right. (B) Quantification of the number of cells harboring aggresomes as a ratio to total number of live cells. Experiments were done in triplicate with 200 cells scored between replicates. Error bars represent the standard error of the mean (SEM).

A.6 References

1. Alzheimer, A., *Concerning unusual medical cases in old age*. Zeitschrift Fur Die Gesamte Neurologie Und Psychiatrie, 1911. **4**: p. 356-385.
2. Graeber, M.B., et al., *Rediscovery of the case described by Alois Alzheimer in 1911: historical, histological and molecular genetic analysis*. neurogenetics, 1997. **1**(1): p. 73-80.
3. Soto, C., *Unfolding the role of protein misfolding in neurodegenerative diseases*. Nat Rev Neurosci, 2003. **4**(1): p. 49-60.
4. Caughey, B. and P. Lansbury, *Protofibrils, pores, fibrils, and neurodegeneration: separating the responsible protein aggregates from the innocent bystanders*. Annu Rev Neurosci, 2003. **26**: p. 267-98.
5. Haass, C. and D. Selkoe, *Soluble protein oligomers in neurodegeneration: lessons from the Alzheimer's amyloid beta-peptide*. Nat Rev Mol Cell Biol, 2007. **8**(2): p. 101-12.
6. Wong, S., W. Chan, and H. Chan, *Sodium dodecyl sulfate-insoluble oligomers are involved in polyglutamine degeneration*. FASEB J, 2008. **22**(9): p. 3348-57.
7. Eisenberg, D. and M. Jucker, *The amyloid state of proteins in human diseases*. Cell, 2012. **148**(6): p. 1188-203.
8. Kopito, R., *Aggresomes, inclusion bodies and protein aggregation*. Trends Cell Biol, 2000. **10**(12): p. 524-30.
9. Johnston, J., C. Ward, and R. Kopito, *Aggresomes: a cellular response to misfolded proteins*. J Cell Biol, 1998. **143**(7): p. 1883-98.
10. Fortun, J., et al., *Emerging role for autophagy in the removal of aggresomes in Schwann cells*. J Neurosci, 2003. **23**(33): p. 10672-80.
11. Opazo, F., et al., *Accumulation and clearance of alpha-synuclein aggregates demonstrated by time-lapse imaging*. J Neurochem, 2008. **106**(2): p. 529-40.
12. Garyali, P., et al., *The malin-laforin complex suppresses the cellular toxicity of misfolded proteins by promoting their degradation through the ubiquitin-proteasome system*. Hum Mol Genet, 2009. **18**(4): p. 688-700.
13. Sha, Y., et al., *A critical role for CHIP in the aggresome pathway*. Mol Cell Biol, 2009. **29**(1): p. 116-28.
14. Miyata, Y., et al., *Molecular chaperones and regulation of tau quality control: strategies for drug discovery in tauopathies*. Future Medicinal Chemistry, 2011. **3**(12): p. 1523-1537.
15. Kovacs, I., et al., *Presenilin 1 forms aggresomal deposits in response to heat shock*. J Mol Neurosci, 2006. **29**(1): p. 9-19.
16. Mishra, A., et al., *The ubiquitin ligase E6-AP is induced and recruited to aggresomes in response to proteasome inhibition and may be involved in the ubiquitination of Hsp70-bound misfolded proteins*. J Biol Chem, 2009. **284**(16): p. 10537-45.

17. Bardag-Gorce, F., et al., *The proteasome inhibitor, PS-341, causes cytokeratin aggresome formation*. *Exp Mol Pathol*, 2004. **76**(1): p. 9-16.
18. Hideshima, T., et al., *Small-molecule inhibition of proteasome and aggresome function induces synergistic antitumor activity in multiple myeloma*. *Proc Natl Acad Sci U S A*, 2005. **102**(24): p. 8567-72.
19. Trottier, Y., et al., *Cellular localization of the Huntington's disease protein and discrimination of the normal and mutated form*. *Nat Genet*, 1995. **10**(1): p. 104-10.
20. Boeddrich, A., R. Lurz, and E. Wanker, *Huntingtin fragments form aggresome-like inclusion bodies in mammalian cells*. *Methods Mol Biol*, 2003. **232**: p. 217-29.
21. Bence, N., R. Sampat, and R. Kopito, *Impairment of the ubiquitin-proteasome system by protein aggregation*. *Science*, 2001. **292**(5521): p. 1552-5.
22. Waelter, S., et al., *Accumulation of mutant huntingtin fragments in aggresome-like inclusion bodies as a result of insufficient protein degradation*. *Mol Biol Cell*, 2001. **12**(5): p. 1393-407.
23. Krobisch, S. and S. Lindquist, *Aggregation of huntingtin in yeast varies with the length of the polyglutamine expansion and the expression of chaperone proteins*. *Proc Natl Acad Sci U S A*, 2000. **97**(4): p. 1589-94.
24. Wang, Y., et al., *Abnormal proteins can form aggresome in yeast: aggresome-targeting signals and components of the machinery*. *FASEB J*, 2009. **23**(2): p. 451-63.
25. Duennwald, M., et al., *A network of protein interactions determines polyglutamine toxicity*. *Proc Natl Acad Sci U S A*, 2006. **103**(29): p. 11051-6.
26. Wisen, S., et al., *Binding of a Small Molecule at a Protein-Protein Interface Regulates the Chaperone Activity of Hsp70-Hsp40*. *Acs Chemical Biology*, 2010. **5**(6): p. 611-622.
27. Bennett, E., et al., *Global changes to the ubiquitin system in Huntington's disease*. *Nature*, 2007. **448**(7154): p. 704-8.
28. Junn, E., et al., *Parkin accumulation in aggresomes due to proteasome impairment*. *J Biol Chem*, 2002. **277**(49): p. 47870-7.
29. Lee, H. and S. Lee, *Characterization of cytoplasmic alpha-synuclein aggregates. Fibril formation is tightly linked to the inclusion-forming process in cells*. *J Biol Chem*, 2002. **277**(50): p. 48976-83.
30. McNaught, K., et al., *Aggresome-related biogenesis of Lewy bodies*. *Eur J Neurosci*, 2002. **16**(11): p. 2136-48.
31. Fratta, P., et al., *Proteasome inhibition and aggresome formation in sporadic inclusion-body myositis and in amyloid-beta precursor protein-overexpressing cultured human muscle fibers*. *Am J Pathol*, 2005. **167**(2): p. 517-26.

32. Kristiansen, M., et al., *Disease-related prion protein forms aggresomes in neuronal cells leading to caspase activation and apoptosis*. J Biol Chem, 2005. **280**(46): p. 38851-61.
33. Garcia-Mata, R., et al., *Characterization and dynamics of aggresome formation by a cytosolic GFP-chimera*. J Cell Biol, 1999. **146**(6): p. 1239-54.
34. Chavez Zobel, A., et al., *Distinct chaperone mechanisms can delay the formation of aggresomes by the myopathy-causing R120G alphaB-crystallin mutant*. Hum Mol Genet, 2003. **12**(13): p. 1609-20.
35. Zaarur, N., et al., *Triggering aggresome formation. Dissecting aggresome-targeting and aggregation signals in synphilin 1*. J Biol Chem, 2008. **283**(41): p. 27575-84.
36. Jinwal, U., et al., *Chemical manipulation of hsp70 ATPase activity regulates tau stability*. J Neurosci, 2009. **29**(39): p. 12079-88.
37. Parrella, E. and V. Longo, *The chronological life span of Saccharomyces cerevisiae to study mitochondrial dysfunction and disease*. Methods, 2008. **46**(4): p. 256-62.